Enzymatic Degradation of Synthetic Polymers

INAUGURALDISSERTATION

zur

Erlangung des akademischen Grades eines

Doktors der Naturwissenschaften

(Dr. rer. nat.)

der

Mathematisch-Naturwissenschaftlichen Fakultät

der

Universität Greifswald

vorgelegt von

Gerlis Maria von Haugwitz

Greifswald, November 2022

Dekan: Prof. Dr. Gerald Kerth

1. Gutachter: Prof. Dr. Uwe T. Bornscheuer

2. Gutachter: Prof. Dr. Thomas Brück

Tag der Promotion: 19.01.2023

Table of Contents

List of Abbreviations

ADH	Alcohol dehydrogenase
BDH	β-diketone hydrolase
BHET	Bis(2-hydroxyethyl) terephthalate
BVMO	Baeyer-Villiger monooxygenase
CHMO	Cyclohexanone monooxygenase
Cryo-EM	Cryo-electron microscopy
DEP	Diethyl phthalate
DNA	Deoxyribonucleic acid
DMT	Dimethyl terephthalate
E. coli	*Escherichia coli*
EG	Ethylene glycol
GPC	Gel permeation chromatography
HPLC	High-performance liquid chromatography
HTS	High throughput screening
*Is*PETase PM	*Is*PETase$^{S121E/D186H/R280A/N233C/S282C}$
I. sakaiensis	*Ideonella sakaiensis*
LCC	Leaf-compost cutinase
LK-ADH	Alcohol dehydrogenase from *Lactobacillus kefir*
LMWPs	Low-molecular-weight products
MEP	Monoethyl phthalate
MHET	Mono-(2-hydroxyethyl)-terephthalic acid
M_n	Average molecular weight
M_w	Weight average molecular weight
NMR	Nuclear magnetic resonance
PA	Phthalic acid
PCR	Polymerase chain reaction

PDI	Polydispersity index
PE	Polyethylene
PET	Polyethylene terephthalate
PETase	PET hydrolase
P. pastoris	*Pichia pastoris*
PQQ	Pyrroloquinoline quinone
PS	Polystyrene
PVA	Polyvinyl alcohol
PVA-DH	PVA dehydrogenases
SA	Succinic anhydrate
TfCa	Carboxylesterase from *T. fusca*
T. fusca	*Thermobifida fusca*
T_g	Glass transition temperature
T_m	Melting temperature
TPA	Terephthalic acid
TTCE	*Thermus thermophilus* carboxylesterase
UHPLC	Ultra-high performance liquid chromatography
wt	Wildtype
3PET	Bis[2-(benzoyloxy)ethyl] terephthalate

In addition to the listed abbreviations, the one-letter codes for proteogenic amino acids, units based on the International System of Units (SI), and SI-derived units were used.

Scope & Outline

This work investigated the enzymatic degradation of polyethylene terephthalate (PET) (**Articles I and II**) and polyvinyl alcohol (PVA) (**Article III**). Physical or chemical degradation of plastic polymers is often performed under extreme conditions like high temperatures or pressure. In comparison to that, recycling of plastics with enzymes can be carried out at ambient temperatures and neutral pH. Enzymes themselves are non-toxic, environmentally friendly, and have been used successfully in a variety of industrial processes.

Enzymatic degradation of polyesters is well studied. Their heteroatomic backbone, which is connecting monomers via ester bonds offers a target for an enzymatic attack. Especially PET, one of the most common polyesters, has been in the focus of research. The first enzyme capable of degrading the polymer was found in 2005. Since then, researchers discovered several enzymes with similar functions and subjected them to enzyme engineering. Improving the enzyme's substrate affinity, activity, and stability aims at making PET recycling more efficient. **Article I** provides an overview of limitations that enzymatic PET recycling is still facing and the research carried out to overcome them. More precisely, enzyme−substrate interactions, thermostability, catalytic efficiency, and inhibition caused by oligomeric degradation intermediates are summarized and discussed in detail.

Article I **Mechanism-Based Design of Efficient PET Hydrolases**
R. Wei, G. von Haugwitz, L. Pfaff, J. Mican, C. P. S. Badenhorst, W. Liu, G. Weber, H. P. Austin, D. Bednar, J. Damborsky, U. T. Bornscheuer, *ACS Catal.*, **2022**, *12*, 3382−3396.

Article II further addresses one of the above-mentioned limitations, namely product inhibition of PET hydrolyzing enzymes. We elucidated the crystal structure of TfCa, a carboxylesterase from *Thermobifida fusca* (*T. fusca*), and applied semi-rational enzyme engineering. The article discusses the structure-function relationship of TfCa based on the apo-structure as well as ligand-soaked structures. Furthermore, it compares the structures of TfCa and MHETase, another PET hydrolase helper enzyme. Lastly, we determined the substrate profile of the carboxylesterase based on terephthalate-based oligo-esters of various lengths and one *ortho*-phthalate ester. In a dual enzyme system, TfCa degraded intermediate products derived from the PET hydrolysis of a variant of PETase hydrolase from *Ideonella sakaiensis* (*I. sakaiensis*). The dual enzyme system utilized PET more efficiently in comparison to solely PETase due to relieved product inhibition. Since TfCa

successfully degraded oligomeric intermediates, the reaction not only released terephthalic acid as the sole product but also increased the overall product yield.

Article II **Structural Insights into (Tere)phthalate-ester Hydrolysis by a Carboxylesterase and its Role in Promoting PET Depolymerization**
G. von Haugwitz, X. Han, L. Pfaff, Q. Li, H. Wei, J. Gao, K. Methling, Y. Ao, Y. Brack, J. Mican, C. G. Feiler, M. S. Weiss, D. Bednar, G. J. Palm, M. Lalk, M. Lammers, J. Damborsky, G. Weber, W. Liu, U. T. Bornscheuer, R. Wei, *ACS Catal.*, **2022**, accepted.

While PET contains an ester bond that can be attacked and hydrolyzed by esterases or lipases, PVA consists of a homoatomic C-C-backbone with repeating 1,3-diol units. The polymer is water soluble with remarkable physical properties such as thermostability and viscosity. PVA is often described as biodegradable, but microbial degradation is slow and frequently involves cost-intensive cofactors. In this study, we present an improved PVA polymer with derivatized side chains and an enzyme cascade that can degrade not only modified but also unmodified PVA in a one-pot reaction. The enzyme cascade consists of a lipase, an alcohol dehydrogenase (ADH), and a Baeyer-Villiger monooxygenase (BVMO). In comparison to the scarcely published research on PVA degradation with free enzyme, this cascade is not only independent from the frequently required cofactor pyrroloquinoline quinone (PQQ) but, in principle, contains an *in vitro* cofactor recycling mechanism.

Article III **Synthesis of Modified Polyvinyl Alcohols and their Degradation Using an Enzymatic Cascade**
G. von Haugwitz, K. Donnelly, M. Di Filippo, D. Breite, M. Phippard, A. Schulze, R. Wei, M. Baumann, U. T. Bornscheuer, *Angew. Chem. Int. Ed.*, *under review*.

1. Background

1.1. Plastic – Advantages and Disadvantages of a Controversial Polymer

Synthetic polymers have been manufactured on industrial scales since the 1950s and have contributed to society with health and safety benefits.[1] Plastics are widely used in a variety of applications, including food packaging and medical applications. The polymer's resistance to degradation was regarded one of the most significant advantages, alongside lightness, low cost, and ease of processing. These material properties make plalstics suitable materials for a broad spectrum of applications.[2] The two largest end-use markets of plastics are packaging and building construction which together make up for over 60 % of the plastic demand.[1] However, due to their persistence, polymers have become a major source of pollution in the environment. Around 307 million tons of plastic were produced worldwide in 2020[1] and it is estimated that 12,000 million metric tons of plastic will accumulate in the environment by 2050 primarily in landfills and oceans making plastic the fourth most common type of waste.[3] This is partly because 40 % of the produced plastic is employed for single-use applications.[4]

In addition to the poor waste management of end-of-life products, the entire lifecycle of plastic products impacts the ecosystem. Microfibers from textile production and maintenance (e.g., from laundry wastewater) and microplastics (MPs) from shower gels or toothpaste, are accumulating in both terrestrial and marine ecosystems.[4–6] The consequences for these ecosystems are tremendous. Aside from the obvious concerns such as physical harm to wildlife animals, there are less obvious and more long-term consequences.[6] Plastic debris can transport invasive species, pathogens, or harmful algal bloom species over long distances and thus from one ecosystem to another.[7,8] Toxic compounds used to gain desired properties of plastics, such as Bisphenol A or plasticizers, and MPs are eaten by fish and can accumulate up the food chain thereby also affecting human health.[9–13]

Even though the research on terrestrial environments is still limited, MPs with a size <5 mm were found in many different soil samples. According to current estimations MPs are present in every terrestrial ecosystem.[14] In soil, MPs potentially impact microbial activity and root growth or provide toxins that penetrate plants.[14,15] Thus, plastic management is an urgent and important issue that researchers from all over the world address in various disciplines. In addition to lowering plastic consumption and reusing plastic items, recycling the polymers is a significant aspect of plastic management with the objective of a circular plastic economy.[16]

1.2. Types of Plastic

Plastics can be categorized into fossil-based chemicals or bio-based polymers with the vast majority of the synthetic polymer being fossil-based.[17] While bio-based polymers derive from renewable sources such as corn, starch, or cellulose, fossil-based plastics are polymers made from petrochemicals and are commonly considered traditional plastics.[16] Fuel-based plastics comprise varying chemical structures and can be further subdivided by the bonds linking the building blocks. Regarding enzymatic degradation, polymers containing a homoatomic carbon-carbon backbone are the most difficult to degrade due to their lack of a functional group for an enzymatic attack. Nevertheless, polymers with a carbon-carbon backbone represent 77 % of global plastics.[3] Examples of synthetic polymers with a homoatomic backbone are polyethylene (PE), polypropylene (PP), and polystyrene (PS). Several kinds of plastics and their respective bond linkages are presented in **Figure 1**.

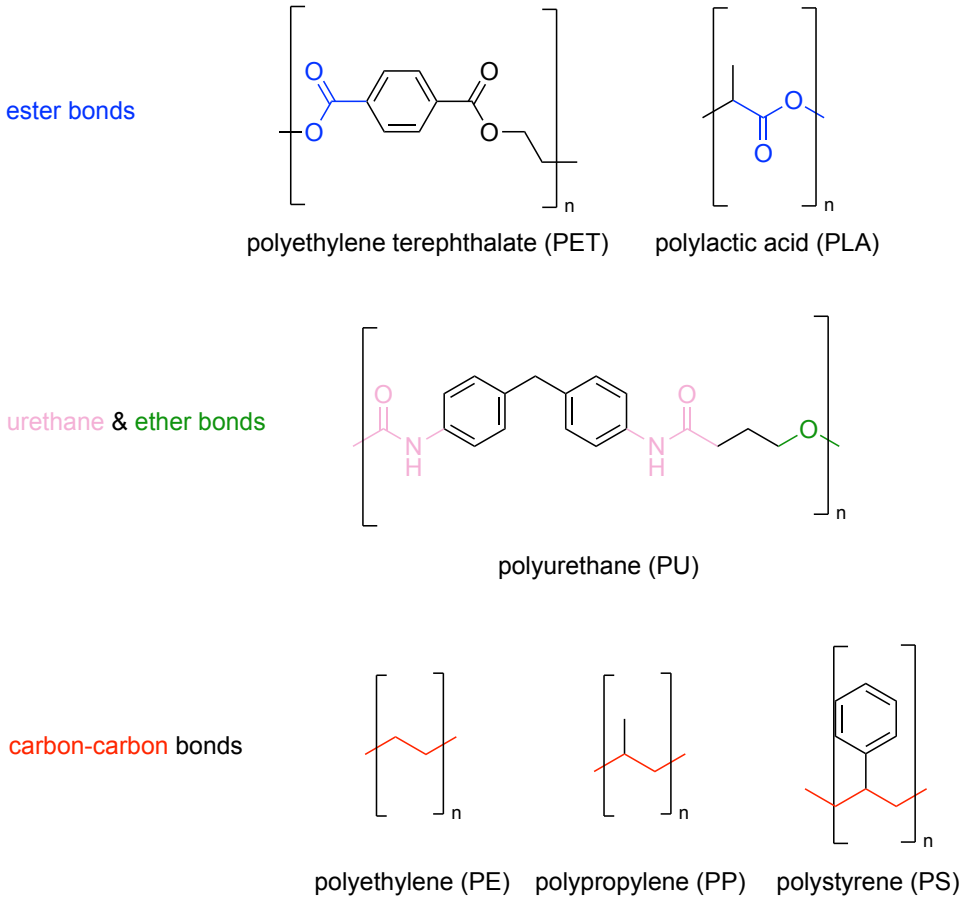

Figure 1: Examples of different types of plastics. The plastics can be subdivided by their chemical structure, or more specifically, by their bond linkages: ester bonds (blue), urethane bonds (pink), ether bonds (green) and carbon-carbon bonds (red). Plastics with a homoatomic carbon-carbon backbone are the most difficult substrate for enzymatic degradation due to the lack of a functional group for biocatalysts to attack.

1.3. Recycling of Plastic

Even though plastic recycling already started in the 1980s, up to today plastic waste management primarily entails accumulation in landfills or incineration for energy recovery.[3] The diversity and complexity of the polymer material, especially in multilayer packaging materials, requires a time- and cost-intensive presorting of post-consumer plastic waste for most recycling methods. High energy costs and a low-quality polymer output of existing recycling methods combined with the low production costs of virgin polymers, render plastic recycling unattractive for the industry.[18] In addition to incineration for energy recovery, plastic recycling can also be achieved mechanically or chemically. All of these pathways have advantages, disadvantages, and limitations which are further discussed in the following.

Mechanical recycling produces secondary items from plastic recycling. These items are mostly low-value products since mechanical processing alters the properties and structure of the recycled polymer.[19] The procedure utilizes large-scale solid waste which is shredded, melted, and remolded into new plastic materials.[4] Prior to mechanical recycling, the post-consumer waste is sorted by material properties such as size, color, and density as well as polymer type. An additional washing step removes organic material and other contaminants.[16] The need for this extensive pretreatment of the diverse material results in increased processing costs.[16] Furthermore, the approach has limited processing cycles, delaying eventual disposal rather than contributing to a circular plastic economy.[20] Combining the outcome of mechanical recycling with virgin plastic, can improve the quality of the resulting product. However, the need for virgin plastic makes mechanical recycling less efficient.

A sub-category of mechanical recycling is primary recycling which refers to reusing the product without altering it. This recycling process is performed for pre-consumer plastic waste that accumulates during plastic manufacturing. After mechanical recycling, the pre-consumer plastic can be returned to the plastic-manufacturing loop.[20] However, primary recycling requires the polymer to be pure and uncontaminated and, as in general mechanical recycling, the recycled material loses its integrity and stability.

In the process of incineration, the polymer itself is not recycled but the energy contained in the polymer is released. The energy content of plastics like PE and PP was measured to be above 40 MJ/kg and thus comparable to gasoline, kerosene, and diesel.[21] At a first glance, recycling energy appears to be a viable approach to recycle plastic. However, burning plastic requires cost-intensive pollution control mechanisms. Furthermore, new plastics must be synthesized from non-renewable resources. As a

result, incineration is a less desirable approach for environmental and economic reasons than mechanical recycling. However, in comparison to other recycling methods, no pre-sorting of plastic waste is needed.

Chemical recycling is for example used for PET post-consumer waste to regain low-molecular-weight products (LMWPs) by thermolysis or monomers by solvolysis. Depending on the chemical reaction, PET can be depolymerized into bis(2-hydroxy-ethyl) terephthalate (BHET), terephthalic acid (TPA), or dimethyl terephthalate (DMT). Methanolysis and glycolysis of PET are performed under high temperature (up to 280 °C) and high pressure (up to 4 MPa) using methanol or glycols such as EG for the depolymerization process.[22] The monomers are subsequently purified and used for the synthesis of virgin polymers.[23]

For the chemical recycling of PE, Jia et. al. published an efficient and selective cascade depolymerization using a co-catalyst system that can perform at comparably low temperatures around 150 °C.[24] However, the authors could not achieve recovery of monomers from their system which is needed for high-quality recycled plastics.

In general, chemical recycling improves the qualitative outcome of the gained polymers in comparison to mechanical recycling techniques. However, the drawback of this method is the need for expensive catalysts, high temperatures, and pressures as well as purity of the post-consumer plastic.[4,25] Furthermore, in chemical recycling, additives such as dye and plasticizers can influence and impede the reaction.[20,26]

Combining different approaches could overcome the limitations of each recycling process. Sullivan et. al. recently reported a hybrid recycling system that uses metal-catalyzed autooxidation to depolymerize mixed plastic waste which is then further used as a substrate for biological conversion by *Pseudomonas putida* to yield useful chemical products such as β-ketoadipate and polyhydroxyalkanoates.[27]

In comparison to the afore-mentioned recycling processes, enzymatic or microbial degradation of plastics have two major advantages: a high selectivity of the biocatalyst which allows the complete depolymerization of the polymer into monomers as well as a performance at ambient temperatures, decreasing the energy costs of the recycling process. However, for cost-efficient enzyme recycling of plastic, much research must still be conducted not only to identify enzymes capable of performing this task but also to improve the activity as well as stability of such enzymes.[4]

1.4. Enzymatic Degradation of Polyethylene Terephthalate

When it comes to enzymatic recycling of plastics, polyesters are currently the most investigated group, especially PET has been the subject of many studies of enzymatic degradation.[28] The aromatic polymer contains repeating TPA and EG and is used for the production of plastic bottles and textiles, among other things. In industry, PET is valued for its hydrophobicity and thermoplastic properties. PET accounts for approximately 10 % of global plastic waste, various recycling routes are described, and, in some cases, industrially applied. Despite that only 10 % of the produced PET is being recycled.[19]

In recent years, enzymatic depolymerization of PET has emerged as an alternative technology to conventional mechanical and chemical plastic recycling approaches. While the microbial and enzymatic degradation of most plastics is still intensively discussed among researchers, enzymatic polyester degradation and recycling evolved fast in recent years. The heteroatomic backbone of PET containing ester bonds makes the polymer accessible for enzymatic hydrolysis.[29] PET degrading enzymes are commonly from the α/β-hydrolase fold family, which cleave ester bonds by the addition of water. Enzymes from this family originate from varying phylogenetic branches and differ in their catalytic function and include lipases, esterases, amidases, and proteases, among others.[30] They are mainly characterized by an α/β-folding motif composed of eight, mostly parallel β-sheets which are stabilized and connected by six α-helices (**Figure 2**).[31]

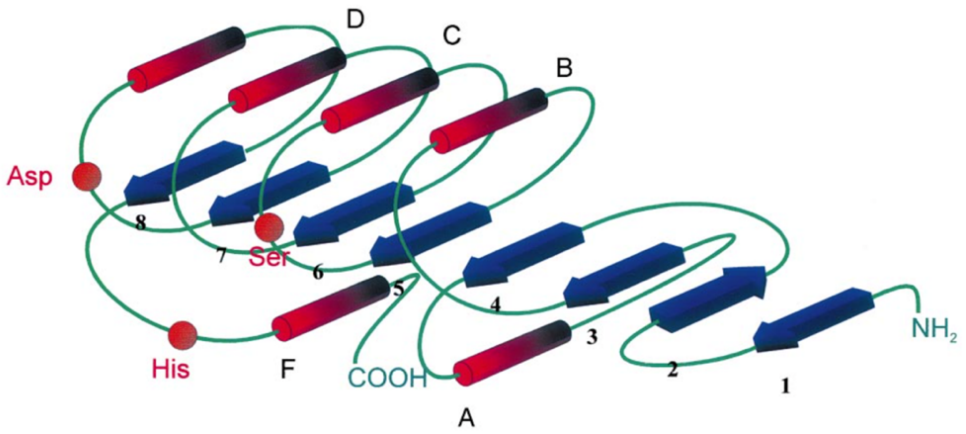

Figure 2: Representation of the α/β-hydrolase fold. Six α-helices are shown as red columns (A-F) which are connecting and stabilizing the eight mostly parallel β-sheets depicted as blue arrows (1-8). Amino acids of the catalytic triad are shown as red spheres. Instead of aspartic acid, the catalytic triad can also contain glutamic acid. The figure was adapted from Bornscheuer et. al..[32]

The catalytic triad of α/β-hydrolases consists of a nucleophilic serine, glutamic acid or aspartic acid, and histidine. The ester hydrolysis is performed in three steps. First, the substrate binds in the active site and is attacked by the nucleophilic serine. The first tetrahedral intermediate is formed and stabilized by an oxyanion hole which is created by

the backbone of conserved amino acids close to the catalytic triad. Second, through the nucleophilic attack, an alcohol is formed as the first product and released from the serine which results in the formation of an acyl-enzyme complex. Lastly, the nucleophilic attack of water forms a second tetrahedral intermediate within the acyl-enzyme complex. The collapse of the second intermediate leads to a carboxylic acid function in the substrate as well as the free enzyme.[32]

Enzymatic PET hydrolysis produces small-molecule degradation products which can be recovered and used for the synthesis of virgin polymers (**Figure 3**).[5,6] In addition to the desired PET monomers TPA and EG, BHET and mono-(2-hydroxyethyl)-terephthalate (MHET) are often gained as intermediate products and can cause inhibition of selected PET hydrolases.[33,34] Biocatalytic recycling of PET is a promising approach which is already successfully performed at laboratory and pilot plant scales.[35,36]

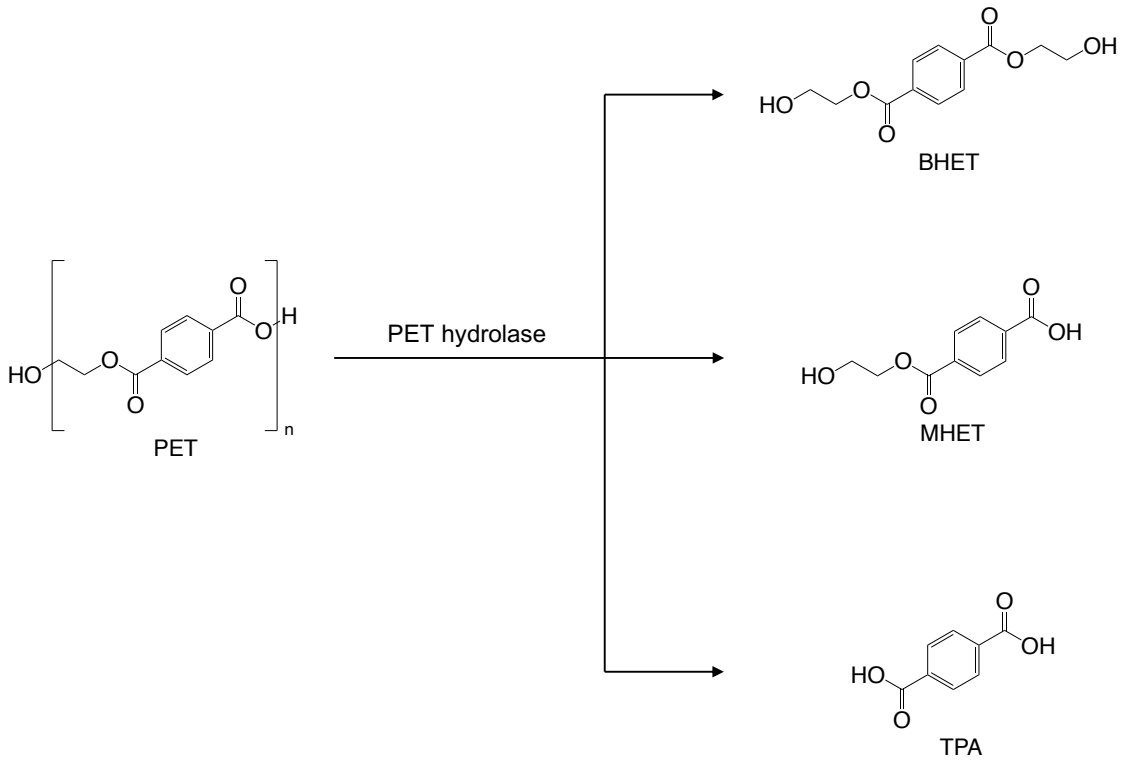

Figure 3: Enzymatic degradation of PET. The PET polymer, consisting of EG and TPA connected by ester bonds, can be degraded by PET hydrolyzing enzymes. The main aromatic products of enzymatic PET degradation are the building block TPA as well as the intermediate substrates BHET and MHET which are known to cause inhibition of selected PET hydrolases.

So far, over 20 enzymes with PET degrading ability have been described and can be classified as esterases (EC 3.1.1.) or more specifically, as carboxylesterases (EC 3.1.1.1.), cutinases (EC 3.1.1.74) and lipases (EC 3.1.1.3.).[37] PET hydrolyzing enzymes are often characterized by an active site close to the surface as well as an active cleft providing enough space for macromolecules and a high affinity towards hydrophobic

materials.[38] The first enzyme with a PET hydrolase-like activity, *Tf*H from *T. fusca*, was discovered in 2005 by Müller et. al.[39] This hydrolase can convert over 50 % of melt-quenched post-consumer PET film at 55 °C within three weeks.[39] In the years after the discovery of *Tf*H, more PET cutinases were found in the *Thermobifida* species which includes *T. fusca*, *T. alba,* and *T. cellulosilytica*.[40–42]

Another milestone in PET degradation was reached in 2016 when Yoshida et. al. discovered that the mesophilic bacterium *I. sakaiensis* can utilize PET as a source of carbon under laboratory conditions.[29] The authors isolated and characterized *Is*PETase, an enzyme with the remarkable ability to degrade highly amorphous PET at ambient temperatures.[29] The enzyme consists of 290 amino acids and can function as a monomer. The crystal structure of *Is*PETase was solved and revealed a central β-sheet composed of nine mixed β-strands as well as seven α-helixes. The overall surface of the biocatalyst is highly polarized, as evident for many PET hydrolases, resulting in an isoelectric point of 9.6.[28,43] Furthermore, the enzyme contains two disulfide bridges, one between C203 and C239 and the other one between C273 and C289, that are stabilizing the protein. The first disulfide bridge is thought to be crucial for the activity of *Is*PETase by providing the structural basis for the positioning of the catalytic histidine.[44,45] In the following years, *Is*PETase was intensively studied[29,46] and engineered towards a higher thermostability[47] and activity[48]. A new enzyme class, the PET hydrolase class, (EC 3.1.1.101) was created.[37]

A variant of leaf-compost cutinase (LCC), so far outperforms all other discovered PET hydrolases and their engineered variants at high temperatures.[35] Tournier et. al. described 90 % depolymerization of amorphized PET into monomers after treatment of the polymer with an improved variant of LCC for 10 h at 72 °C.[35] The enzyme also folds as an α/β-hydrolase and is composed of nine β-strands forming the β-sheet as well as eight α-helices and strongly resembles the previously elucidated structure of a cutinase from *T. alba*.[49] A protruding groove that is built from a hydrophobic amino acid patch and extended from the catalytic pocket promotes the binding of long-chain substrates.[49] Molecular docking of a model substrate confirmed the role of the groove in substrate binding and made it a target for enzyme engineering. Eleven residues within the hydrophobic groove were chosen by Tournier et. al. for mutagenesis. Two mutations (F243I/W) showed improved activity and four others an enhanced melting point (T69M, Y127G, N246D/M) in comparison to the wildtype enzyme.[35] The combination of the mutations resulted in the LCC^{ICCG} mutant (F243I/D238C/S283C/Y127G). The crystal structure of this mutant was recently elucidated

by Zeng et. al. in complex with MHET revealing the enzyme-substrate interaction network.[50]

Next to the bacterial enzymes, PET hydrolases also exist in eukaryotes. Among them are *Thermomyces insolens* (formerly *Humicola insolens*), the fungus *Fusarium solani pisi,* and *Fusarium oxysporum*.[51–53] *Hi*C, a cutinase from *T. insolens* with an optimal temperature of 70 °C[54], was successfully commercialized and optimized in terms of process engineering.[52,55,56] Using low-crystallinity PET (7 % crystallinity) as a substrate, Ronkvist et. al. reported 97 % of degradation within 96 h at 70 °C, determined by weight loss measurements.[52]

1.4.1. Improving the Reaction Performance of PET Hydrolases

Even though many enzymes were found to degrade PET, the degradation performance is mostly too inefficient for an industrial application. Hence, many strategies were developed to improve the enzymes themselves as well as the degradation process.[37]

Improved thermostability of PET hydrolases is required to overcome the issue of crystallinity in enzymatic PET degradation. The degree of crystallinity of the thermoplastic can range from 2-40 % and is the result of uniformly packed crystalline regions in combination with randomly arranged amorphous regions.[37,57] Enzymes preferentially hydrolyze the flexible amorphous regions of the polymer. The glass transition temperature (T_g) marks the temperature at which the amorphous parts of the polymer become flexible and therefore, better accessible for an enzymatic attack. For PET T_g lies in a range of 65-71 °C[58–60] but can be influenced, at least on the surface, by solvents e.g., water which is used in most attempts of enzymatic degradation of PET. In water, T_g can be lowered by up to 16 °C.[61,62] Nonetheless, a lot of research is focused on increasing enzyme stability since the optimal working temperature of most enzymes lies even below the reduced T_g of PET.[35,47,52,63] In general, wildtype PET hydrolases often possess a low catalytic activity as well as low thermostability, which is why enzyme engineering is needed to improve the enzymes.[64]

Furthermore, the adsorption and desorption of the PETase to the polymer as well as the complexation are being researched for efficient PET degradation. The enzyme activity largely depends on the enzyme-substrate interaction; however, the system of PET hydrolysis is heterogenic and hence, not ideal for enzymatic activity. While the PET polymer is mostly insoluble, the biocatalyst is soluble which prevents the enzyme from efficiently binding to the polymer in larger amounts.[37,65] To promote the adsorption, natural

substrate-binding modules e.g., from cellulases are used as model systems to enhance the adsorption of the PET hydrolyzing enzyme to the polymer surface. The degradation performance of PETases could thus be increased by fusing cellulose-binding domains[66–68], polyhydroxyalkanoate-binding modules[67,] or chitin-binding modules[69] to the enzyme. Graham et. al. reported that CBMs can be beneficial for the degradation of PET with LCC if the solid loading is below 10 weight percent.[70]

To improve the complexation of the enzyme and the substrate, information about the detailed mechanism of PET degradation with a biocatalyst are of utmost importance.[71] In a recent study, various substrate-binding modes were identified in ligand-soaked PES-H1 and PES-H2 crystal structures.[71] From these structures, several key residues involved in the binding of PES-H1 and PES-H2 to PET could be identified. Furthermore, the study revealed that substrate intermediates MHET and BHET bind too far from the catalytic triad for a nucleophilic attack supporting previous studies about product inhibition of PETases.[71] Further studies using substrate homologs could elucidate the enzyme-substrate interaction network of LCC and its variants as well as *Is*PETase.[44,50]

1.4.2. PET Oligo- and Monomer Degrading Enzymes

Methods for mitigating the product inhibition during enzymatic PET hydrolysis include the continuous removal of small-molecule products using ultrafiltration membranes,[8] the use of engineered PETase variants that are less affected by the inhibitors,[9] or the introduction of a helper enzyme with specific hydrolytic activity on the inhibitors. In nature, the degradation of recalcitrant polymers is often achieved by a synergistic enzyme system.[33] In the plastic-utilizing bacterium *I. sakaiensis* the issue of product inhibition was relieved by the helper enzyme MHETases.[72] Also *in vitro* introduction of MHETase or other helper enzymes can decrease product inhibition and thus increase the yield of the monomeric products TPA and EG.[33,72] Knott et. al. generated a chimeric enzyme from *Is*PETase and MHETase. The chimeric enzyme performed approximately four times better in comparison to *Is*PETase alone in the degradation of PET. Additionally, TPA was the sole degradation product in reactions with the chimeric enzyme whereas in reactions with only *Is*PETase approximately one-third of the reaction product was MHET.[73]

Mrigwani et. al. reported a two-enzyme system with free enzyme using LCC as the polymer-degrading enzyme and a carboxylesterase from *Thermus thermophilus* (TTCE) as the oligomer hydrolyzing enzyme.[74] The high melting point of both enzymes allows for performance at 60 °C, which gives this system an advantage over the system proposed by Knott et al., which performed at 30 °C. Even though the two systems cannot be

compared easily due to different substrates and reaction conditions, it should be mentioned here that Knott et. al. reached a 400 % higher overall product outcome with TPA as the sole product using 550 nM of each enzyme.[73] Mrigwani et. al. increased the yield of TPA by 30-100 % when using the dual enzyme system in comparison to solely LCC and applied 2 µM of each enzyme to the reaction. Despite the helper enzyme TTCE, small amounts of MHET were detected in the reaction.[74]

Billig et. al.[75] first described the carboxylesterase TfCa, another PET oligomer-degrading enzyme, which originates from *T. fusca.* The enzyme was shown to function with a typical serine hydrolase mechanism and retained 37 % of its activity over 96 h at 50 °C.[75] Billig et. al. could furthermore show that the enzyme hydrolyzes cyclic PET trimers.[75] Immobilized TfCa was successfully deployed in a dual enzyme system together with LCC or TfCut2. The addition of the carboxylesterase to the reaction with LCC and TfCut2 led to a 91 % and 104 % increase in overall product outcome respectively. The immobilization via a sulfo-link resin made the enzyme more resistant to increased reaction temperatures of up to 60 °C.[76]

1.5. Protein Engineering

As mentioned before, many of the discovered PET hydrolases and their helper enzymes for oligomer hydrolysis are lacking either activity, thermostability, or both to function efficiently for enzymatic PET recycling on an industrial scale.[28] Thus, protein engineering is used to modify proteins in order to improve the affinity for their substrate, turnover number, or stability at higher reaction temperatures and over longer reaction periods.[77–79] Protein engineering is subdivided into two main strategies: directed evolution and rational design.[80] Depending on the information available the respective strategies can be more or less advantageous.[81]

Directed evolution deploys diversity and evolution to influence enzymatic behavior and has developed into a common laboratory tool.[82,83] As a result, directed evolution not only aids in the evolution of new protein functions but also with the characterization and understanding of natural protein function and stability.[84,85] The Darwinian cycle of mutation, selection, and amplification is employed with the gene of interest.[83,86,87] For example, through error-prone polymerase chain reaction (PCR) or deoxyribonucleic acid (DNA) shuffling, random mutations are introduced into a target gene sequence, mimicking evolutionary processes.[82,87] The *ex vivo* diversification results in a large gene library which is subsequently transformed into cells where proteins are expressed and undertaken a selection process. Importantly, in each of the iterative cycles, the stringency of the

selection is enhanced through competition or changing experimental conditions.[82] Due to the vast size of the resulting library, well-established high-throughput screening (HTS) methods are essential for successful directed evolution. However, due to a lack of robust assays, HTS is also frequently limiting directed evolution.[88] HTS is mostly based on spectrophotometric or fluorometric assays which can be automated using a robotic screening platform.[89] For the degradation of PET, Bell et. al. used directed evolution to improve the thermostability of *Is*PETase. Starting from an *Is*PETase variant with a melting point of 56.8 °C, the authors yielded the HotPETase with a melting point of 82.5 °C by employing sequential rounds of saturation mutagenesis of the gene of interest and using ultra-high performance liquid chromatography (UHPLC) as the screening method.[90]

In comparison to directed evolution, the rational design uses mechanistic and structural information as well as molecular modeling for a targeted alteration of the enzyme property. Targeted mutations result in significantly smaller enzyme libraries in comparison to directed evolution, opening possibilities for screening methods without high throughput.[91] Recently, the development of an artificial intelligence system e.g., DeepMind Technologies' AlphaFold2 brought new opportunities for rational enzyme design. In experimental approaches, enzyme structures are commonly solved by X-ray crystallography, nuclear magnetic resonance (NMR) spectroscopy, or cryo-electron microscopy (cryo-EM).[92–95] In contrast, AlphaFold2 can predict the enzyme's structure with atomic accuracy and within hours. The prediction is solely based on the amino acid sequence of the target protein.[96] Furthermore, computational methods and tools such as Rosetta which uses the atomic representation of protein structures and energy functions as models or molecular dynamics can be used to understand the structure-function relationship of enzymes.[97]

Directed evolution and rational design methods, can also be employed together in a combined approach called semi-rational enzyme design. Here, the creation of small and smart libraries is of the essence. The reduced libraries allow for less screening effort and at the same time might overcome potentially false predictions from rational approaches. Site-saturation mutagenesis is often applied in semi-rational enzyme design, exchanging one amino acid of a predicted hotspot with all possible mutations at this position. Hence, the choice of the mutated position remains rational whereas the amino acid exchange becomes random as in the directed evolution approach.[98]

1.6. Degradation of Polyvinyl Alcohol

PVA is a water-soluble synthetic vinyl polymer consisting of a carbon-carbon backbone with repeating 1,3-diol groups. Due to its versatile properties such as tensile strength, flexibility, and thermostability, PVA is used in many industrial applications e.g., fabric and paper sizing, fiber coating, films for packaging, and many more.[99] Its water solubility made the polymer furthermore an easy solution for water-dissolvable laundry and dishwasher detergent packaging. The polymer's low cytotoxicity[100] and the alleged biodegradability make the material also a widespread choice in biomedical[101] and biomaterial[102] research fields. In biomedical applications, PVA is used to form hydrogels by crosslinking the polymer chemically (e.g., boric acid or sulfosuccinic acid), physically (e.g. freeze-thaw cycles), or through radiation treatment.[103-105] The hydrogels can subsequently be used for vascular grafts, wound dressings, drug delivery, and many more.[101,106,107] Furthermore, PVA is deployed for immobilization e.g., as a carrier for enzymes or microbes.[108,109]

The vinyl polymer is considered biodegradable and thus, a more sustainable alternative in comparison to other plastics. However, the requirements for microbial decomposition are highly specific and microorganisms for PVA degradation are not omnipresent.[99] Additionally, PVA is released in large quantities into the environment, making the polymer a major pollutant.[110] A recent study by Rolsky and Kelkar revealed that over 70 % of PVA used as packaging for laundry and dish detergent pods ends up in the environment.[110] The presence of the polymer in the environment, even though solubilized in water, can be tremendous due to the potential of mobilizing heavy metals and other hydrophilic contaminants.[10,111,112] Furthermore, the polymer forms a foam that inhibits oxygen from being recovered in water and therefore, threatens marine life.[38]

The printing and dyeing industries in particular are major PVA emitters. As a sizing agent, PVA is applied to act as a protective layer on the final product. Treatment of PVA wastewater with chemical or physical methods such as adsorption, filtration, ultrasonic degradation, and Fenton’s reaction are cost intensive, less efficient, and can cause secondary pollution.[113] Therefore, alternative and more sustainable approaches (e.g., with microorganisms or enzymes) are required for the remediation of wastewater contaminated by PVA.[99] Additionally, in comparison to conventional desizing methods, enzymatic PVA degradation can be carried out under mild conditions.[114] Enzymes themselves are non-toxic, environmentally friendly, and have been used successfully in a variety of industrial processes for many years.

1.6.1. Microbial Degradation of Polyvinyl Alcohol

Microbial degradation of PVA was already described for bacterial strains such as *Pseudomonas putida* and *Spingomonas* sp. SA3 and SA2.[115,116] The degradability of PVA is thereby dependent on factors such as the degree of polymerization, the tacticity of the main chain, and the degree of saponification.[38] The latter results from the process of manufacturing PVA which involves the hydrolysis of polyvinyl acetate. PVA can either be fully hydrolyzed with solely the 1,3-diol groups remaining on the C-C-backbone or it can be partially hydrolyzed, with individual acetate groups remaining in the polymer (**Figure 4**).[99] However, the acetylated PVA causes complications for the degradation of PVA since the microorganism also needs to express an enzyme for hydrolysis of the acetate group.

Shimao et. al.[116] and Sakazawa et. al.[115] already reported in the 1980s that the strain *Pseudomonas sp.* VM15C depends on a growth stimulant for effective PVA degradation. The unique stimulant was produced by another strain *Pseudomonas putida* VM15A in a symbiotic manner and was identified as PQQ.

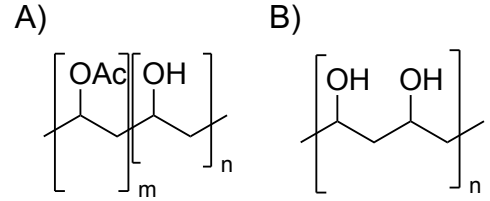

Figure 4: Different structures of PVA resulting from the manufacturing process of PVA. PVA is yielded from either **A)** partially hydrolyzed or **B)** fully hydrolyzed polyvinyl acetate. In partially hydrolyzed PVA irregular repetitions of hydroxyl groups and acetate groups occur whereas fully hydrolyzed PVA solely consists of the repetition of 1,3-diols on the C-C-backbone.

Kim et. al.[117] observed the same symbiotic behavior for the strains *Sphingomonas sp.* SA3 and SA2 with *Sphingomonas sp.* SA2 being the PQQ-producing strain.

However, PQQ-independent strains for PVA degradation were reported as well. *Pseudomonas vesicularis* var. *povalolyticus* PH can degrade PVA independently of PQQ but relies on thiamin as a growth factor as well as the amino acids tyrosine or phenylalanine, isoleucine and cystine for PVA degradation.[118] Recently, Wu et. al. published the degradation of simulated PVA wastewater by mixed PVA-degrading bacterial strains using 1 g/L of the substrate.[119] Higher concentration of substrate, however, led to a decrease of degradation by the mixed bacteria. The authors claim that PVA was degraded into ketones, fatty acids, and alcohols which were then further processed by microbes into carbon dioxide, hydrogen, and methane.[119] These findings are in accordance with the observations from many other studies that led to the proposal of

microbial degradation of fully hydrolyzed PVA (**Figure 4 B**) by bacteria as a two-step process (**Figure 5**), i) the oxidation of one or two adjacent hydroxyl groups and ii) the subsequent cleavage of the resulting mono- or di-ketone structure. Step one is carried out by PVA oxidases or PQQ-dependent PVA dehydrogenases (PVA-DH) while an aldolase or a β-diketone hydrolase (BDH) catalyzes the second step.[113,119–121]

Kawai and Hu[113] hypothesized that the polymer is cleaved extracellularly by PVA oxidases which results in fragments small enough to enter the periplasmic space. They based their suggestion on two observations: I) PVA oxidases were found extracellularly whereas PVA-DHs were discovered membrane-bound or periplasmatic[122] and II) oxidized PVA can be hydrolyzed by enzymes[123] but can also undergo spontaneous oxidation[121]. In the periplasm, the smaller PVA fragments are further oxidized by the PQQ-dependent PVA-DH. Aldolases or diketone hydrolases subsequently degrade the PVA further until it can be taken up by the organism through the inner membrane.[113] However, some organisms express only PVA-DH and no PVA oxidases, which suggests that extracellular PVA degradation plays a secondary role.[113]

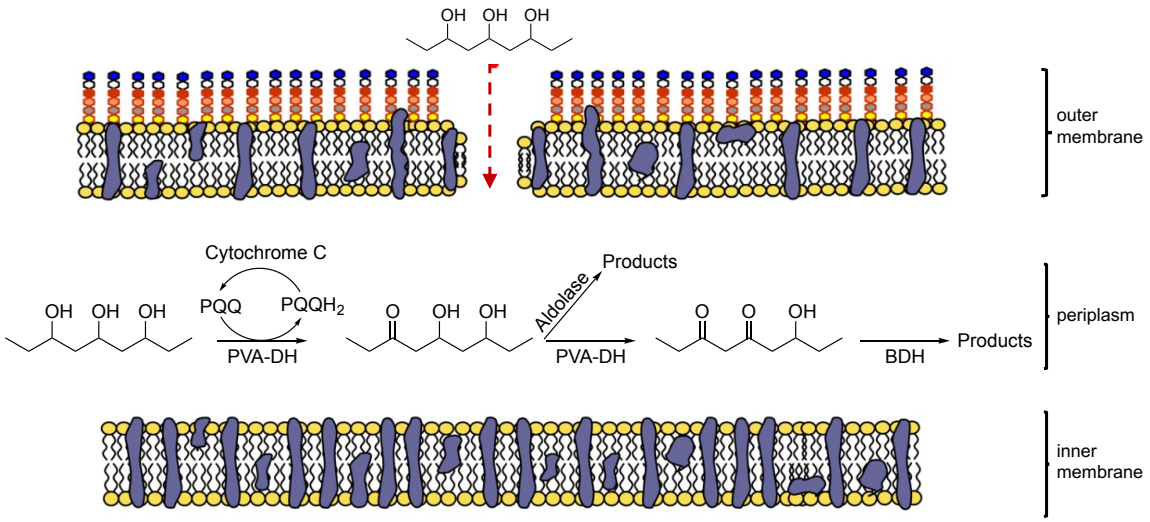

Figure 5: Proposed microbial degradation of PVA in the periplasm. After entering the bacterial periplasm through the outer membrane, PVA is firstly oxidized by the PQQ-dependent PVA-DH. Depending on the second step, oxidation needs to occur either on one or two adjacent hydroxyl groups. The ketone is subsequently cleaved by an aldolase whereas the di-ketone is cleaved by a BDH. The Figure was adapted and modified from Kawai and Hu.[113]

In summary, the current literature suggests that microbial degradation of PVA relies on highly specific organisms, growth factors, cofactors, and environmental conditions.[115–117,119] Taken together with the vast amounts of PVA being released by the industry and from packaging, complete biodegradation of PVA is highly unlikely.

1.6.2. Enzymatic Degradation of Polyvinyl Alcohol

Although the microbial mechanism for PVA degradation has been known for a long time and some enzymes involved in PVA degradation were purified and characterized[124-127], research has been scarce on the degradation of PVA with free enzymes. More recently, the crystal structure (PDB ID: 3WL6) of a hydrolase from *Sphingopyxis* sp. 113P3 and *Pseudomonas* sp. VM15C utilizing oxidized PVA was elucidated and the first enzyme engineering approaches were implemented.[124] Further investigations of the PVA-DH from *Sphingopyxis* sp. 113P3, the enzyme carrying out the first step of PVA degradation according to the proposed mechanism of Kawai et. al. (**Figure 5**), have failed because the recombinantly expressed enzyme formed largely insoluble inclusion bodies.[128] Wei et. al. investigated *Stenotrophomonas rhizophila* QL-P4 and were able to efficiently express a novel PQQ-independent PVA oxidase.[125] Nonetheless, current literature suggests that PQQ-dependent enzymes are needed for the complete degradation of PVA. Since PQQ is an expensive cofactor, this method is unattractive for industrial purposes.

2. Results & Discussion

2.1. Mechanism and Structural Insights into PET Degrading Enzymes

PET is one of the most investigated plastics when it comes to enzymatic degradation. In its heteroatomic backbone, the building blocks TPA and EG are connected by ester bond linkages making the polymer a suitable substrate for hydrolases. However, only a few hydrolases have been subject to a thorough characterization, and subsequent enzyme engineering. The degradation performances of PET hydrolases are still partly limited due to low thermostability, unbalanced enzyme-substrate interaction, low catalytic efficiency, and product inhibition. The following articles (**Article I** and **II**) provide an overview of the current benchmark PET hydrolases, their limitations, and the research of the scientific community on overcoming them.

Furthermore, we elucidated the crystal structure and the degradation mechanism of TfCa, a PET hydrolase helper enzyme. Using semi-rational enzyme design, we improved the activity of the enzyme and employed both, the wildtype and the improved variant, in a dual enzyme system for enhanced PET degradation.

2.1.1. Mechanism-Based Design of Efficient PET Hydrolases (Article I)

In a Perspective article, **Article I**, we analyzed the limitations of benchmark PET hydrolases for efficient industrial applications of enzymatic PET degradation. More precisely, we discussed the engineering of PET hydrolases towards higher thermostability as well as the de/adsorption properties of the enzymes and the release of product inhibition.

After Müller et. al. discovered *Tf*H, the first enzyme capable of hydrolyzing amorphous PET[39], scientific attention was soon drawn towards the material properties of PET including the glass transition temperature T_g and its importance for the enzymatic degradation of the polyester.[52,129] It was found that for efficient enzymatic PET hydrolysis, the amorphous regions of the polymer need to transition from hard and brittle to a rubbery state.[57,130] The T_g of PET is in the range of 65-71 °C but can be influenced by experimental factors.[58–60] For instance water, a reactant, and solvent in enzymatic PET degradation has a plasticization effect on the polyester and can decrease its T_g by up to 16 °C.[58,131,132] Additionally, Shinotsuka et. al. observed for PET films with different thicknesses that the T_g on the surface up to about 13 nm depth is significantly lower (approx. 48.1 °C).[133] Both effects taken together explain the comparably fast degradation of amorphous PET by

mesophilic enzymes such as *Is*PETase.[29] However, many studies showed that thermophilic and thermostable enzymes are more capable biocatalysts in comparison to mesophilic enzymes.[47,52,134] Hence, enzyme engineering as well as process optimization were carried out to enhance the degradation performance (**Figure 6 A**). For instance, the optimal temperature of some bacterial PET hydrolases was increased by up to 10 °C in the presence of bivalent ions like Ca^{2+} or Mg^{2+}.[135,136] However, since Ca^{2+} reacts with terephthalate, one of the aromatic products from PET degradation, and forms insoluble byproducts, the Ca^{2+} binding site was substituted by a salt bridge or a putative disulfide bridge.[35,47,137–140] Furthermore, varying the expression host resulted in an increased thermostability. For LCC the melting temperature (T_m) was increased by >4 °C or >12 °C, respectively, when it was expressed in *Bacillus subtilis* or *Pichia pastoris* (*P. pastoris*) in comparison to *Escherichia coli* (*E. coli*). In *P. pastoris* the large increase in T_m is due to glycosylation of the protein.[141,142]

Protein engineering was performed for many PET hydrolases, increasing their T_m by stabilizing the enzyme. Over years of research, the T_m of an *Is*PETase variant (HotPETase) was increased by 42.5 °C in comparison to the wildtype enzyme.[9] The BhrPETase, expressed in *B. subtilis* even reached a T_m of 101 °C.[142] However, increasing the reaction temperature for enzymatic PET degradation from 65 to over 75 °C causes the polymer microstructure to transform from a less-ordered amorphous state to a nondegradable crystalline state.[35] Furthermore, at higher T_m the enzymatic degradation reaction has to compete against the physical aging of the polymer with increasing reaction temperature.[143] Hence, a higher T_m of enzymes is not always desirable.

Additionally, the stabilization of the enzyme and the subsequent thermostability often come with lower flexibility of catalytic regions and thus possibly impede the activity of the enzyme. Focusing on a thermo-active approach in protein engineering for an optimal reaction temperature of around 75 °C is therefore indispensable. **Figure 6 A** shows the progress made by enzyme and process engineering in the enhancement of the optimal temperature for benchmark PET hydrolases as well as their degradation performance.

In the Perspective article, we furthermore discussed the understanding of interfacial enzymatic PET hydrolysis from a structure-function perspective. Water, which acts as both the solvent and reactant, as well as the enzyme itself can only interact with the surface of the PET polymer. This limits accessible ester bonds and thus implies that the reaction occurs under enzyme-excess conditions.[144] PET degradation kinetics are therefore commonly calculated with the inverse Michaelis-Menten equation or the derivation of the Langmuir adsorption isotherm.[33,52,145–150] The binding of PET hydrolases to the surface of

PET was investigated using biophysical methods such as quartz crystal microbalance[67,151,152], chemiluminescence[67], and fluorescence[69].

In nature, the binding of enzymes to polymers is promoted by binding modules. In PET hydrolysis binding modules such as the cellulose-binding domains (CBM) CenA from *Cellulomonas fimi*[66] and cellobiohydrolase I from *Trichoderma reesei*[67,153] were fused to PET hydrolases which increased the degradation performance of the enzyme. The binding modules can be further optimized for PET binding. CBM's tryptophan residues were found to be mutational hotspots. Protein engineering of these hot spots resulted in an enhanced hydrogen bond formation with the PET substrate.[66,68] Furthermore, binding of PET hydrolases to the substrate surface was shown to be improved by hydrophobins[154-156], lytic polysaccharide monooxygenase (LPMO) derived from the white-rot fungus *Pycnoporus coccineus*[157] and a zwitterionic polymer (EKylation)[158]. Hydrophobins are produced by filamentous fungi.[159] They are small amphiphilic proteins with a surfactant-like activity that can enhance the binding affinity of PET hydrolases to their substrate when applied as free molecules or pre-treatment for the degradation reaction. However, the hydrophobins were most effective when directly fused to the PET hydrolase.[154–156]

So far, only a few co-crystallized PETase hydrolase structures were published in complex with a monomer which is why most investigations regarding enzyme-substrate interactions were performed using molecular docking.[35,43,160–163] For bacterial PET hydrolases, the surface landscape in close vicinity to the active site is comparable. The favored angle of the substrate requires a high conformational selectivity.[43,162,164] The highest activation free energy barrier for the catalytic reaction was determined using quantum mechanics/molecular mechanics (QM/MM) adiabatic mapping which suggested the nucleophilic attack as the rate-limiting step.[165,166] **Chapter 1.4** describes the catalytic mechanism of hydrolases in detail. **Figure 6 B** depicts the schematical hydrolysis reaction with the activation free energy barriers for each step. The well-conserved residue W185 was found in *Is*PETase and many other PET hydrolases and is thought to be part of a dynamic catalytic site with aromatic subsites that are locally stabilized upon substrate binding.[43,44,160,167] Substitution of this residue decreased the activity of the biocatalyst drastically.[44,167] The steric hindrance of W185 within the active site is uniquely reduced in *Is*PETase due to two residues (S214 and I218) which allow higher flexibility of the indole side chain and thus a higher hydrolysis rate.[168] Further enhancement of the enzymatic activity of PET hydrolases was approached by widening the substrate binding pocket.[150,169] Since the free energy barrier and hydrolytic reaction thermodynamics are similar in both the thermophilic LCC^{ICCG} and the mesophilic *Is*PETase[165], we concluded that the increase in activity is mostly due to better accessibility of the PET at elevated temperatures rather

than to the fundamental interaction affinity. In further studies, it was also observed that an enzyme variant with a narrower substrate binding pocket in comparison to the wildtype enzyme can still exhibit increased activity.[35,160,170] These findings suggest that polymer binding is a dynamic rather than static process.[171,172] Thus, to gain a better understanding of the rate-limiting interactions of PET hydrolases it could be beneficial to systematically engineer all variable amino acids in the substrate binding pocket.

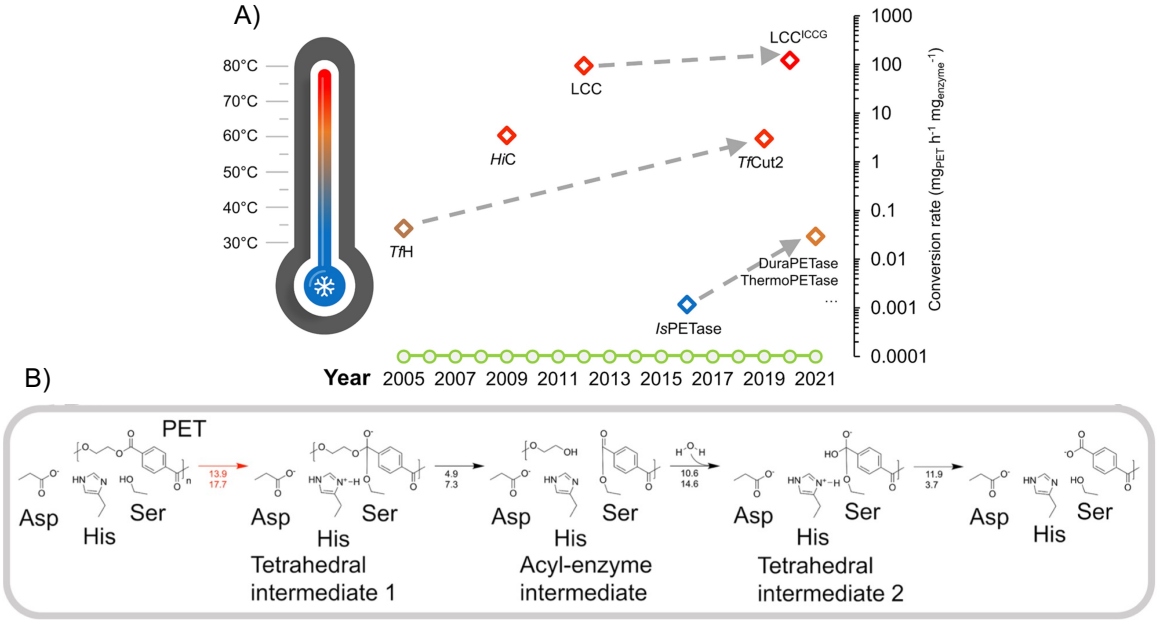

Figure 6: Identification and improvement of selected PET hydrolases over a course of 16 years and their reaction mechanism. A The normalized maximal conversion rates of *Is*PETase, *Tf*H, *Hi*C, and LCC as well as their mutants were calculated based on various publications[29,35,47,49,52,63,143,173–175] and plotted on a logarithmic scale. The optimal temperature of each enzyme is shown in varying colors. The improvement of the degradation performance (dashed arrows) was gained by either enzyme or process engineering. **B** The hydrolysis reaction mechanism of PET hydrolases starts with the nucleophilic attack of the substrate by the catalytic serine. The tetrahedral intermediate one which is formed during this step is stabilized by the catalytic residues histidine and glutamate or aspartate as well as the oxyanion hole. Upon the collapse of intermediate one into an acyl-enzyme and an alcohol, the catalytic aspartate or glutamate as well as the histidine activate a water molecule that attacks the acyl-enzyme's carbonyl and thus forms a second tetrahedral intermediate. The subsequent diacylation of the second intermediate releases a carboxylic acid. The activation free energy barriers of each step are indicated in kcal/mol with the rate-limiting step marked in red. Values are summarized from different studies calculating the Boltzmann-weighted average from 20 QM/MM MD simulations (top number) or derived from adiabatic mapping studies (bottom number).[165,166] The figure was adapted and modified from Wei et. al.[176]

However, varying experimental conditions such as pH, buffer, agitation speed and substrate material properties which have a major impact on the outcome of the enzymatic degradation performance are making it difficult to compare different studies, even when the same hydrolyzing enzyme was used.[177–179] Additionally, under laboratory conditions post-consumer low-crystallinity PET packaging is often used as a substrate in various forms such as powder, foil, sheet, and others.[180,181] In relevant industrial applications,

however, the substrate contains all crystallinity patterns. Furthermore, contaminants in the substrate impeding the enzymatic degradation have to be removed which is typically done by a washing step prior to thermomechanical processing followed by amorphization and micronization.[35,182,183] Using such pre-treated PET in laboratory research would thus result in more reliable and comparable data for industrial applications.

2.1.2. Structural Insights into (Tere)phthalate-ester Hydrolysis by a Carboxylesterase and its Role in Promoting PET Depolymerization (Article II)

As mentioned in **Chapters 1.4.1.** and **2.1.1.**, one of the restrictions in enzymatic PET degradation is the product inhibition of selected PET hydrolases by the degradation intermediates MHET and BHET.[34,71,72] Helper enzymes for PET hydrolases can be used to overcome this inhibition and thus expedite and improve the degradation performance as described in detail in **Chapter 1.4.2**. In **Article II** we elucidated the apo-structure of TfCa, a carboxylesterase from *T. fusca*. Additionally, we elucidated the crystal structure of TfCa in complex with PET monomers and a monomer analog and investigated the structure-function relationship between the enzyme and various *ortho*- and *para*-phthalate esters. Further, we conducted enzyme engineering in a semi-rational approach, resulting in a TfCa variant with 3.3-fold enhanced activity. Both the wildtype and the variant of TfCa were introduced to a dual enzyme system with a recently published *Is*PETase variant.[47]

The carboxylesterase TfCa has been subject to research in PET degradation for over ten years.[75,76,184] However, the crystal structure of the enzyme was never solved, making rational enzyme engineering of the hydrolase rely on homology models only. In this work, we elucidated the apo-structure of TfCa (PDB-ID: 7W1K, 1.40 Å) in collaboration with the groups of Prof. Dr. Weidong Liu at the Tianjin Institute of Industrial Biotechnology and the University of Chinese Academy of Sciences in Beijing, Prof. Dr. Manfred Weiss at the Helmholtz-Zentrum Berlin für Materialien und Energie GmbH, and Prof. Dr. Lammers at the Institute of Biochemistry. The apo-structure of TfCa folds has a canonical α/β-hydrolase with a central antiparallel β-sheet surrounded by α-helices, a lid domain A, and a lid domain B (**Figure 7 A**). The strictly conserved catalytic triad consists of S185, E319, and H415. The ligand-soaked structures of TfCa with BHET (PDB-ID: 7W1L, 2.43 Å), MHET and BHET (PDB-ID: 7W1I, 1.67 Å) as well as MHETA (PDB-ID: 7W1J, 1.92 Å), a substrate analog for MHET, which were elucidated in the same collaboration, revealed a deep active site cleft containing the hydrophobic residues L282, L322, and V376. When the ligand-soaked structure of TfCa with MHETA is compared to the ligand-soaked structure of MHETase with MHETA (**Figure 7**), three hydrogen bonds (H-bonds) form with

the amide bond and the neighboring hydroxyl end of the substrate (**Figure 7 B**), whereas five H-bonds form with both ends of the ligand in MHETase (**Figure 7 D**).

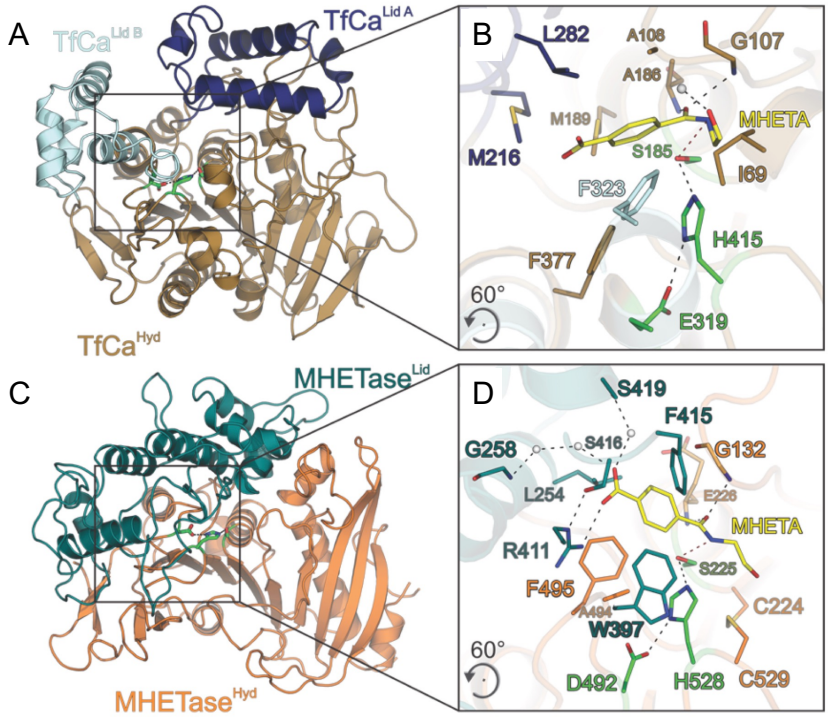

Figure 7: Comparison of ligand-free and ligand-soaked structures of TfCa from *T. fusca* and MHETase from *I. sakaiensis*. A Elucidation of the crystal structure of TfCa revealed three subdomains: a hydrolase domain ($TfCa^{Hyd}$, brown), a lid domain A ($TfCa^{LidA}$, dark blue), and a lid domain B ($TfCa^{LidB}$, cyan). In **B** the active site of TfCa with bound MHETA (yellow) is shown (PDB-ID: 7W1J, 1.92 Å). Residues from different domains are depicted in brown ($TfCa^{Hyd}$), dark blue ($TfCa^{LidA}$), and cyan ($TfCa^{LidB}$). **C** The MHETase structure from *I. sakaiensis* contains two domains: the hydrolase domain ($MHETase^{Hyd}$, orange) and the lid domain ($MHETase^{Lid}$, dark aquamarine) (PDB-ID: 6QGA).[72] In **D** the view of the active site of TfCa with bound MHETA in yellow is shown. Dark aquamarine ($MHETase^{Hyd}$) and orange ($MHETase^{Hyd}$) represent residues from various domains ($MHETase^{Lid}$). H-bond formation is indicated by dashed lines, and molecules and interacting residues are colored according to the kind of atom: oxygen is red, nitrogen is blue, and carbon is a variety of colors. Green sticks represent the catalytic triad residues. This figure was adapted from von Haugwitz et. al. 2022.[185]

Using terephthalate-based oligo-esters of various lengths we determined the substrate profile of TfCa and suggested a degradation pathway for the longest substrate bis[2-(benzoyloxy)ethyl] terephthalate (3PET) which we determined from the high-performance liquid chromatography (HPLC)-derived product profile. Furthermore, we estimated the specific activity of TfCa for the various substrates (**Figure 8 A**). The highest specific activity of TfCa was calculated for the first hydrolytic step from BHET to MHET and EG. The second hydrolytic step of BHET (MHET into TPA and EG), however, is approximately 500 times slower compared to the first one. Interestingly, the specific activity of TfCa for the *ortho*-phthalate ester diethyl phthalate (DEP) is three times lower in comparison to BHET and only one hydrolysis step occurs, leaving monoethyl phthalate (MEP) as the product. Phthalic acid (PA), the product of the second hydrolysis step for DEP was not observed in

the reactions suggesting that MEP is a less preferred substrate for TfCa. Molecular docking revealed that MEP binds unproductively to the active site of TfCa (**Figure 8 B**). Overall, the estimated specific activities suggest diesters as the preferred substrates of the carboxylesterase.

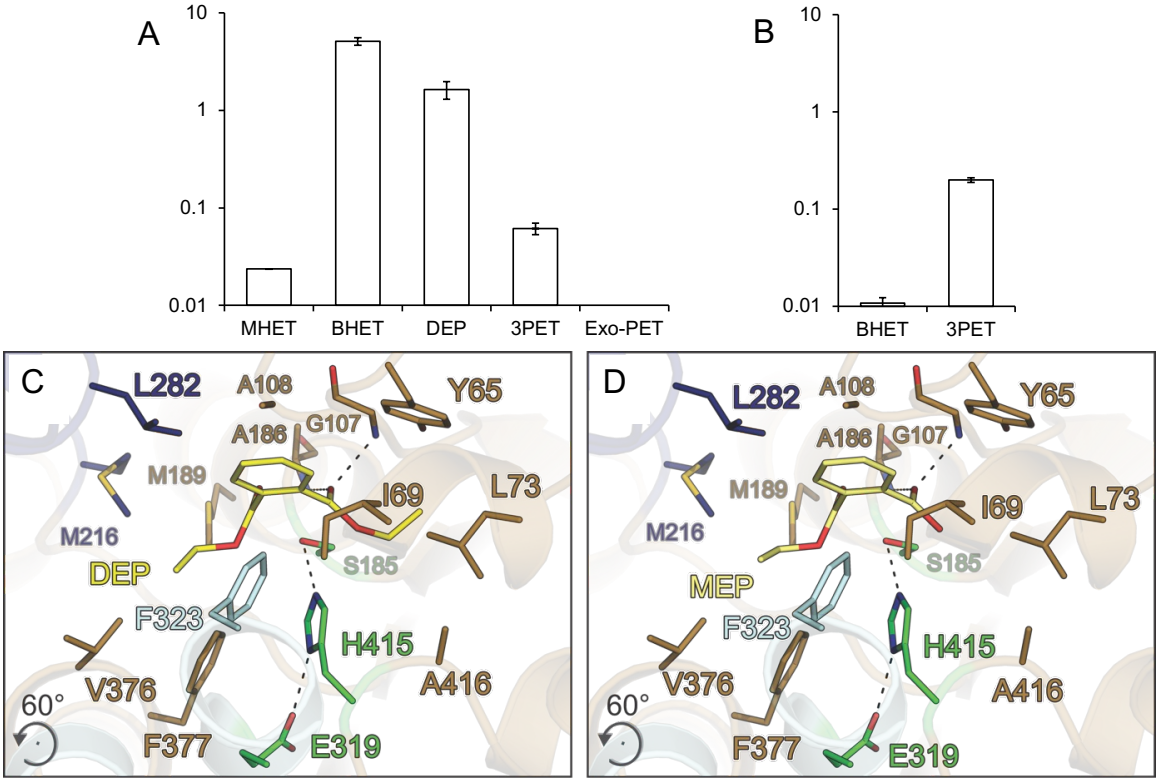

Figure 8: Estimated specific activity of TfCa for terephthalate-based oligo-esters of various lengths and molecular docking results for TfCa with DEP and MEP. The specific activity for TfCa with the indicated substrates was calculated and is shown on a logarithmic scale. **A** shows the specific activity for the first hydrolysis of the respective substrate and **B** the specific activity of the second hydrolysis step which only occurs for the substrates BHET and 3PET. Error bars indicate the standard deviations calculated from at least three replicates. **C+D** show molecular docking results for TfCa with DEP (**C**) and MEP (**D**). One of the esters in DEP is in close proximity to the catalytic S185 and allows the cleavage into EG and MEP. The most favorable docking pose of MEP reveals that its only hydrolyzable ester bond is positioned too far from the oxyanion hole and the catalytic triad. Thus, MEP binds unproductively to the active site of TfCa. Residues from different enzyme domains are shown in brown ($TfCa^{Hyd}$), dark blue ($TfCa^{LidA}$), and cyan ($TfCa^{LidB}$). Ligands are shown as yellow sticks and the catalytic triad as green sticks. This figure was adapted and modified from von Haugwitz et. al. 2022.[185]

Based on the elucidated structures of TfCa, semi-rational enzyme engineering was performed within the substrate binding pocket of TfCa. Amino acid residues within 5 Å of the soaked ligands were mutated to alanine (alanine scan) except alanine, glycine, proline residues, the catalytic triad, and the highly conserved GxSxG motif. Two variants exceeded the activity of the wildtype enzyme by over 1.2-fold while the mutation I69A resulted in a loss of function for the enzyme. Thereafter, site-saturation mutagenesis was performed with residue 69 and the variant $TfCa^{I69W}$ was found to be over 2-fold more active in comparison to the wildtype enzyme. The three more active mutants were subsequently

combined in double and triple mutants leading to the most active mutant TfCa$^{I69W/V376A}$ with a 3.3-fold increased activity which was titled TfCa WA and characterized regarding its optimal temperature and its activity in BHET and MHET hydrolysis. Furthermore, both, the wildtype of TfCa and the variant with increased activity were subjected to a dual enzyme system for PET degradation using the recently published *Is*PETase$^{S121E/D186H/R280A/N233C/S282C}$ (*Is*PETase PM)[47] as the polymer degrading enzyme. Using different PET substrates (PET nanoparticles, PET powder, or PET film) we could show that the main product of *Is*PETase PM is MHET, independently of the substrate used. Adding either TfCa wildtype (TfCa wt) or TfCa WA to the reaction mixture resulted in TPA as the sole degradation product. With the substrates PET powder and PET film as well as with higher amounts of PET nanoparticles, the dual enzyme system generated an overall increased product yield. The best results with the dual enzyme system were gained using the variant TfCa WA for the hydrolysis of the intermediate products BHET and MHET. TPA yields were thus increased up to 14-fold in comparison to reactions containing solely *Is*PETase PM.

2.2. Synthesis of Modified Polyvinyl Alcohols and their Degradation Using an Enzymatic Cascade (Article III)

Compared to the heteroatomic polyester PET, polymers with a homoatomic backbone such as PVA raise another challenge for degradation by microbes and enzymes as specified in **Chapter 1.2**. PVA is a synthetic but water-soluble vinyl polymer containing a carbon-carbon backbone and repeating 1,3-diols. Despite its classification as biodegradable by microorganisms, the vast amount of PVA released into the environment causes pollution. Microbial degradation of PVA is slow and often relies on the expensive cofactor PQQ which makes it an inefficient process for the industry. In **Article III** we present a modified PVA with derivatized side chains that results in better properties for biodegradation. This section presents an enzymatic cascade, consisting of three enzymes that can degrade the modified PVA in four steps and the unmodified PVA in three steps in a one-pot reaction.

In collaboration with the group of Dr. Marcus Baumann from the School of Chemistry at the University College Dublin (Ireland), we used a simple ester-forming reaction introducing succinate groups to the hydroxyl groups of the polymer to alter the properties of PVA towards better biodegradability. Succinic anhydrate (SA) was chosen because of its renewable, non-toxic, and inexpensive characteristics. Different amounts of SA (2, 4, and 6 g per 30 g PVA) were explored and will be referred to as PVA-2 (2 g SA), PVA-4

(4 g SA), and PVA-6 (6 g SA). External testing revealed that critical metrics such as tensile strength and puncture can be efficiently altered in response to the amount of the utilized succinic anhydride. All modified PVA materials retained water solubility.

Furthermore, we developed an enzymatic cascade that can degrade the derivatized and unmodified PVA in a one-pot reaction (**Figure 9**). All steps are carried out by well-characterized enzymes[186,187] which are either easily expressible in *E. coli* or commercially available. In the first step, the ester-bound modifications (acetylation and succinylation) are hydrolyzed by the commercially available and immobilized lipase originating from *Thermomyces lanuginosus* (TL-IM) which utilizes water for the reaction. The resulting unmodified PVA with 1,3-repeating diols can be oxidized to ketones by an alcohol dehydrogenase from *Lactobacillus kefir* (LK-ADH) in step 2 using nicotinamide adenine dinucleotide phosphate ($NADP^+$) as the cofactor and converting it into NADPH. NADPH is used in the next reaction step by cyclohexanone monooxygenase (CHMO) variant M15, originating from *Acinetobacter calcoaceticus*. CHMO M15 belongs to the class of BVMOs which catalyze the insertion of an oxygen atom between C-C bonds in ketones and aldehydes and thus introduces an ester bond into the polymer. The cofactor NADPH is converted into $NADP^+$ by CHMO M15 which, in theory, results in an advantageous cofactor recycling within the enzymatic cascade. In the last step of the reaction, the ester bond is hydrolyzed by TL-IM which produces smaller PVA fragments.

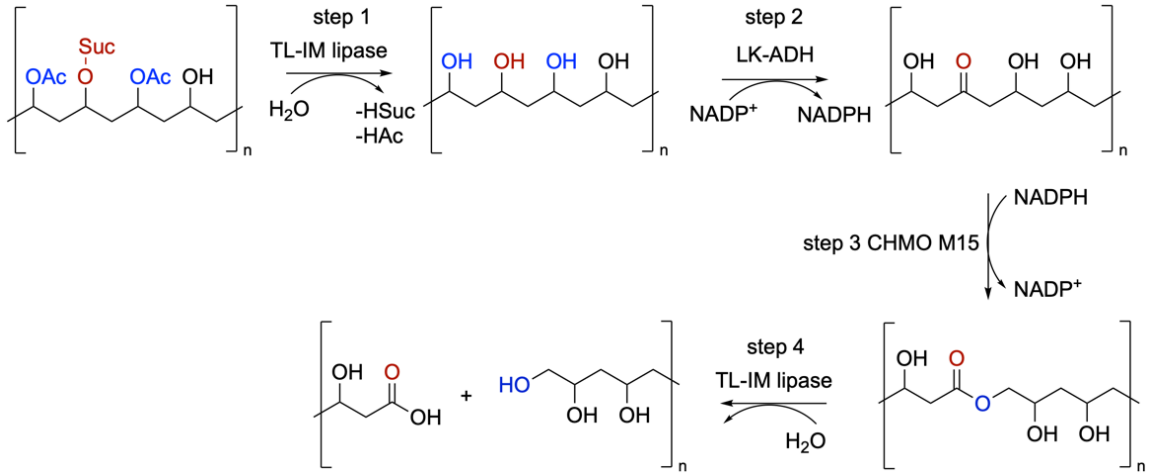

Figure 9: Reaction scheme of the proposed enzymatic cascade for the degradation of PVA. The ester bonds of PVA modifications, namely acetylation and succinylation, are cleaved by the lipase TL-IM. The enzymatic reaction utilizes water and results in unmodified PVA. Next, LK-ADH oxidizes one or more of the 1,3 repeating hydroxyl groups on PVA into ketones using $NADP^+$ as a cofactor. During the reaction, LK-ADH converts $NADP^+$ into NADPH. The BVMO CHMO M15 implements an ester bond while utilizing NADPH and converting it into $NADP^+$. Finally, in step 4 the newly introduced ester bond is cleaved by the same lipase that performed step 1 resulting in a carboxylic acid and an alcohol. This figure was adapted from von Haugwitz et. al. 2022.[188]

The reaction of the enzyme cascade was investigated using the Finley method. Finley reported that PVA forms a green complex with iodide in the presence of boric acid[189] which can be spectrophotometrically detected at 500 nm. The degradation of film PVA-4 was investigated regarding the effects of reaction temperature, buffer pH, initial $NADP^+$ amount, enzyme stability, and LK-ADH to CHMO ratio (**Figure 10**).

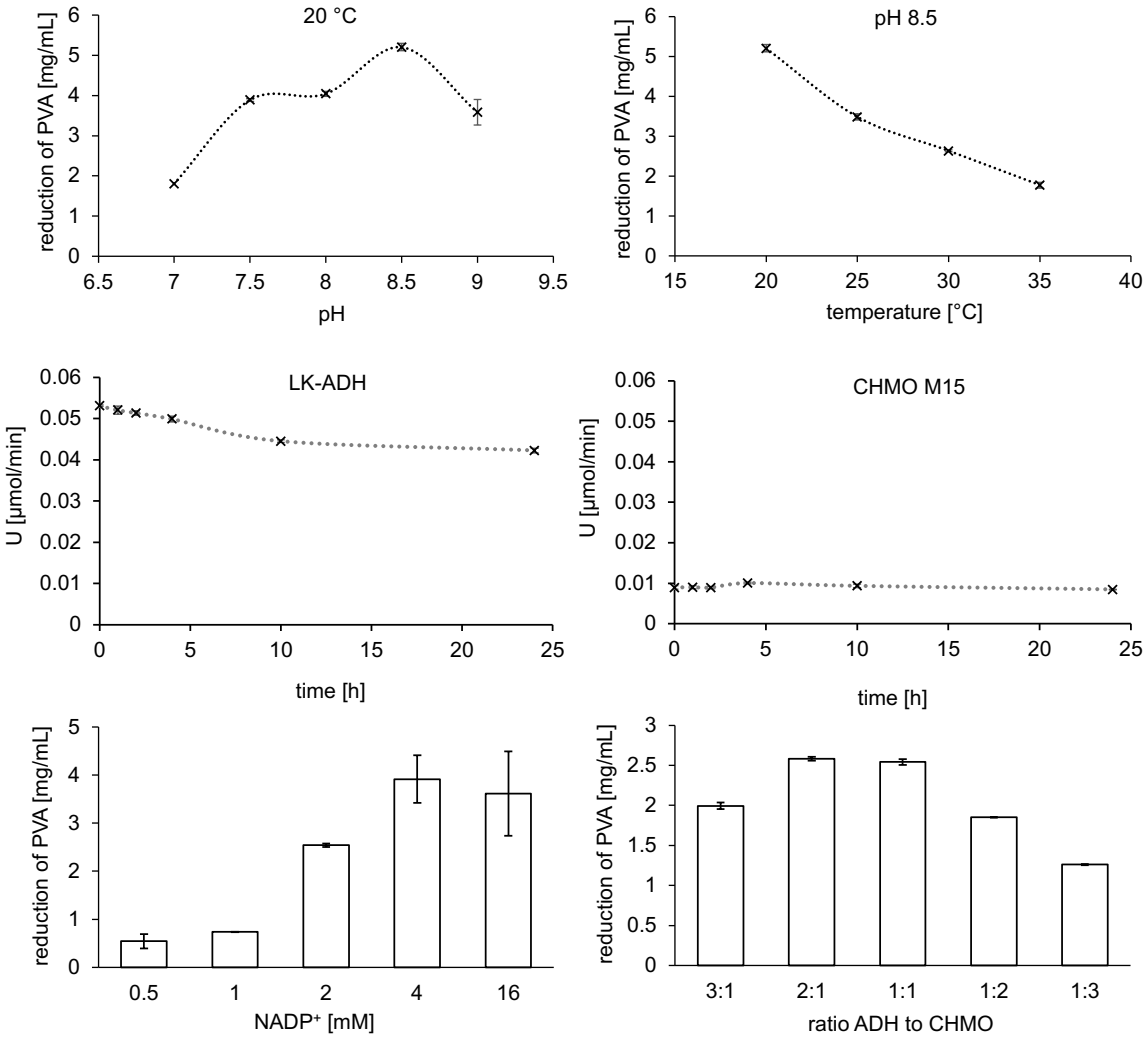

Figure 10: Analyzing the impact of different reaction conditions on PVA-4 degradation. The degradation of PVA-4 was investigated regarding temperature, pH, reaction time, amount of cofactor, and ADH to CHMO ratio. pH 8.5, 20 °C, 4 mM of $NADP^+$, and a ratio of 1:1 or 2:1 of ADH to CHMO were shown to be the ideal reaction conditions in the range tested. Using the model substrates (*R*)-1-phenyl ethanol (LK-ADH) and cyclohexanone (CHMO M15), the stability of the indicated enzymes was investigated over 24 h by following NADP/H decrease or increase. One unit was defined as the amount of substrate converted by 1 µL enzyme lysate per minute. Error bars originate from the standard deviation of at least three replicates. This figure was adapted and modified from von Haugwitz et. al. 2022.[188]

Firstly, we investigated the optimal temperature for single enzymes by incubating them for one hour at a temperature range of 4 to 50 °C and subsequently determining the residual activity using model substrates. LK-ADH and CHMO M15 were found to be less stable than TL-IM which is in agreement with the manufacturer's information regarding the

lipase. Step 2 and step 3 of the enzymatic cascade reaction were thus considered the crucial steps of the reaction.

With the Finley method, the optimal settings for the enzymatic cascade were found to be pH 8.5, 20 °C, and 4 mM $NADP^+$ out of the range of parameters evaluated. The optimal enzyme ratio of LK-ADH to CHMO M15 is important for sufficient cofactor recycling. The ratios 2:1 and 1:1 were observed with equal efficiency and thus, in the subsequent gel permeation chromatography (GPC) measurements both ratios were further investigated.

GPC measurements were performed with PVA-2, PVA-4, PVA-6, and unmodified PVA using the optimized reaction conditions for PVA-4. The number average molecular weight (M_n), the weight average molecular weight (M_w), and the polydispersity index (PDI) were determined from the GPC measurements. In all measurements taken, the PDI increased when PVA was treated with the enzyme cascade in comparison to untreated PVA. The increase in PDI indicates a broader distribution of molecular weight in the sample and hence, indicates degradation of the PVA film by the enzyme cascade. For PVA-4, independently of the enzyme ratio of ADH to CHMO, M_n decreased by 10 %, confirming the results gained with the Finley method that the enzyme ratio does not significantly impact the reaction. However, it should be noted that the amount of cofactor and the enzyme ratio are most likely interdependent, and the GPC analysis was only performed with 4 mM $NADP^+$.

With film PVA-4, the largest decrease in M_n (10 %) was observed, independently of the LK-ADH to CHMO ratio. However, the largest reduction in M_w was measured for unmodified PVA. When using a 2:1 LK-ADH to CHMO ratio, M_w decreased by 10 % for unmodified PVA and 7 % for PVA-4. In general, the proportional decrease of M_w was lower in comparison to M_n in most cases except for unmodified PVA film. After enzymatic treatment with an enzyme ratio of 2:1, M_w was reduced by 10 % and M_n by 9 %. With an enzyme ratio of 1:1 M_w was reduced by 4 % and M_n by 7 %. These findings indicate that the enzyme ratio of LK-ADH to CHMO M15 has a higher impact on PVA without modification in comparison to modified PVA.

LK-ADH has been shown to accept a wide range of substrates, including those with bulky side chains.[190] Nevertheless, the polymer is likely a difficult substrate for the biocatalyst. An increase in the enzyme's concentration may aid in the degradation of larger molecules. Further increasing the rate of PVA breakdown may be possible by genetically modifying the enzyme LK-ADH to accept larger side chains.

3. Conclusion

Enzymatic PET degradation has evolved impressively in the past 17 years since the first PET hydrolase was discovered. A lot of research was conducted, using protein or process engineering to make enzymatic PET degradation more and increasingly efficient. Many limitations of the natural enzymes such as low stability, low activity, low substrate binding affinity, and product inhibition are already being addressed in multiple studies. These limitations were summarized and discussed in **Article I**, giving an overview of methods employed to overcome these challenges. However, varying experimental conditions have a major impact on the outcome of the enzymatic degradation performance.[177–179] Additionally, in relevant industrial applications the substrate is likely to contain contaminants that can impede the enzymatic degradation and must be removed prior to the reaction. Using such pre-treated PET in laboratory research and comparable reaction conditions would therefore result in more reliable data with industrial relevance. In **Article II** we addressed one of the above-mentioned limitations in PET degradation, substrate inhibition, which was reported for several PET hydrolases. Using the carboxylesterase TfCa we performed a dual enzyme reaction using a recently published variant of *Is*PETase. We elucidated the enzymes' structure and employed enzyme engineering to create a more active mutant. TfCa WA was 3.3-fold more active and increased the TPA yield in the dual enzyme system up to 14-fold with various PET substrates in comparison to solely the PET hydrolase.

In addition to PET, researchers are also interested in degrading other synthetic polymers. Among them is PVA, a polymer that was claimed to be degradable by microorganisms. However, microbial biodegradation occurs at a small scale which is not sufficient for the PVA amounts being released into the environment. In **Article III** we studied PVA degradation using an enzymatic cascade in a one-pot reaction. So far, most enzymes that were characterized and performed PVA degradation are PQQ-dependent. The herein-reported conceptionally new enzymatic cascade is PQQ-independent and contains an advantageous cofactor recycling system. All enzymes used in the cascade are either easily expressible in *E. coli* or commercially available. The cascade can degrade PVA with derivatized side chains in four steps and unmodified PVA in three steps.

In summary, in this work, enzymatic plastic degradation was performed using PET and PVA as the substrates. The structure-function relationship of TfCa was investigated by comparing its hydrolytic activity on various *ortho*-and *para*-phthalate esters of different lengths and the enzymatic activity improved using semi-rational enzyme engineering.

Lastly, an enzymatic cascade was shown to degrade unmodified PVA in a three- and the modified PVA in a four-step reaction.

4. References

1. PlasticEurope-Association of Plastics Manufactures (2021) Plastic- the Facts. Plastic Europe. https://plasticseurope.org/knowledge-hub/plastics-the-facts-2021/. Accessed Oct 25th, 2022.
2. Wang, M.-L., Chang, R.-Y. & Hsu, C.-H. Molding Simulation: Theory and Practice., *Carl Hanser Verlag* (2018).
3. Geyer, R., Jambeck, J. R. & Law, K. L. P *Sci. Adv.* **3**, e1700782 (2017).
4. Verschoor, J.-A., Kusumawardhani, H., Ram, A. F. J. & de Winde, J. H. *Front. Microbiol.* **13**, 821629 (2022).
5. Henry, B., Laitala, K. & Klepp, I. G. *Sci. Total Environ.* **652**, 483–494 (2019).
6. Thushari, G. G. N. & Senevirathna, J. D. M. *Heliyon* **6**, e04709 (2020).
7. Zettler, E. R., Mincer, T. J. & Amaral-Zettler, L. A. *Environ. Sci. Technol.* **47**, 7137–7146 (2013).
8. Amaral-Zettler, L. A., Zettler, E. R. & Mincer, T. J. *Nat. Rev. Microbiol.* **18**, 139–151 (2020).
9. Rochman, C. M., Hoh, E., Kurobe, T. & Teh, S. J. *Sci. Rep.* **3**, 1–7 (2013).
10. Cole, M., Lindeque, P., Halsband, C. & Galloway, T. S. *Mar. Pollut. Bull.* **62**, 2588–2597 (2011).
11. Gola, D. et al. *Environ. Nanotechnol. Monit. Manag.* **16**, 100552 (2021).
12. Lu, Y. et al. *Environ. Sci. Technol.* **50**, 4054–4060 (2016).
13. Rochman, C. M. et al. *Sci. Rep.* **5**, 14340 (2015).
14. Khalid, N., Aqeel, M. & Noman, A. *Environ. Pollut. Barking Essex 1987* **267**, 115653 (2020).
15. Lozano, Y. M. & Rillig, M. C. *Environ. Sci. Technol.* **54**, 6166–6173 (2020).
16. Law, K. L. & Narayan, R. *Nat. Rev. Mater.* **7**, 104–116 (2022).
17. Walker, S. & Rothman, R. *J. Clean. Prod.* **261**, 121158 (2020).
18. Garcia, J. M. & Robertson, M. L. *Science* **358**, 870–872 (2017).
19. Schaerer, L. G. et al. *Trends Biotechnol.* S0167-7799(22)00152-4, (2022).
20. Dogu, O. et al. *Prog. Energy Combust. Sci.* **84**, 100901 (2021).

21. Anuar Sharuddin, S. D., Abnisa, F., Wan Daud, W. M. A. & Aroua, M. K. *Energy Convers. Manag.* **115**, 308–326 (2016).

22. Benyathiar, P., Kumar, P., Carpenter, G., Brace, J. & Mishra, D. K. *Polymers* **14**, 2366 (2022).

23. Vollmer, I. et al. *Angew. Chem., Int. Ed.* **59**, 15402–15423 (2020).

24. Jia, X., Qin, C., Friedberger, T., Guan, Z. & Huang, Z. *Sci. Adv.* **2**, e1501591 (2016).

25. Thiounn, T. & Smith, R. C. *J. Polym. Sci.* **58**, 1347–1364 (2020).

26. Gu, F., Guo, J., Zhang, W., Summers, P. A. & Hall, P. *Sci. Total Environ.* **601–602**, 1192–1207 (2017).

27. Sullivan, K. P. et al. *Science* **378**, 207–211 (2022).

28. Magalhães, R. P., Cunha, J. M. & Sousa, S. F. *Int. J. Mol. Sci.* **22**, 11257 (2021).

29. Yoshida, S. et al. *Science* **351**, 1196–1199 (2016).

30. Blow, D. *Nature* **343**, 694–695 (1990).

31. Ollis, D. L. et al. *Protein Eng.* **5**, 197–211 (1992).

32. Bornscheuer, U. T. *FEMS Microbiol. Rev.* **26**, 73–81 (2002).

33. Wei, R. *et al. Biotechnol. Bioeng.* **113**, 1658–1665 (2016).

34. Barth, M. *et al. Biochem. Eng. J.* **93**, 222–228 (2015).

35. Tournier, V. *et al. Nature* **580**, 216–219 (2020).

36. Wei, R. *et al. Nat. Catal.* **3**, 867–871 (2020).

37. Carniel, A., Waldow, V. de A. & Castro, A. M. de. *Biotechnol. Adv.* **52**, 107811 (2021).

38. Kawai, F., Kawabata, T. & Oda, M. *Appl. Microbiol. Biotechnol.* **103**, 4253–4268 (2019).

39. Müller, R.-J., Schrader, H., Profe, J., Dresler, K. & Deckwer, W.-D. *Macromol. Rapid Commun.* **26**, 1400–1405 (2005).

40. Herrero Acero, E. et al. *Macromolecules* **44**, 4632–4640 (2011).

41. Ribitsch, D. et al. *Biocatal. Biotransformation* **30**, 2–9 (2012).

42. Ribitsch, D. et al. *Polymers* **4**, 617–629 (2012).

43. Joo, S. et al. *Nat. Commun.* **9**, 382 (2018).

44. Han, X. et al. **8**, 2106 (2017).

45. Liu, B. et al. *ChemBioChem* **19**, 1471–1475 (2018).

46. Kan, Y., He, L., Luo, Y. & Bao, R. *ChemBioChem* **22**, 1706–1716 (2021).

47. Brott, S. et al. *Eng. Life Sci.* **n/a**,.

48. Lu, H. et al. *Nature* **604**, 662–667 (2022).

49. Sulaiman, S., You, D.-J., Kanaya, E., Koga, Y. & Kanaya, S. *Biochemistry* **53**, 1858–1869 (2014).

50. Zeng, W. et al. *ACS Catal.* **12**, 3033–3040 (2022).

51. Alisch-Mark, M., Herrmann, A. & Zimmermann, W. *Biotechnol. Lett.* **28**, 681–685 (2006).

52. Ronkvist, Å. M., Xie, W., Lu, W. & Gross, R. A. *Macromolecules* **42**, 5128–5138 (2009).

53. Dimarogona, M. et al. *Biochim. Biophys. Acta* **1850**, 2308–2317 (2015).

54. Fabbri, F., Bertolini, F. A., Guebitz, G. M. & Pellis, A. *Int. J. Mol. Sci.* **22**, 8493 (2021).

55. Carniel, A., Gomes, A. da C., Coelho, M. A. Z. & de Castro, A. M. *Bioprocess Biosyst. Eng.* **44**, 507–516 (2021).

56. Kaabel, S. et al. *Proc. Natl. Acad. Sci. U. S. A.* **118**, e2026452118 (2021).

57. Jog, J. P. *J. Macromol. Sci. Part C* **35**, 531–553 (1995).

58. Langevin, D., Grenet, J. & Saiter, J. M. *Eur. Polym. J.* **30**, 339–345 (1994).

59. Alves, N. M., Mano, J. F., Balaguer, E., Meseguer Dueñas, J. M. & Gómez Ribelles, J. L. *Polymer* **43**, 4111–4122 (2002).

60. Wellen, R. M. R., Canedo, E. & Rabello, M. S. *J. Mater. Res.* **26**, 1107–1115 (2011).

61. Ito, E. & Kobayashi, Y. *J. Appl. Polym. Sci.* **25**, 2145–2157 (1980).

62. Jabarin, S. A. & Lofgren, E. A. *Polym. Eng. Sci.* **26**, 620–625 (1986).

63. Son, H. F. et al. *ACS Catal.* **9**, 3519–3526 (2019

64. Gao, R., Pan, H. & Lian, J. *Enzyme Microb. Technol.* **150**, 109868 (2021).

65. Wei, R., Oeser, T. & Zimmermann, W. *Adv. Appl. Microbiol.* vol. 89, 267–305 (2014).

66. Zhang, Y., Wang, L., Chen, J. & Wu, J. *Carbohydr. Polym.* **97**, 124–129 (2013).

67. Ribitsch, D. et al. *Biomacromolecules* **14**, 1769–1776 (2013).

68. Weber, J. et al. *Appl. Microbiol. Biotechnol.* **103**, 4801–4812 (2019).

69. Xue, R. et al. *Front. Bioeng. Biotechnol.* **9**, (2021).

70. Graham, R. et al. *Chem Catal.* **2**, 2644–2657 (2022).

71. Pfaff, L. et al. *ACS Catal.* 9790–9800 (2022).

72. Palm, G. J. et al. *Nat. Commun.* **10**, 1717 (2019).

73. Knott Brandon C. et al. *Proc. Natl. Acad. Sci.* **117**, 25476–25485 (2020).

74. Mrigwani, A., Thakur, B. & Guptasarma, P. *Green Chem.* **24**, 6707–6719 (2022).

75. Billig, S., Oeser, T., Birkemeyer, C. & Zimmermann, W. *Appl. Microbiol. Biotechnol.* **87**, 1753–1764 (2010).

76. Barth, M. et al. *Biotechnol. J.* **11**, 1082–1087 (2016).

77. Lehmann, M. & Wyss, M. *Curr. Opin. Biotechnol.* **12**, 371–375 (2001).

78. Samak, N. A. et al. *Environ. Int.* **145**, 106144 (2020).

79. Li, C., Zhang, R., Wang, J., Wilson, L. M. & Yan, Y. *Trends Biotechnol.* **38**, 729–744 (2020).

80. Behrens, G. A., Hummel, A., Padhi, S. K., Schätzle, S. & Bornscheuer, U. T. *Adv. Synth. Catal.* **353**, 2191–2215 (2011).

81. Buchholz K., Kasche V. & Bornscheuer U. T. Biocatalysts and Enzyme Technology, *Wiley-Blackwell*, 2nd edition (2012).

82. Zhao H., Lee S. Y., Nielsen J. & Stephanopoulos G. Protein Engineering: Tools and Applications*, Wiley*, vol. 10 (2021)

83. Romero, P. A. & Arnold, F. H. *Nat. Rev. Mol. Cell Biol.* **10**, 866–876 (2009).

84. McLure, R. J., Radford, S. E. & Brockwell, D. J. *Trends Chem.* **4**, 378–391 (2022).

85. Newberry, R. W., Leong, J. T., Chow, E. D., Kampmann, M. & DeGrado, W. F. *Nat. Chem. Biol.* **16**, 653–659 (2020).

86. Bornscheuer, U. T. et al. *Nature* **485**, 185–194 (2012).

87. Bornscheuer, U. T., Hauer, B., Jaeger, K. E. & Schwaneberg, U. *Angew. Chem., Int. Ed.* **58**, 36–40 (2019).

88. You, L. & Arnold, F. H. *Protein Eng. Des. Sel.* **9**, 77–83 (1996).

89. Dörr, M. et al. *Biotechnol. Bioeng.* **113**, 1421–1432 (2016).

90. Bell, E. L. et al. *Nat. Catal.* **5**, 673–681 (2022).

91. Xiong, W., Liu, B., Shen, Y., Jing, K. & Savage, T. R. *Biochem. Eng. J.* **174**, 108096 (2021).

92. Smyth, M. S. & Martin, J. H. J. *Mol. Pathol.* **53**, 8–14 (2000).

93. Wüthrich, K. *Nat. Struct. Biol.* **8**, 923–925 (2001).

94. Bai, X., McMullan, G. & Scheres, S. H. W. *Trends Biochem. Sci.* **40**, 49–57 (2015).

95. Jaskolski, M., Dauter, Z. & Wlodawer, A. *FEBS J.* **281**, 3985–4009 (2014).

96. Jumper, J. et al. *Nature* **596**, 583–589 (2021).

97. Egbe, E., Levy, C. W. & Tabernero, L. *PLoS ONE* **15**, e0235133 (2020).

98. Chica, R. A., Doucet, N. & Pelletier, J. N. *Curr. Opin. Biotechnol.* **16**, 378–384 (2005).

99. Halima, N. B. *RSC Adv.* **6**, 39823–39832 (2016).

100. DeMerlis, C. C. & Schoneker, D. R. *Food Chem. Toxicol.* **41**, 319–326 (2003).

101. Chaouat, M. et al. *Adv. Funct. Mater.* **18**, 2855–2861 (2008).

102. Paradossi, G., Cavalieri, F., Chiessi, E., Spagnoli, C. & Cowman, M. K. *J. Mater. Sci. Mater. Med.* **14**, 687–691 (2003).

103. Stauffer, S. R. & Peppast, N. A. *Polymer* **33**, 3932–3936 (1992).

104. Ma, S. et al. *Ind. Eng. Chem. Res.* **56**, 7971–7976 (2017).

105. Rynkowska, E., Fatyeyeva, K., Marais, S., Kujawa, J. & Kujawski, W. *Polymers* **11**, 1799 (2019).

106. Kamoun, E. A., Chen, X., Eldin, M. S. M. & Kenawy, E.-R. S. *Arab. J. Chem.* **8**, (2014).

107. Zhou, X., Hou, C., Chang, T.-L., Zhang, Q. & Liang, J. F. *Colloids Surf. B Biointerfaces* **187**, 110645 (2020).

108. El-Naas, M. H., Mourad, A.-H. I. & Surkatti, R. *Int. Biodeterior. Biodegrad.* 413–420 (2013).

109. Shinde, P., Musameh, M., Gao, Y., Robinson, A. J. & Kyratzis, I. *Biotechnol. Rep.* **19**, e00260 (2018).

110. Rolsky, C. & Kelkar, V. *Int. J. Environ. Res. Public. Health* **18**, 6027 (2021).

111. Brennecke, D., Duarte, B., Paiva, F., Caçador, I. & Canning-Clode, J. *Estuar. Coast. Shelf Sci.* **178**, 189–195 (2016).

112. Li, J., Zhang, K. & Zhang, H. *Environ. Pollut.* **237**, 460–467 (2018).

113. Kawai, F. & Hu, X. *Appl. Microbiol. Biotechnol.* **84**, 227–237 (2009).

114. Zhang, Y., Wang, Q. & Yuan, J. *Advances in Textile Biotechnology (Second Edition),* 21–36 (2019).

115. Sakazawa, C., Shimao, M., Taniguchi, Y. & Kato, N. *Appl. Environ. Microbiol.* **41**, 261–267 (1981).

116. Shimao, M., Fukuta, I., Kato, N. & Sakazawa, C. *Appl. Environ. Microbiol.* **48**, 751–754 (1984).

117. Kim, B. C., Sohn, C. K., Lim, S. K., Lee, J. W. & Park, W. *J. Ind. Microbiol. Biotechnol.* **30**, 70–74 (2003).

118. Hashimoto, S. *J. Ferment. Technol.* **63**, 471–474 (1985).

119. Wu, H. F. et al. *Water Sci. Technol.* **79**, 2005–2012 (2019).

120. Matsumura, S., Tomizawa, N., Toki, A., Nishikawa, K. & Toshima, K. *Macromolecules* **32**, 7753–7761 (1999).

121. Sakai, K., Hamada, N. & Watanabe, Y. *Agric. Biol. Chem.* **48**, 1093–1095 (1984).

122. Shimao, M., Taniguchi, Y., Shikata, S., Kato, N. & Sakazawa, C. *Appl. Environ. Microbiol.* **44**, 28–32 (1982).

123. Klomklang, W. et al. *Microbiology* **151**, 1255–1262.

124. Yang, Y. et al. *ChemBioChem* **15**, 1882–1886 (2014).

125. Wei, Y. et al. *Appl. Environ. Microbiol.* **84**, e01898-17 (2017).

126. Suzuki, T. *Agric. Biol. Chem.* **42**, 1187–1194 (1978).

127. Sakai, K., Hamada, N. & Watanabe, Y. *Agric. Biol. Chem.* **49**, 817–825 (1985).

128. Jia, D. et al. *Appl. Biochem. Biotechnol.* **172**, 2540–2551 (2014).

129. Mueller, R.-J. *Process Biochem.* **41**, 2124–2128 (2006).

130. Keller, A., Lester, G. R., Morgan, L. B. & Melville, H. W. *Philos. Trans. R. Soc. Lond. Ser. Math. Phys. Sci.* **247**, 1–12 (1954).

131. Bianchi, R., Chiavacci, P., Vosa, R. & Guerra, G. *J. Appl. Polym. Sci.* **43**, 1087–1089 (1991).

132. Launay, A., Thominette, F. & Verdu, J. *J. Appl. Polym. Sci.* **73**, 1131–1137 (1999).

133. Shinotsuka, K., Bliznyuk, V. N. & Assender, H. E. *Polymer* **53**, 5554–5559 (2012).

134. Baker, P. J., Poultney, C., Liu, Z., Gross, R. & Montclare, J. K. *Appl. Microbiol. Biotechnol.* **93**, 229–240 (2012).

135. Oda, M. et al. *Appl. Microbiol. Biotechnol.* **102**, 10067–10077 (2018).

136. Miyakawa, T. et al. *Appl. Microbiol. Biotechnol.* **99**, 4297–4307 (2015).

137. Then, J. et al. *Biotechnol. J.* **10**, 592–598 (2015).

138. Then, J. et al. *FEBS Open Bio* **6**, 425–432 (2016).

139. Emori, M. et al. *Proteins Struct. Funct. Bioinforma.* **89**, 502–511 (2021).

140. Zhong-Johnson, E. Z. L., Voigt, C. A. & Sinskey, A. J. *Sci. Rep.* **11**, 928 (2021).

141. Shirke, A. N. et al. *Biochemistry* **57**, 1190–1200 (2018).

142. Xi, X. et al. *Enzyme Microb. Technol.* **143**, 109715 (2021).

143. Wei, R. et al. *Adv. Sci.* **6**, 1900491 (2019).

144. Kari, J., Andersen, M., Borch, K. & Westh, P. *ACS Catal.* **7**, 4904–4914 (2017).

145. Erickson, E. et al. *ChemSusChem* **15**, e202101932 (2022).

146. Vogel, K. et al. *Sci. Total Environ.* **773**, 145111 (2021).

147. Bååth, J. A., Borch, K., Jensen, K., Brask, J. & Westh, P. *ChemBioChem* **22**, 1627–1637 (2021).

148. Wei, R. et al. *J. Mol. Catal. B Enzym.* **103**, 72–78 (2014).

149. Wei, R. et al. *AMB Express* **4**, 44 (2014).

150. Silva, C. et al. *Biotechnol. J.* **6**, 1230–1239 (2011).

151. Zumstein, M. T., Kohler, H.-P. E., McNeill, K. & Sander, M. *Environ. Sci. Technol.* **50**, 197–206 (2016).

152. Weinberger, S. et al. *Green Chem.* **19**, 5381–5384 (2017).

153. Dai, L. et al. *J. Biotechnol.* **334**, 47–50 (2021).

154. Espino-Rammer, L. et al. *Appl. Environ. Microbiol.* **79**, 4230–4238 (2013).

155. Ribitsch, D. et al. *Appl. Environ. Microbiol.* **81**, 3586–3592 (2015).

156. Puspitasari, N., Tsai, S.-L. & Lee, C.-K. *Int. J. Biol. Macromol.* **176**, 157–164 (2021).

157. Dai, L. et al. *Int. J. Biol. Macromol.* **190**, 456–462 (2021).

158. Chen, K., Hu, Y., Dong, X. & Sun, Y. *ACS Catal.* **11**, 7358–7370 (2021).

159. Berger, B. W. & Sallada, N. D. *J. Biol. Eng.* **13**, 10 (2019).

160. Austin, H. P. et al. *Proc. Natl. Acad. Sci.* **115**, E4350–E4357 (2018).

161. Fecker, T. et al. *Biophys. J.* **114**, 1302–1312 (2018).

162. da Costa, C. H. S. et al. *Proteins Struct. Funct. Bioinforma.* **89**, 1340–1352 (2021).

163. Roth, C. et al. *Appl. Microbiol. Biotechnol.* **98**, 7815–7823 (2014).

164. Taniguchi, I. et al. *ACS Catal.* **9**, 4089–4105 (2019).

165. Boneta, S., Arafet, K. & Moliner, V. *J. Chem. Inf. Model.* **61**, 3041–3051 (2021).

166. Feng, S. et al. *ACS Sustain. Chem. Eng.* **9**, 9823–9832 (2021).

167. Chen, C.-C., Han, X., Ko, T.-P., Liu, W. & Guo, R.-T. *FEBS J.* **285**, 3717–3723 (2018).

168. Chen, C.-C. et al. *Nat. Catal.* **4**, 425–430 (2021).

169. Araújo, R. et al. *J. Biotechnol.* **128**, 849–857 (2007).

170. Furukawa, M., Kawakami, N., Tomizawa, A. & Miyamoto, K. *Sci. Rep.* **9**, 16038 (2019).

171. Wei, R. et al. *Nat. Commun.* **10**, 5581 (2019).

172. Falkenstein, P., Wei, R., Matysik, J. & Song, C. *Methods Enzymol.*, **648**, 231–252 (2021).

173. Chen, S., Su, L., Chen, J. & Wu, J. *Biotechnol. Adv.* **31**, 1754–1767 (2013).

174. Sulaiman, S. et al. *Appl. Environ. Microbiol.* **78**, 1556–1562 (2012).

175. Cui, Y. et al. *ACS Catal.* **11**, 1340–1350 (2021).

176. Wei, R. et al. *ACS Catal.* **12**, 3382–3396 (2022).

177. Schmidt, J. et al. *FEBS Open Bio* **6**, 919–927 (2016).

178. Kim, H. T. et al. *ChemSusChem* **14**, 4251–4259 (2021).

179. Rogers, B. A. et al. *Nat. Chem.* **14**, 40–45 (2022).

180. Gundupalli, S. P., Hait, S. & Thakur, A. *Waste Manag.* **60**, 56–74 (2017).

181. Hahladakis, J. N. & Iacovidou, E. *J. Hazard. Mater.* **380**, 120887 (2019).

182. Tsochatzis, E. D., Lopes, J. A. & Corredig, M. *Resour. Conserv. Recycl.*

179, 106096 (2022).

183. Singh, A. et al. Joule 5, 2479–2503 (2021).

184. Oeser, T. et al. *J. Biotechnol.* 146, 100–104 (2010).

185. von Haugwitz, G. et. al., *ACS Catal.,* accepted, (2022).

186. Becker, A. et al. *Appl. Microbiol. Biotechnol*. 105, 4189–4197 (2021).

187. Engel, J., Mthethwa, K. S., Opperman, D. J. & Kara, S. *Mol. Catal.* 468, 44–51 (2019).

188. von Haugwitz, G. et. al. *Angew. Chem., Int. Ed.,* under review.

189. Finley, J. H. *Anal. Chem.* 33, 1925–1927 (1961).

190. Bradshaw, C. W., Hummel, W. & Wong, C. H. J. *Org. Chem.* 57, 1532–1536(1992).

5. Author Contributions

Article I **Mechanism-Based Design of Efficient PET Hydrolases**
R. Wei, G. von Haugwitz, L. Pfaff, J. Mican, C. P. S. Badenhorst, W. Liu, G. Weber, H. P. Austin, D. Bednar, J. Damborsky, U. T. Bornscheuer, *ACS Catal.*, **2022**, *12*, 3382−3396.

Conceptualization, R.W.; resources, U.T.B.; writing—original draft preparation, R.W., G.H., L.P., J.M. C.P.S.B.; writing, review and editing, all authors; visualization, R.W.; supervision, U.T.B.; project administration, U.T.B.

Article II **Structural Insights into (Tere)phthalate-ester Hydrolysis by a Carboxylesterase and its Role in Promoting PET Depolymerization**
G. von Haugwitz, X. Han, L. Pfaff, Q. Li, H. Wei, J. Gao, K. Methling, Y. Ao, Y. Brack, J. Mican, C. G. Feiler, M. S. Weiss, D. Bednar, G. J. Palm, M. Lalk, M. Lammers, J. Damborsky, G. Weber, W. Liu, U. T. Bornscheuer, R. Wei, *ACS Catal.*, **2022**, accepted.

Conceptualization, R.W., W.L., and U.T.B.; Protein crystallographic studies, J.G., X.H., C.G.F., Q.L., G.J.P., M.L., and W.L.; Computational simulations, G.W., J.M., D.B., J.D., and W.L.; Protein engineering and characterization, G.H.; Substrate generation and characterization, Y.A. and L.P.; Product identification, G.H., K.M., M.L. and R.W.; Generation of the phylogenetic tree, Y.B.; Writing – original draft, G.H., J.M., W.L., and R.W.; Writing, review and editing, all authors; Supervision and funding acquisition, J.D., W.L., U.T.B., and R.W.

Article III **Synthesis of Modified Polyvinyl Alcohols and their Degradation Using an Enzymatic Cascade**
G. von Haugwitz, K. Donnelly, M. Di Filippo, D. Breite, A. Schulze, R. Wei, M. Baumann, U. T. Bornscheuer, *Angew. Chem. Int. Ed.*, *under review*.

Conceptualization, U.T.B., M.B.; Substrate generation and characterization, K.D., M.D.F., and M.B.; Enzyme expression, characterization and enzymatic reactions, G.H.; Gas permeation chromatography measurements, D.B.; Writing – Original Draft, G.H., and M.B.; Writing, review and editing, all authors; supervision and funding acquisition, R.W., M.B., and U.T.B.

Gerlis Maria von Haugwitz

Prof. Dr. Uwe T. Bornscheuer

Articles

Article I

ACS Catalysis

pubs.acs.org/acscatalysis Perspective

Mechanism-Based Design of Efficient PET Hydrolases

Ren Wei,* Gerlis von Haugwitz, Lara Pfaff, Jan Mican, Christoffel P. S. Badenhorst, Weidong Liu, Gert Weber, Harry P. Austin, David Bednar, Jiri Damborsky, and Uwe T. Bornscheuer*

Cite This: ACS Catal. 2022, 12, 3382−3396 Read Online

ACCESS | Metrics & More | Article Recommendations

ABSTRACT: Polyethylene terephthalate (PET) is the most widespread synthetic polyester, having been utilized in textile fibers and packaging materials for beverages and food, contributing considerably to the global solid waste stream and environmental plastic pollution. While enzymatic PET recycling and upcycling have recently emerged as viable disposal methods for a circular plastic economy, only a handful of benchmark enzymes have been thoroughly described and subjected to protein engineering for improved properties over the last 16 years. By analyzing the specific material properties of PET and the reaction mechanisms in the context of interfacial biocatalysis, this Perspective identifies several limitations in current enzymatic PET degradation approaches. Unbalanced enzyme−substrate interactions, limited thermostability, and low catalytic efficiency at elevated reaction temperatures, and inhibition caused by oligomeric degradation intermediates still hamper industrial applications that require high catalytic efficiency. To overcome these limitations, successful protein engineering studies using innovative experimental and computational approaches have been published extensively in recent years in this thriving research field and are summarized and discussed in detail here. The acquired knowledge and experience will be applied in the near future to address plastic waste contributed by other mass-produced polymer types (e.g., polyamides and polyurethanes) that should also be properly disposed by biotechnological approaches.

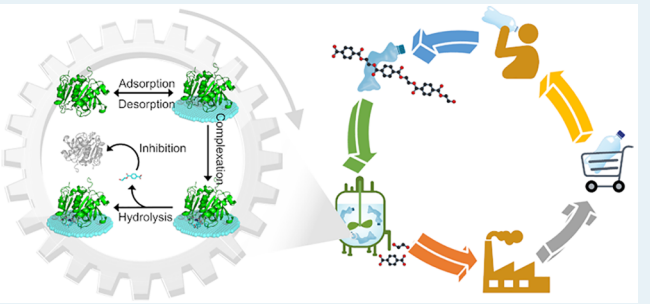

KEYWORDS: *Hydrolase, enzymatic degradation, interfacial biocatalysis, plastic recycling, protein engineering, polyethylene terephthalate (PET), product inhibition, thermostability*

1. INTRODUCTION

Scientists began to study biological degradation of plastic waste in the early 1970s.[1] Around the same time, the distribution of plastic waste in the Pacific Ocean was first quantified.[2] After nearly 50 years, climate change and environmental pollution caused by mass production, mass consumption, and improper end-of-life management of petroleum-based plastic products have become unprecedented challenges for human society.[3−5] Consciousness of these issues spreading among governments and policymakers, industries producing or relying on plastics, and end-users of plastic products, has recently boosted research and development of novel plastic replacement materials and waste plastic valorization strategies to enable a transition from a linear to a circular plastic economy.[6−9]

To this end, biotechnological plastic recycling has become a thriving research area in recent years.[6,9,10] The biodegradation of hydrophobic vinyl polymers, such as polyolefins and polystyrene, which represent over 80% of all conventional plastics produced,[11] is still an intensively debated topic.[9,12,13] In contrast, the biocatalytic degradation of polyester-type plastics, such as polyethylene terephthalate (PET), has evolved in the last two decades from verifying trace amounts of released monomers after weeks of incubation to highly efficient depolymerization within several hours.[14−17] PET is a heteroatomic polymer consisting of terephthalic acid (TPA) and ethylene glycol (EG) connected by ester bonds. It is a semicrystalline thermoplastic composed of crystalline regions with uniformly packed molecules and amorphous regions with randomly arranged microstructures.[18] With a first patent filed for its synthesis in 1941 and commercialization starting in the early 1950s,[19] particularly as synthetic polyester fabric for the textile industry and as packaging materials for food and beverages,[20,21] PET has become one of the most important mass-produced petrochemical plastics.[22] The majority of PET products have a high crystalline fraction (usually 30−40% crystallinity)[23,24] benefiting their durability against mechanical and chemical stress.[25] Post-consumer PET accounts for a considerable fraction of the global solid waste stream, and its

Received: December 20, 2021
Revised: February 4, 2022

https://doi.org/10.1021/acscatal.1c05856
ACS Catal. 2022, 12, 3382−3396

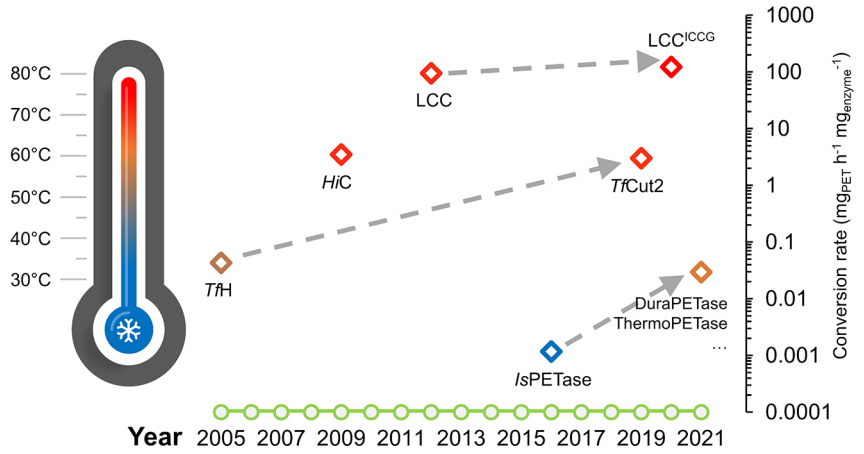

Figure 1. Selected milestones of a 16-year-long history of identifying and engineering PET hydrolases. Both optimal reaction temperatures (in varying colors) for PET degradation and normalized maximal conversion rates (diamonds corresponding to logarithmic values on the vertical axis) calculated based on various publications are denoted, regardless of the material properties of applied PET substrates. The successes in raising the degradation performance using certain benchmark enzymes by both protein and process engineering are indicated by arrows with broken lines. *Tf*H: hydrolase from *T. fusca* DSM43793;[31] *Hi*C: *Humicola insolens* cutinase;[42] LCC: leaf-branch compost cutinase;[33,52] *Is*PETase: *I. sakaiensis* PET hydrolase;[16,34] *Tf*Cut2: *T. fusca* KW3 cutinase;[53] LCC^{ICCG}: LCC variant with indicated quadruple substitutions;[16] DuraPETase, ThermoPETase, etc.: various thermostabilized *Is*PETase variants.[54−56]

breakdown is a source of microplastics and microfibers that further pollute the environment.[11,26−28]

Tokiwa et al. suggested in the 1970s that aromatic polymers are resistant to enzymatic and microbial attack.[29] Later research found, however, that crude enzyme preparations from specific fungal species can induce surface modifications on high-crystallinity PET materials.[30] The first breakthrough was achieved with the cutinase *Tf*H (from the filamentous actinomycete *Thermobifida fusca*) which caused >50% weight loss of melt-quenched post-consumer PET bottles (10% crystallinity) following 3 weeks of incubation.[31] During 16 years of extensive research, the initial low PET degradation activity of *T. fusca* PET hydrolase has been considerably enhanced by more than an order of magnitude (Figure 1) as a result of both protein and process engineering.[32] The development of metagenomic approaches has allowed for the identification of a more active leaf-branch-compost cutinase LCC,[33] which has emerged as the most promising benchmark thermophilic PET hydrolase. In 2020, *Nature* published a breakthrough article on engineered LCC variants which can rapidly depolymerize amorphized (i.e., by lowering the crystallinity through a thermomechanical process to allow for enzymatic degradation) PET waste at an industrially relevant scale within 10 h, and the recovered monomers were readily used to synthesize virgin polymers, thereby closing the recycling loop.[16] *Is*PETase and the related monoester-hydrolyzing *Is*MHETase, both derived from the bacterium *Ideonella sakaiensis*, which was isolated from plastic-contaminated sediment samples, have also been intensively studied.[34,35] The uniqueness of this bacterium in degrading and metabolizing highly amorphous PET led not only to the discovery of a tandem polymer degradation pattern by two distinct enzyme classes,[36] but also to its utility in the efficient bio-upcycling of PET waste to other useful biopolymers when it was applied as a whole cell-based catalyst.[37]

Based on >65 crystal structures so far elucidated,[38] these bacterial PET hydrolases exhibit conserved structural properties and can be classified into a single subclass of the α/β-hydrolase fold enzyme superfamily as represented by the first solved *Streptomyces exfoliates* lipase structure (PDB ID: 1JFR).[39,40] This subclass is distinct from the polyester-hydrolyzing fungal cutinases (EC 3.1.1.74) with shorter polypeptides and more compact structures.[41] *Thermomyces insolens* (formerly named *Humicola insolens*) cutinase *Hi*C is a prominent member of the fungal PET hydrolase family. It has been successfully commercialized and also received broad attention in recent years by researchers working on PET waste degradation. However, here the emphasis was more on process engineering and improvement rather than protein engineering.[42−45]

This Perspective intends to provide a deeper understanding of important obstacles in the engineering of effective industrially applicable PET hydrolases, as well as to provide guidance for further efforts in this intriguing research field. Previous research has indicated that enzymatic polyester hydrolysis occurs preferentially in its amorphous parts rather than the well-ordered crystalline regions with poor chain mobility.[46] Understanding the accessibility of amorphous polymer chains around the polymer glass transition temperature, in conjunction with tailoring the thermostability of biocatalysts, has thus become a focus of contemporary research.[38,47] As a typical surface erosion process, it is not yet fully understood how the adsorption and desorption of biocatalysts onto the polymer surface influence the overall degradation kinetics and performance. This problem is reminiscent of the decades spent investigating the relationship between the binding of cellulases onto crystalline cellulose and catalytic activity.[48] Altering their affinity to polymer substrates by protein engineering, on the other hand, has proven to be a viable approach to maximize the catalytic capacity of both cellulose and PET depolymerases. Similar to the aforementioned natural polymer-degrading enzymes such as cellulases, mass transfer of certain degradation intermediates that can function as inhibitors of the biocatalysts, has been identified as the third main bottleneck that must be addressed with a low-cost solution for adequate reaction efficiency.[49−51] This Perspective summarizes and discusses special efforts devoted to the engineering of thermostability (Section 2), to study the de/adsorption properties, and to address the product inhibition (Sections 3 and 4).

https://doi.org/10.1021/acscatal.1c05856
ACS Catal. 2022, 12, 3382−3396

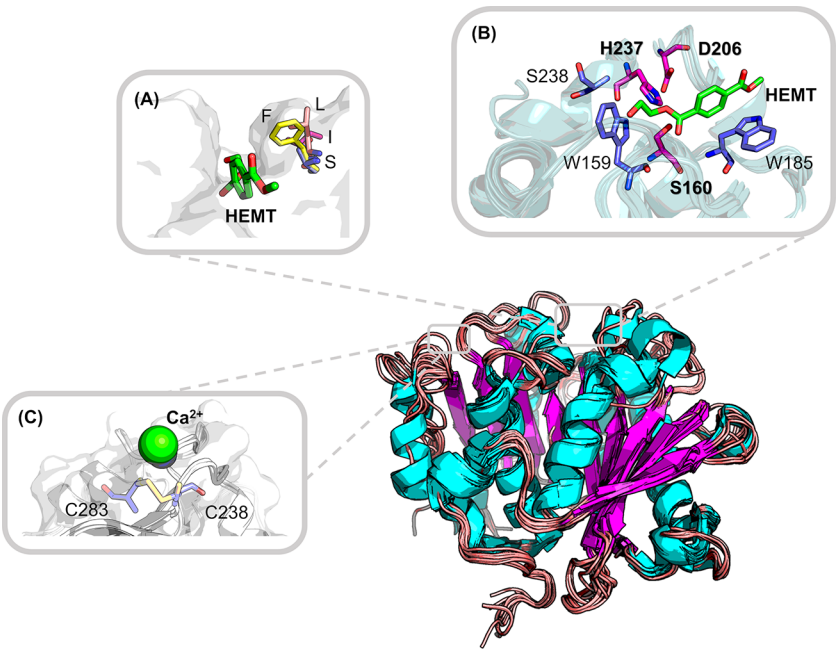

Figure 2. Frequently reported mutation hot spots illustrated on the superposed crystal structures of known bacterial PET hydrolases. Backbones shown in the cartoon are derived from the structural superposition with selected homologous enzymes. The catalytic triad (S160, D206, and H237) as well as two aromatic residues (W159 and W185) are involved in the interaction with the monomer analogue 1-(2-hydroxyethyl)-4-methyl terephthalate (HEMT) (A, B) based on the *Is*PETase structure (PDB ID: 5XH3; the numbering of residues is modified consistently with other structures solved later for easy comprehension). (A) One frequently reported mutation hotspot equivalent to S209 (B) in *Is*PETase can adopt various residues which might influence the widths of the binding pocket:[65,90] F found in 4CG1, 4EB0, and 7OSB and also conserved in many other PET hydrolases; S found in the *Is*PETase structure 5XH3; I found in an LCC mutant 6THT; L found in another PET hydrolase 7CUV. (C) One of the putative Ca^{2+} binding sites revealed by cocrystallized structures such as 4WFJ, 5LUL, and 5ZNO can be replaced by a disulfide bridge (6THT, 7CTS, and 7CTR) to thermostabilize several PET hydrolases.

2. DESIGN OF THERMOSTABLE PET HYDROLASES BASED ON MATERIAL PROPERTIES

Earlier research on enzymatic degradation of aromatic and aliphatic copolyesters suggested that increasing the proportion of aromatic moieties raises the melting point, thus lowering the polymer chain mobility and biodegradability at the optimal reaction temperatures of the applied hydrolases.[57,58] For a long time, enzymatic depolymerization of PET with a melting point over 260 °C was thought to be unachievable according to this idea, until, in 2005, Müller et al. showed significant weight loss of amorphized PET waste using *Tf*H.[31] This discovery drew attention to the preferential (or perhaps exclusive) degradation of amorphous PET, as well as the importance of its glass transition temperature (T_g) in understanding enzymatic degradation.[42,46] T_g is the temperature range in which the glass transition process occurs, i.e., the amorphous polymer structure transitions from a "glassy" (hard and brittle) state into a sticky-liquid or rubbery one as a function of increasing temperature.[18,59] The T_g of bulk amorphous PET is in the range of 65−71 °C, estimated based on data collected with differential scanning calorimetry (DSC) at zero heating rate.[60−62] This has so far been accepted as a standard value by research communities working on enzymatic PET hydrolysis.[31,42,53,63−65] In addition to its role as both a solvent and a reactant in enzymatic PET degradation, water has a plasticization effect on the PET polymer, as reported since the early 1980s,[66,67] by lowering the T_g of bulk polymer by up to 16 °C.[60,68,69] This influence is more pronounced on the surface polymer layer of about 13 nm which has an intrinsically lower T_g (~48.1 °C) than that of the bulk polymer even when water is not present.[70] With both effects taken into account, the superficial PET layer exposed to enzymatic degradation in an aqueous milieu can indeed have a biocatalysis-relevant $T_g \lesssim 40$ °C, explaining the considerably fast degradation of amorphous PET by, for example, *I. sakaiensis* and its *Is*PETase at ambient temperature.[34] The enhanced segmental mobility of the surface polymer, on the other hand, may decrease to a level similar to that of the bulk polymer as a result of superficial crystallization.[71] For example, as a result of UV-treatment-induced crystallization, the overall degradation performance could be significantly impaired.[72]

Based on these PET material characteristics, the advantage of using thermophilic and thermostable enzymes in depolymerization, over their mesophilic counterparts, is obvious and evident from preliminary studies.[42,56,73,74] In this regard, searching for new thermophilic enzymes, such as those found in metagenomic libraries,[33,75] as well as known thermostabilizing ones, provides viable options for improving degradation performance.[74] In the presence of selected bivalent ions such as Ca^{2+} or Mg^{2+}, the overall thermostability of many bacterial PET hydrolases has been improved, as indicated by increased midpoints of thermal denaturation (T_m) by 10−16 °C and enhanced optimal temperatures (T_{opt}) for PET degradation by at least 10 °C.[52,76−78] The probable Ca^{2+} binding site was found to be close to the catalytic triad based on cocrystallized structures (Figure 2) and molecular dynamics simulations.[76−81] The interaction with Ca^{2+} controls the process of opening and closing the active site during substrate binding and unbinding by Cut190 from *Saccharomonospora viridis*.[78,80] Because Ca^{2+} will precipitate terephthalate to generate insoluble byproducts from the reaction super-

https://doi.org/10.1021/acscatal.1c05856
ACS Catal. 2022, 12, 3382−3396

Table 1. Selected *Is*PETase Engineering Studies Designed to Improve Thermal Stability

nomenclature and introduced mutations	improved stability[a]	design approach and interpretation	refs
S238F/W159H	T_m = 56.5 °C, ΔT_m = +9.7 °C	Structural and sequence comparison with homologous PET hydrolases	65,90
ThermoPETase: S121E/D186H/R280A	T_m = 57.6 °C, ΔT_m = +8.8 °C	Structure-based design; Water-mediated hydrogen bond between E121 and H186	54
DuraPETase: A214H/I168R/W159H/S188Q/R280A/A180I/G165A/Q119Y/L17F/T140D	T_m = 77.0 °C, ΔT_m = +31.0 °C	Structure-based design and machine learning approach; Multiple stabilizing interactions	55
W159H/F229Y	ΔT_m = +10.4 °C	Sequence comparison with other homologous PET hydrolases	91
DuraPETase+N233K	T_m = 83.5 °C, ΔT_m = +38.4 °C	Machine learning; Introduction of salt bridge between K233 and E204	88
FAST-PETase: ThermoPETase+R224Q/N233K	T_m= 67.4 °C, ΔT_m = +22.3 °C	Machine learning; Introduction of a hydrogen bond between Q224 and S192	88
TS-PETase: ThermoPETase+N233C/S282C	T_m = 69.4 °C, ΔT_m = +22.3 °C	Structural comparison with other homologous PET hydrolases	83
TM3: ThermoPETase+K95N/F201I/N233C/S282C	T_m = 70.8 °C, ΔT_m = +25.8 °C	Random mutagenesis based on error prone PCR and structural comparison with LCC^{ICCG} mutant	56
D1: DuraPETase+N233C/S282C	T_m = 81.1 °C, ΔT_m = +36.1 °C	Structural comparison with LCC^{ICCG} mutant	56
HotPETase: TS-PETase+P181V/S207R/S214Y/Q119K/S213E/R90T/Q182M/N212K/R224L/S58A/S61V/K95N/M154G/N241C/K252M/T270Q	T_m= 82.5 °C, ΔT_m = +37.5 °C	Directed evolution	89

[a] ΔT_m was estimated compared to T_m of the wild-type *Is*PETase either determined in the same publication or that of 45.1 °C determined by Brott et al.[56] T_m values were determined by circular dichroism, differential scanning calorimetry, or differential scanning fluorimetry.

natants,[82] relying on Ca^{2+} salts for high degradation efficiency is undesirable and can be minimized by tailoring the Ca^{2+}-binding sites of the biocatalysts. Earlier research was carried out by substituting one major Ca^{2+}-binding site with a salt bridge or a putative disulfide bond, resulting in an increased T_m of the *T. fusca* cutinase *Tf*Cut2 by up to 25 °C.[77,79] The latter strategy was then adopted in engineering other homologous PET hydrolases, resulting in increased T_m by up to 26 °C,[16,56,81,83] although the formation of this disulfide bond was indeed validated by protein crystallography for only two enzymes.[16,81] More recently, Nakamura et al. have also introduced cysteine pairs to form putative disulfide bonds at alternative positions in the homologous hydrolase PET2, but this led only to a marginal increase of T_m by less than 3.1 °C.[84]

Enhanced thermostability of PET hydrolases has also been reported when they were recombinantly expressed in alternative hosts other than *Escherichia coli*, for example, *Bacillus subtilis*[53,85] or *Pichia pastoris*.[86] Compared to the wild-type LCC obtained from *E. coli*, an increased T_m of >4 °C or >12 °C has been described when it was expressed in *B. subtilis* or *P. pastoris*, respectively.[85,86] The remarkable improvement with the latter host was attributed to glycosylation which mitigated the enzyme thermal aggregation at high reaction temperatures.[86]

Despite the fact that *Is*PETase is distinguished by its high PET hydrolyzing activity at ambient temperature, an effect which is presumably due to its more flexible and open substrate binding cleft,[87] efforts to thermostabilize this enzyme have been widely reported recently, with the goal of outperforming other cutinase-like PET hydrolases also at higher temperature ranges (Table 1). A ThermoPETase mutant with three residue substitutions, generated based on a structure-based engineering strategy, exhibited an increased T_m by 8.8 °C and up to 14-fold improved PET hydrolyzing activity compared to the wild-type *Is*PETase at 40 °C.[54] DuraPETase is an *Is*PETase variant with ten mutated residues, discovered by a novel GRAPE (*greedy accumulated strategy for protein engineering*) computational method.[55] Compared to wild-type *Is*PETase, DuraPETase showed a T_m increase of 31 °C and over 300-fold higher hydrolytic activity against high-crystallinity PET powder. By applying a convolutional neural network, MutCompute, trained for stability optimization, Lu et al. reported in a recent preprint the most thermostable *Is*PETase variant based on a single N233K substitution in addition to the DuraPETase, resulting in a T_m of 83.5 °C.[88] FAST-PETase, the most promising variant based on additional mutations of ThermoPETase, demonstrated significantly improved PET degradation activity against low-crystallinity PET waste at 50 °C compared to the wild-type and other known mutants of *Is*PETase. By screening a randomized *Is*PETase library based on error-prone PCR, at least one of their computationally targeted stability-related hot spots was also discovered.[56] Further substitutions related to thermostabilizing *Is*PETase found by other protein engineering strategies have been reported to be distributed across the entire sequence (Table 1). In another recent preprint, >13,000 *Is*PETase variants were evaluated by applying catalytic activity at elevated temperatures as a primary selection pressure. This directed evolution procedure afforded a HotPETase variant with 21 mutations compared to wild-type *Is*PETase and a T_m of 82.5 °C.[89] Therefore, the thermostability of *Is*PETase and other homologous enzymes depends on the interplay of many effects, necessitating further comprehensive research.

By raising the reaction temperature from 65 to 75 °C, the transition of the polymer microstructure from a less-ordered amorphous state to a nondegradable crystalline state can occur significantly earlier and faster.[16] This "physical aging" reaction competes with the enzymatic depolymerization and thus becomes the main determining factor of the total achievable degradation level.[53] As a result, using biocatalysts with only very high thermostability, such as the BhrPETase with a T_m of 101 °C,[85] is not always a good way to improve the degradation performance. As thermostabilizing an enzyme usually comes at the expense of lowering the flexibility of certain catalysis-relevant structural segments, a more balanced protein engineering strategy focusing on a thermo-active biocatalyst with T_{opt} at 75 °C and sufficient long-term robustness will hold promise for industrial applications. A recent techno-economic

https://doi.org/10.1021/acscatal.1c05856
ACS Catal. 2022, 12, 3382−3396

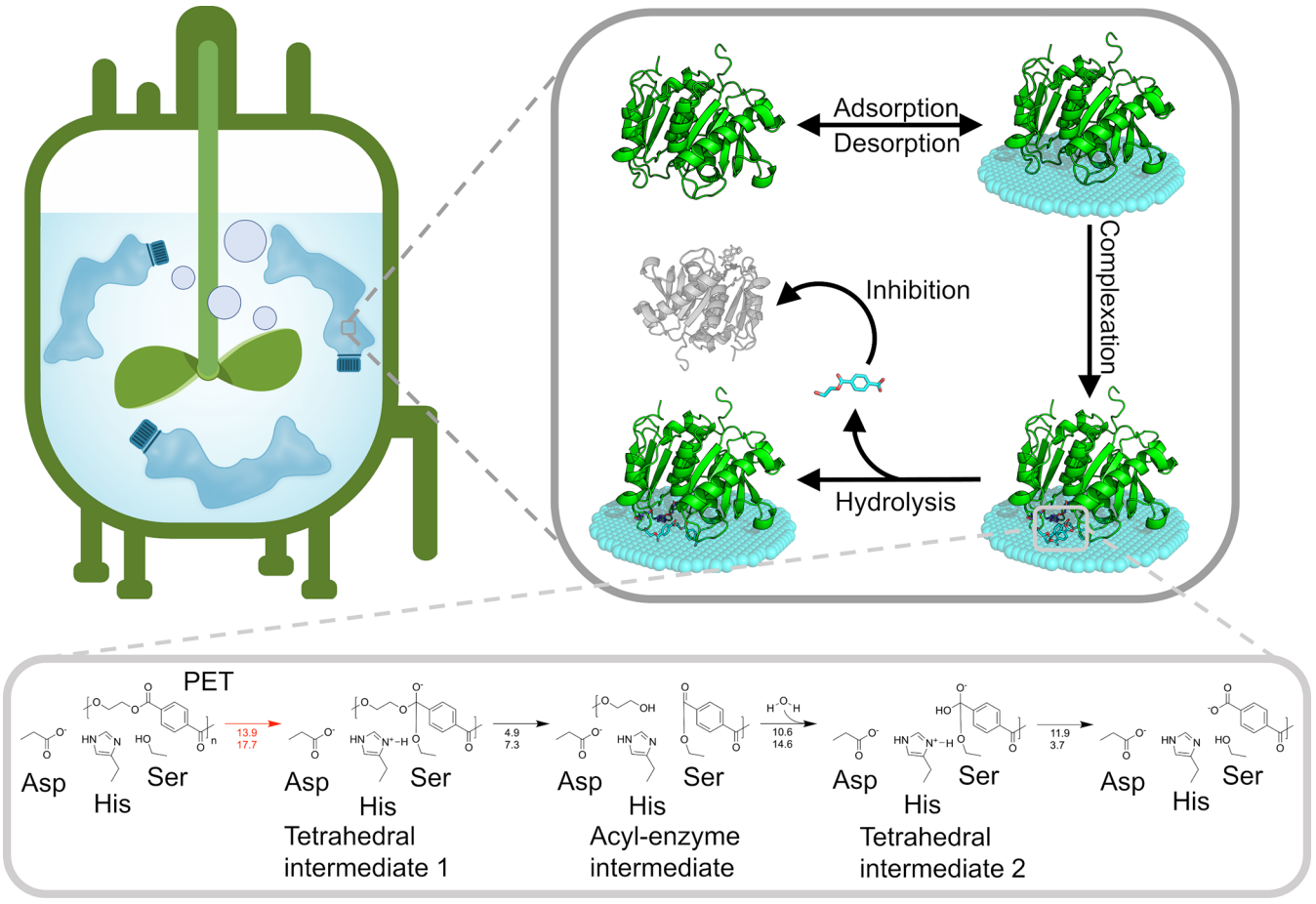

Figure 3. Interfacial biocatalytic hydrolysis of PET and its reaction mechanism. The states of a PET hydrolase are schematically illustrated in the upper right panel. In the lower panel, individual steps of the hydrolysis reaction are schematically shown in line with their activation free-energy barriers in kcal·mol^{-1} summarized based on different studies.[107,108] The reaction is initiated by a nucleophilic attack by a catalytic serine resulting in a tetrahedral intermediate stabilized by a catalytic histidine, an aspartic acid, and the oxyanion hole, followed by breakdown of the tetrahedral intermediate 1 into an acyl−enzyme intermediate and release of an alcohol. The aspartate−histidine pair activates the water for attack on the acyl−enzyme intermediate carbonyl, resulting in the formation of the second tetrahedral intermediate. The deacylation of this tetrahedral intermediate releases the carboxylic acid product. The rate-limiting step is regarded as the initial nucleophilic attack and highlighted in red with two free-energy activation barriers denoted. The top number is the Boltzmann-weighted average from 20 QM/MM MD simulations,[108] and the bottom number comes from adiabatic mapping studies.[107]

analysis of a simulated enzymatic PET recycling process revealed that the reaction duration and enzyme price have a greater influence on process costs than the energy cost to maintain an operating temperature of up to 80 °C.[92] Therefore, a commercially viable biocatalytic PET degradation process will rely on highly efficient enzymes rather than more heat-stable ones, which have, for example, T_{opt} in a higher temperature range but are less active at 75 °C.

3. UNDERSTANDING INTERFACIAL ENZYMATIC PET HYDROLYSIS FROM A STRUCTURE−FUNCTION PERSPECTIVE

Enzymatic PET hydrolysis is a surface erosion process characterized by the primary degradation of the exterior polymer to expose the inside of the material.[42,46,93] Because neither water (as both a solvent and a reactant) nor the biocatalysts can permeate the inner core of the polymer, only a limited number of superficial ester bonds can be accessed, implying that the reaction occurs primarily under conditions using an excess of enzyme.[94] As a consequence of this, research on PET hydrolysis kinetics has commonly employed an inverse Michaelis−Menten equation[90,95,96] or its mathematically equivalent expression based on the derivation of the Langmuir adsorption isotherm.[42,63,97−99] By simultaneous analysis using the conventional Michaelis−Menten equation, which is typically used to analyze bulk reactions on soluble substrates in great excess to enzymes, the accessible enzyme attack sites on the PET surface can be estimated using the ratio of parameters derived from these swapped kinetic models.[90,96]

The degradation-relevant binding of these PET hydrolases and variants was investigated by various biophysical approaches, such as quartz crystal microbalance,[100−102] chemiluminescence,[100] and fluorescence.[103] Binding isotherms have been directly estimated based on the concentrations of free enzymes determined in the supernatant after incubation with PET.[104−106] Selected PET hydrolases were shown to have a high affinity for the PET surface, as evidenced by the rapid formation of a monolayer, although this was thought to be mainly contributed by nonspecific adsorption.[106] A related kinetic study indicated that PET polymers were hydrolyzed at a remarkably lower rate than PET oligomers, regardless of their water solubility.[96] The conversion rates of these oligomers were found to be comparable to those of small-molecule *para*-

https://doi.org/10.1021/acscatal.1c05856
ACS Catal. 2022, 12, 3382−3396

Table 2. Selected PET Hydrolase Engineering Studies in the Presence of Binding Modules

binding module	enzyme	fold improvement	reaction condition	ref
PcAA14A	ThermoPETase	1.3	PET granules (3 g/L) incubated with 8.3 mg_{Enzyme}/g_{PET} in glycine-NaOH buffer (pH 9) for 5 days	137
RolA	*Is*PETase	1.2 (by weight loss) 1.5 (by HPLC)	Preincubation with RolA for 3 h, then degradation of PET fiber waste and high-crystallinity PET powder (15 g/L) at pH 8, 30 °C with 1.3 g_{Enzyme}/g_{PET} for 5 days	136
HGFI	*Is*PETase	1.3 (by weight loss) 1.6 (by HPLC)		
Zwitterionic polypeptide (EK)	*Is*PETase	11	Degradation of amorphous Goodfellow PET film and high-crystallinity (45.2%) beverage bottle with 200 nM enzyme in glycine-NaOH-buffer at pH 9 and 30−40 °C for up to 6 days	138
CBM	A cutinase from *T. fusca*	1.4−1.5 (only affinity)	Incubated with PET fiber and 50 μM enzyme in 50 mM Tris-buffer (pH 8) at 50 °C for 24 h	104
ChBD	LCC^{ICCG}	1.2	With 0.6 g/L amorphous Goodfellow PET film, post-consumer waste PET (16% crystallinity), or high crystallinity (40%) PET at 65 °C for 12 h	103
CBM	LCC^{ICCG}	1.3		
CBM	ThC_Cut1	1.4	With amorphous Goodfellow PET film and 25 mM enzyme in 100 mM potassium phosphate buffer (pH 7) at 50 °C	100
PBM	ThC_Cut1	3.8		

nitrophenyl esters. This suggests that the complexation or dissociation with the degradable polyester strands requires large activation barriers, determining the overall conversion rate rather than the chemical catalysis itself, which showed, in addition, a similar hydrolysis enthalpy to those reported in the literature for other readily accessible esters.[95] Recently, the hydrolysis reaction mechanism of several PET hydrolases against PET-related oligomers was investigated using QM/MM molecular dynamics (MD) simulations or adiabatic mapping to resemble polyester degradation.[107−110] Because there is only one cocrystallized *Is*PETase structure in a complex with a PET monomer analogue available so far, molecular docking of oligomeric aromatic esters has been widely used to study the substrate interaction in the binding groove as well as with the catalytic triad of various PET hydrolases.[16,65,87,111−113] The protein surface landscapes of bacterial PET hydrolases are comparable in close vicinity to the catalytic triad, requiring a high conformational selectivity of accommodated PET repeating units directly around the target ester bond at favored twisting angles.[112−114] In contrast, it is unclear and unlikely if distal PET repeating units are involved in a catalysis-related interaction with additional surface residues which requires a long PET strand to adopt a specific conformation.[113,115] Nonetheless, the defined polymer segment conformation directly next to the target ester bond will require a steric reconfiguration of the polymer chains with adequate mobility in order to form the productive tetrahedral intermediate via the initial nucleophilic attack by the catalytic serine.[115] This is evidenced by the highest activation free-energy barrier determined by QM/MM adiabatic mapping, suggesting the nucleophilic attack as a probable rate-limiting step (Figure 3).[107,108] Further reaction steps of the PET hydrolysis mechanism are canonically the same as for other conventional ester hydrolases, in agreement with the recent findings in kinetic studies.[96]

PET hydrolases are thought to possess dynamic catalytic sites with aromatic subsites which are locally stabilized upon substrate binding.[65,112,116] For example, the conserved W185 in *Is*PETase was also found in many other known PET hydrolases (Figure 2B).[116,117] A substitution of this residue usually resulted in a drastically reduced hydrolytic activity on PET.[112,118] Recently, Chen et al. identified that S214 and I218 are uniquely present in *Is*PETase to reduce the steric hindrance of W185, therefore enabling a higher flexibility of the indole side chain, allowing a higher polymer hydrolysis rate.[119] Introduction of the corresponding double-residue substitutions into homologous polyester hydrolases indeed boosted PET hydrolyzing activity, albeit at the expense of stability at temperatures >60 °C.

Large polymer segments may be unable to fit into a binding cleft that is too narrow. The overall catalytic properties of several PET hydrolases can be changed by widening or narrowing the binding clefts.[97,120] Interestingly, the free energy barrier and hydrolytic reaction thermodynamics do not differ significantly between the thermophilic $LCCI^{ICCG}$ mutant and the mesophilic *Is*PETase.[107] This suggests that the high activity of thermostable PET hydrolases is attributable mostly to the increased accessibility of PET polymer to nucleophilic attack at elevated temperatures, rather than to the fundamental interaction affinity. Austin et al. measured the width of the substrate binding cleft of *Is*PETase via the residue pair T88/S238.[65] By substituting S238 to F, which is highly conserved in homologous cutinase-like PET hydrolases, increased hydrolytic activity on PET was determined when accompanied by the mutation W159H, although the binding cleft width appeared to be narrowed. This phenomenon suggests that the polymer binding in the surface groove is more likely a dynamic rather than static process, as supported by an NMR analysis of PET chain mobility in the context of enzymatic hydrolysis.[115,121] The residue equivalent of the *Is*PETase S238 is F in *Tf*Cut2 and LCC.[52,111] By substitution to A, I, and W, significantly increased PET hydrolysis activity was reported.[16,122] These findings suggest that further systematic iterative engineering of all variable residues in the PET hydrolase binding pocket may be beneficial for gaining a thorough understanding of the rate-limiting interactions with aromatic polyesters and, as a result, improving the overall degradation performance.

Mono(2-hydroxyethyl) terephthalate (MHET) and bis(2-hydroxyethyl) terephthalate (BHET) are degradation intermediates well-known to inhibit the efficiency of depolymerization catalyzed by various PET hydrolases, except for *Hi*C and Cut190.[50,78,123,124] MHET has a stronger inhibitory effect and can hardly be hydrolyzed by the wild-type *Is*PETase.[96] Thus, *I. sakaiensis* produces a distinct MHETase to yield TPA and EG for its growth.[34] This serves as a template for developing a dual enzyme system for effective PET degradation containing an oligo-ester-specific helper enzyme.[123] Recently, a chimeric dual-enzyme system with MHETase linked to *Is*PETase resembling their natural microbial host was established, resulting in PET degradation efficiency improved by at least

https://doi.org/10.1021/acscatal.1c05856
ACS Catal. 2022, 12, 3382−3396

2.8-fold.[125] Additional MHETase-like enzymes from *Comamonas thiooxydans* and *Hydrogenophaga sp*. PML113[125] and an enzyme from a marine consortium[126] with similar structures but considerably lower substrate affinity for MHET than the *Is*MHETase[127] were also identified. This distinction in catalytic characteristics may provide a wide range of choices for combining with other depolymerizing enzymes, particularly for the use in whole cell-based multiple enzyme systems.[128,129] While *Is*PETase has been successfully stabilized, additionally thermostabilizing MHETase-like enzymes would provide a robust two-enzyme system with industrial promise. Other technical solutions have been proposed in this regard, such as employing enzyme mutants that are less susceptible to product inhibition[99] or a membrane reactor for continuous removal of the inhibitors.[130]

4. ENGINEERING ENZYMATIC DE/ADSORPTION ONTO PET SURFACES BY INCLUDING BINDING MODULES

To resemble other natural polymer degrading enzymes, specific polymer binding modules were either directly added in the reaction mixture or covalently fused to appropriate PET hydrolases. Among these, the cellulose-binding domains (CBM) CenA from *Cellulomonas fimi*[104] and that of cellobiohydrolase I from *Trichoderma reesei*,[100,131] the polyhydroxyalkanoate (PHA)-binding module of PHA depolymerase from *Alcaligenes faecalis*,[100] and the chitin-binding module from the chitinase CmChi1 from *Chitinolyticbacter meiyuanensis* SYBCH1[103] increased the degradation performance when they were fused to the C-termini of PET hydrolases (Table 2). Selected tryptophan residues in CBMs were identified as mutation hot spots for enhanced hydrogen bond formation with aromatic moieties at the PET surface.[104,132]

Hydrophobins are small amphiphilic proteins (about 20 kDa) produced by filamentous fungi with surfactant-like activity.[133] Although the highest boosting effect with hydrophobins was discovered when fused to a PET hydrolase, they can already improve the enzymatic binding affinity to the PET surface when introduced to the degradation mixtures as free molecules or applied to material as a pretreatment.[134−136]

In this regard, the lytic polysaccharide monooxygenase (LPMO) from the white-rot fungus *Pycnoporus coccineus* (PcAA14A)[137] and a zwitterionic polymer based on positively charged lysine and negatively charged glutamate[138] were both recently shown to improve PET degradation performance when added to *Is*PETase. LPMO and the so-called EKylation, on the other hand, appear to promote the enzymatic degradation via different mechanisms than hydrophobins or other binding modules.

While the necessity of binding modules for effective cellulase-catalyzed cellulose degradation has been questioned,[139] their presence was recently found to alter the binding and hydrolysis kinetics at various solid loading levels.[140] The CBM was shown to favor low solid loading level in an adsorption-controlled scenario where higher catalytic efficiency is associated with tighter substrate binding but disfavored at high substrate concentrations, as shown by a so-called "volcano plot" of specific reaction rates against the binding strengths.[140] Accordingly, optimal PET hydrolases are suspected to also follow this Sabatier principle and will function at an intermediate substrate binding strength. Future research should be conducted to confirm this hypothesis based on comprehensive binding and hydrolysis kinetic studies with various PET hydrolases, as well as those containing artificially introduced polymer binding modules, to clarify their roles for the interfacial biocatalysis, which is obviously missing so far. This is of great interest for potential industrial applications, where a very high solid loading level is generally preferred, in terms of an economical use of biocatalysts.

5. CONCLUDING REMARKS AND FUTURE PERSPECTIVES

More than 16 years have elapsed since the first microbial PET hydrolase was reported. Many research efforts have been expended in the quest for new PET hydrolases as well as in the optimization of known enzymes. A large number of high-quality studies have been conducted using a few benchmark enzymes, such as cutinase(-like) enzymes from *Thermobifida* species,[141] the plant compost-derived LCC cutinase, and *Is*PETase. Different research groups employed varying experimental conditions, such as pH, buffer compositions (different salts) and concentrations (different ionic strengths), and agitation techniques and speeds, making a balanced comparison of the degradation data very challenging, even when the same benchmark enzyme was used. Selected experimental parameters can also have a significant impact on the degradation performance as well as the related data interpretation in terms of interfacial biocatalysis mechanisms. For example, buffer salts can influence the enzyme performance[142] and the solubility of degradation products or inhibitors,[143] and they can also fundamentally modify the water interaction with polymeric substrates.[144] When simultaneous mechanical treatment is occurring, the ideal water volume for enzymatic PET degradation can vary dramatically.[44] More crucially, studies employed PET materials from various suppliers, with varying crystallinity (even that of the widely used amorphous Goodfellow PET film may differ from batch to batch) and in various forms (powder, foil, sheet, etc.). As a result, standardization of PET hydrolysis tests and conditions using polymer samples with defined material sources and properties should be applied in future investigations to allow for a straightforward data comparison. Several recent studies used manually picked post-consumer low-crystallinity PET packaging in order to achieve striking enzymatic degradation performance at a small laboratory scale.[88,145] However, in a real-world scenario, post-consumer PET packaging with all crystallinity patterns ends up in mixed household plastic waste which is collected and then separated in an industrial plastic sorting system according to polymer type and color, but not crystallinity.[146,147] To remove the contaminants which may hamper the subsequent recycling process, a washing step (e.g., with hot soda water) is usually applied prior to thermomechanical reprocessing (e.g., shredding and drying).[148] These processes will age the sorted waste polymer considerably and consequently eliminate the low-crystallinity fraction of PET. Following additional amorphization and micronization steps, these waste plastic flakes can be readily used for biotechnological recycling.[16,92] Therefore, for lab-scale research in the field of PET hydrolases, using equally pretreated real-world PET waste (e.g., with the same amorphization and micronization equipment and protocols) instead of biased selection of a low-crystallinity fraction will deliver more reliable standardized data on the enzymatic degradation performance of industrial relevance.

As an alternative to the energy-consuming amorphization step,[92] the challenge in lowering the polymer crystallinity is

https://doi.org/10.1021/acscatal.1c05856
ACS Catal. 2022, 12, 3382−3396

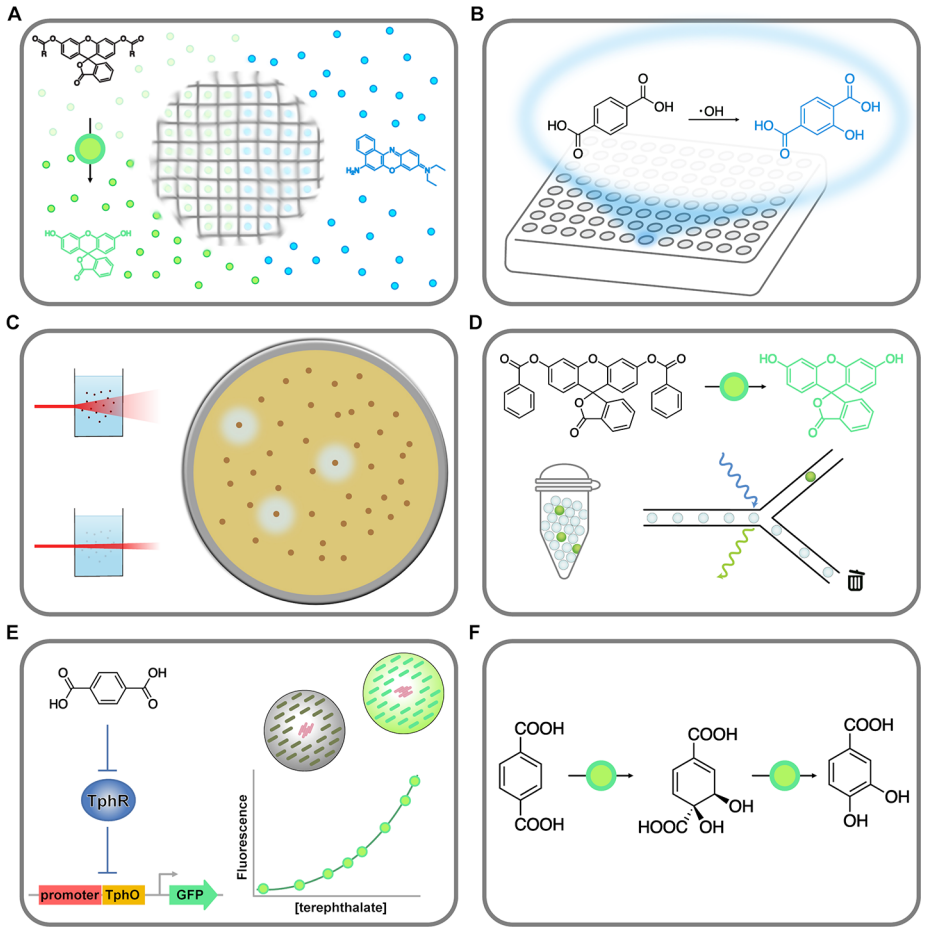

Figure 4. Potential PET hydrolase screening methods arranged in order of increasing potential throughput. (A) Fluorogenic substrates like fluorescein dilaurate can be trapped in polyester films or particles[175,176] and can be released and hydrolyzed upon polymer hydrolysis, generating a fluorescence signal. (B) Fluorimetric method based on the reaction of terephthalic acid with hydroxyl radicals to form the fluorophore 2-hydroxyterephthalic acid.[177−179] Tens of thousands of clones can be screened using microtiter plate-based assays (A, B). (C) Agar plate assay based on the hydrolysis of polyester (PET) nanoparticles.[75,180,181] Clear zones (halos) form around clones expressing active polyester-hydrolyzing enzymes, allowing simple visual identification. Millions of clones can easily be screened using this method. (D) Recently reported ultra-high-throughput droplet-based assay for PETase activity.[182] The use of the fluorogenic surrogate substrate fluorescein dibenzoate indicates a low selectivity, since many other esterases would also be identified using this assay. Tens of millions of clones could be analyzed using this method. Combinations of the turbidimetric assay (C) and droplet-based methods (D) seem promising. (E) Ultra-high-throughput assay based on a terephthalic acid biosensor.[183] Cells could be entrapped in hydrogel beads[184] containing reporter cells that express GFP in response to terephthalic acid formed by clones expressing active PET-hydrolyzing enzymes. Because fluorescence-activated cell sorting (FACS) can be used to sort the beads, the throughput of this method is potentially in the hundreds of millions. (F) Envisaged growth selection approach based on the conversion of terephthalic acid to protocatechuic acid, which could be catabolized by engineered strains of *E. coli* or other model organisms.[183,185] The throughput of this method would be limited only by library size and transformation efficiencies, making it one of the most attractive methods.

envisaged to be possibly solved with a specific crystalline PET depolymerase, like those found in natural cellulase systems to decrystallize cellulose.[149] To this end, continuously growing PET hydrolase sequence data from large-scale sequencing projects can be used for exploring this missing enzyme activity and other novel PET hydrolases in genomic and metagenomic databases. EnzymeMiner and other available *in silico* tools provide useful computational platforms for automated identification of promising enzyme candidates for experimental validation.[150] Pan-genome analysis focusing on microbes which produce known PET hydrolases, e.g., in the *Thermobifida* and *Ideonella* genera, could facilitate finding yet-unknown MHETase-like enzymes to address the product-inhibition problem. Nevertheless, as the substrates of identified PET hydrolases and carbon sources for the host strains are unlikely to be synthetic polyester in their natural habitats, the probability of success of such a research activity is hard to predict. The explored sequence space can also be used to predict enzymes with improved properties by machine learning and ancestral sequence reconstruction.[151−153] Robust proteins can be designed by sequence-based approaches and fully automated computational workflows, like FireProt^{ASR}, making complex protocols of ancestral inference accessible to nonexperts.[154] Recent developments of highly accurate protein structure prediction methods, like AlphaFold2 and RoseTTA-Fold, can assist a structure-based design of novel PET hydrolases identified by database searches.[155−157] While hydrolytic biocatalysis might fundamentally be unable to crack the well-ordered crystalline PET, oxidative enzymes, which may have a mechanistically comparable function to LPMOs known from lignin and cellulose degrading systems,[158] can offer further options for mining for polyester decrystallizing activities.

https://doi.org/10.1021/acscatal.1c05856
ACS Catal. 2022, 12, 3382−3396

High-quality structures incorporating PET relevant ligands will be required for further understanding of the structure−function relationship and related engineering of PET hydrolases. Application of novel cryoEM techniques to examine the binding of bigger polymer substrates may be required for a thorough understanding of the substrate−enzyme interaction at the solid−liquid interface. To date, these mechanistic insights have primarily been derived from docking and simulation experiments using flexible PET oligomers, which overlook the inherent mobility and steric constraints given by neighboring polymers under realistic reaction conditions. The utilization of particular force fields designed for interface reactions, as well as taking into account real-world material properties, will help *in silico* protein engineering even more.[159] The calculated energy barriers for PET hydrolysis are balanced for individual reaction stages (Figure 3), implying that more than one catalytic step would need to be enhanced at the same time. This is typically difficult to address rationally, providing room for directed evolution and machine learning. Hence, the future development of suitable screening assays applicable to large enzyme libraries is of particular relevance in this regard. Due to technical limitations of individual approaches, achieving ultra-high-throughput screening specifically for PET degradation activity still remains a challenge (Figure 4).

Furthermore, researchers may investigate the power and specific advantages of using biocatalysts over chemical catalysts, such as when combined with living cells as whole-cell catalysts, which can potentially allow for a one-pot process that simultaneously includes an enzyme cascade not only to degrade the plastics but also to convert the degradation intermediates into a variety of products with added value.[32] The utility of mesophilic enzymes can potentially be reemphasized using such a procedure, because numerous metabolic pathways converting monomers to other value-added compounds are currently only available/engineerable in mesophilic microbial frameworks. Aside from the well-engineered frameworks such as *Pseudomonas putida*, *E. coli*, and *P. pastoris*,[160−164] *I. sakaiensis* has recently emerged as a new promising strain for genomic engineering with considerably high conversion efficiency from PET substrates to PHA biopolymers.[37,129] On the other hand, thermophilic whole-cell biocatalysts such as *Clostridium thermocellum* can be easily employed for faster PET depolymerization, for example, targeting textile waste also containing cellulose, which may be degraded and valorized simultaneously.[21,165] For more details regarding the biotechnological potential of enzymatic textile recycling, readers are referred to a recent comprehensive review by Jönsson et al.[21] In this regard, designing the PET degrading multienzyme complex by combining the advantages of various enzyme classes to resemble an architecture similar to the natural cellulosome might be a viable option.[128]

A photosynthetic microalga, *Phaeodactylum tricornutum*, has been engineered to functionally express *Is*PETase and is able to degrade selected PET-related materials in a saltwater environment at 21−30 °C.[166] This has been suggested to be a potential bioremediation approach for seawater polluted by PET microplastics, although the conversion rate was very low and the application of genetically engineered microorganisms in an open environment is currently strictly forbidden worldwide.[9] Although a recent study has reported wild-type marine microbes with PET-metabolizing activity,[167] microplastics present in aquatic ecosystems can hardly support microbial growth and will therefore remain as persistent xenobiotics that cannot be remediated easily.[168]

Scientists have thus far succeeded in identifying and creating biocatalysts that appear to fit the need for PET waste depolymerization on an industrial and commercial scale. The fundamental understanding of interfacial biocatalysis on PET should be extended and transferred to address the challenges associated with the biotechnological degradation of other more abundant plastics such as polyolefins or more similar plastics such as polyamides (PA) and polyurethanes (PUR) with hydrolyzable backbones.[21,32,169] While the breakdown of carbon−carbon backbones in polyolefins can be energetically very challenging,[170,171] chemical and thermal pretreatments have been shown to enable subsequent biochemical transformation[172,173] and thus should be extensively studied in future research. On the other hand, the identification of putative PUR or PA hydrolases is envisioned as a result of collaborative large-scale research activities (e.g., the MIX-UP project[174] and the upPE-T project) on plastic recycling. A combination of these novel biocatalysts will pave a new path for the valorization of unsorted mixed plastic waste that cannot be efficiently recycled via other disposal approaches at an industrial scale.

AUTHOR INFORMATION

Corresponding Authors

Uwe T. Bornscheuer − *Institute of Biochemistry, Department of Biotechnology & Enzyme Catalysis, University of Greifswald, D-17487 Greifswald, Germany;* orcid.org/0000-0003-0685-2696; Email: uwe.bornscheuer@uni-greifswald.de

Ren Wei − *Institute of Biochemistry, Department of Biotechnology & Enzyme Catalysis, University of Greifswald, D-17487 Greifswald, Germany;* orcid.org/0000-0003-3876-1350; Email: ren.wei@uni-greifswald.de

Authors

Gerlis von Haugwitz − *Institute of Biochemistry, Department of Biotechnology & Enzyme Catalysis, University of Greifswald, D-17487 Greifswald, Germany*

Lara Pfaff − *Institute of Biochemistry, Department of Biotechnology & Enzyme Catalysis, University of Greifswald, D-17487 Greifswald, Germany*

Jan Mican − *Loschmidt Laboratories, Department of Experimental Biology and RECETOX, Faculty of Science, Masaryk University, 625 00 Brno, Czech Republic; International Clinical Research Center, St. Anne's University Hospital and Faculty of Medicine, Masaryk University, 656 91 Brno, Czech Republic*

Christoffel P. S. Badenhorst − *Institute of Biochemistry, Department of Biotechnology & Enzyme Catalysis, University of Greifswald, D-17487 Greifswald, Germany;* orcid.org/0000-0002-5874-4577

Weidong Liu − *Tianjin Institute of Industrial Biotechnology, Chinese Academy of Sciences, Tianjin 300308, China*

Gert Weber − *Macromolecular Crystallography, Helmholtz-Zentrum Berlin für Materialien und Energie, D-12489 Berlin, Germany;* orcid.org/0000-0003-3624-1060

Harry P. Austin − *Institute of Biochemistry, Department of Biotechnology & Enzyme Catalysis, University of Greifswald, D-17487 Greifswald, Germany*

David Bednar − *Loschmidt Laboratories, Department of Experimental Biology and RECETOX, Faculty of Science,*

https://doi.org/10.1021/acscatal.1c05856
ACS Catal. 2022, 12, 3382−3396

Masaryk University, 625 00 Brno, Czech Republic; International Clinical Research Center, St. Anne's University Hospital and Faculty of Medicine, Masaryk University, 656 91 Brno, Czech Republic

Jiri Damborsky − *Loschmidt Laboratories, Department of Experimental Biology and RECETOX, Faculty of Science, Masaryk University, 625 00 Brno, Czech Republic; International Clinical Research Center, St. Anne's University Hospital and Faculty of Medicine, Masaryk University, 656 91 Brno, Czech Republic*

Complete contact information is available at: https://pubs.acs.org/10.1021/acscatal.1c05856

Notes

The authors declare no competing financial interest.

■ ACKNOWLEDGMENTS

The authors gratefully acknowledge the financial support received from the European Union's Horizon 2020 research and innovation program (MIX-UP, grant number 870294; upPE-T, grant number 953214; CETOCOEN Excellence, grant number 857560), from the Czech Ministry of Education (CZ.02.1.01/0.0/0.0/16_026/0008451) and the Alexander von Humboldt foundation.

■ REFERENCES

(1) Brown, B. S.; Mills, J.; Hulse, J. M. Chemical and Biological Degradation of Waste Plastics. *Nature* **1974**, *250*, 161−163.
(2) Wong, C. S.; Green, D. R.; Cretney, W. J. Quantitative Tar and Plastic Waste Distributions in the Pacific Ocean. *Nature* **1974**, *247*, 30−32.
(3) Borrelle, S. B.; Ringma, J.; Law, K. L.; Monnahan, C. C.; Lebreton, L.; McGivern, A.; Murphy, E.; Jambeck, J.; Leonard, G. H.; Hilleary, M. A.; Eriksen, M.; Possingham, H. P.; Frond, H. D.; Gerber, L. R.; Polidoro, B.; Tahir, A.; Bernard, M.; Mallos, N.; Barnes, M.; Rochman, C. M. Predicted Growth in Plastic Waste Exceeds Efforts to Mitigate Plastic Pollution. *Science* **2020**, *369*, 1515−1518.
(4) MacLeod, M.; Arp, H. P. H.; Tekman, M. B.; Jahnke, A. The Global Threat from Plastic Pollution. *Science* **2021**, *373*, 61−65.
(5) Meys, R.; Kätelhön, A.; Bachmann, M.; Winter, B.; Zibunas, C.; Suh, S.; Bardow, A. Achieving Net-Zero Greenhouse Gas Emission Plastics by a Circular Carbon Economy. *Science* **2021**, *374*, 71−76.
(6) Ellis, L. D.; Rorrer, N. A.; Sullivan, K. P.; Otto, M.; McGeehan, J. E.; Román-Leshkov, Y.; Wierckx, N.; Beckham, G. T. Chemical and Biological Catalysis for Plastics Recycling and Upcycling. *Nat. Catal.* **2021**, *4*, 539−556.
(7) Kakadellis, S.; Rosetto, G. Achieving a Circular Bioeconomy for Plastics. *Science* **2021**, *373*, 49−50.
(8) Coates, G. W.; Getzler, Y. D. Y. L. Chemical Recycling to Monomer for an Ideal, Circular Polymer Economy. *Nat. Rev. Mater.* **2020**, *5*, 501−516.
(9) Wei, R.; Tiso, T.; Bertling, J.; O'Connor, K.; Blank, L. M.; Bornscheuer, U. T. Possibilities and Limitations of Biotechnological Plastic Degradation and Recycling. *Nat. Catal.* **2020**, *3*, 867−871.
(10) Cornwall, W. The Plastic Eaters. *Science* **2021**, *373*, 36−39.
(11) Geyer, R.; Jambeck, J. R.; Law, K. L. Production, Use, and Fate of All Plastics Ever Made. *Sci. Adv.* **2017**, *3*, No. e1700782.
(12) Inderthal, H.; Tai, S. L.; Harrison, S. T. L. Non-Hydrolyzable Plastics - an Interdisciplinary Look at Plastic Bio-Oxidation. *Trends Biotechnol.* **2021**, *39*, 12−23.
(13) Li, Z.; Wei, R.; Gao, M.; Ren, Y.; Yu, B.; Nie, K.; Xu, H.; Liu, L. Biodegradation of Low-Density Polyethylene by *Microbulbifer hydrolyticus* IRE-31. *J. Environ. Manage.* **2020**, *263*, 110402.
(14) Yoon, M.-Y.; Kellis, J.; Poulose, A. J. Enzymatic Modification of Polyester. *AATCC Review* **2002**, *2*, 33−36.
(15) Wei, R.; Zimmermann, W. Biocatalysis as a Green Route for Recycling the Recalcitrant Plastic Polyethylene Terephthalate. *Microb. Biotechnol.* **2017**, *10*, 1302−1307.
(16) Tournier, V.; Topham, C. M.; Gilles, A.; David, B.; Folgoas, C.; Moya-Leclair, E.; Kamionka, E.; Desrousseaux, M. L.; Texier, H.; Gavalda, S.; Cot, M.; Guémard, E.; Dalibey, M.; Nomme, J.; Cioci, G.; Barbe, S.; Chateau, M.; André, I.; Duquesne, S.; Marty, A. An Engineered PET Depolymerase to Break Down and Recycle Plastic Bottles. *Nature* **2020**, *580*, 216−219.
(17) Kawai, F. Emerging Strategies in Polyethylene Terephthalate Hydrolase Research for Biorecycling. *ChemSusChem* **2021**, *14*, 4115−4122.
(18) Jog, J. P. Crystallization of Polyethyleneterephthalate. *J. Macromol. Sci. Part C* **1995**, *35*, 531−553.
(19) Xin, J.; Zhang, Q.; Huang, J.; Huang, R.; Jaffery, Q. Z.; Yan, D.; Zhou, Q.; Xu, J.; Lu, X. Progress in the Catalytic Glycolysis of Polyethylene Terephthalate. *J. Environ. Manage.* **2021**, *296*, 113267.
(20) Welle, F. Twenty Years of PET Bottle to Bottle Recycling—an Overview. *Resour. Conserv. Recycl.* **2011**, *55*, 865−875.
(21) Jönsson, C.; Wei, R.; Biundo, A.; Landberg, J.; Schwarz Bour, L.; Pezzotti, F.; Toca, A.; M. Jacques, L.; Bornscheuer, U. T.; Syrén, P.-O. Biocatalysis in the Recycling Landscape for Synthetic Polymers and Plastics Towards Circular Textiles. *ChemSusChem* **2021**, *14*, 4028−4040.
(22) Nicholson, S. R.; Rorrer, N. A.; Carpenter, A. C.; Beckham, G. T. Manufacturing Energy and Greenhouse Gas Emissions Associated with Plastics Consumption. *Joule* **2021**, *5*, 673−686.
(23) Karacan, I. An in Depth Study of Crystallinity, Crystallite Size and Orientation Measurements of a Selection of Poly(Ethylene Terephthalate)Fibers. *Fibers Polym.* **2005**, *6*, 186−199.
(24) Bashir, Z.; Al-Aloush, I.; Al-Raqibah, I.; Ibrahim, M. Evaluation of Three Methods for the Measurement of Crystallinity of PET Resins, Preforms, and Bottles. *Polym. Eng. Sci.* **2000**, *40*, 2442−2455.
(25) Webb, H. K.; Arnott, J.; Crawford, R. J.; Ivanova, E. P. Plastic Degradation and Its Environmental Implications with Special Reference to Poly(Ethylene Terephthalate). *Polymers* **2013**, *5*, 1−18.
(26) Suaria, G.; Achtypi, A.; Perold, V.; Lee, J. R.; Pierucci, A.; Bornman, T. G.; Aliani, S.; Ryan, P. G. Microfibers in Oceanic Surface Waters: A Global Characterization. *Sci. Adv.* **2020**, *6*, No. eaay8493.
(27) Deng, H.; Wei, R.; Luo, W.; Hu, L.; Li, B.; Di, Y.; Shi, H. Microplastic Pollution in Water and Sediment in a Textile Industrial Area. *Environ. Pollut.* **2020**, *258*, 113658.
(28) Worm, B.; Lotze, H. K.; Jubinville, I.; Wilcox, C.; Jambeck, J. Plastic as a Persistent Marine Pollutant. *Annu. Rev. Environ. Resour.* **2017**, *42*, 1−26.
(29) Tokiwa, Y.; Suzuki, T. Hydrolysis of Polyesters by Lipases. *Nature* **1977**, *270*, 76−78.
(30) Sato, M. Deterioration of Filaments and Films of Polyethyleneterephthalate with Enzyme of *Cladosporium Cladosporioides* FERM J-8. *Sen-i Gakkaishi* **1983**, *39*, 67−77.
(31) Mueller, R.-J.; Schrader, H.; Profe, J.; Dresler, K.; Deckwer, W.-D. Enzymatic Degradation of Poly(Ethylene Terephthalate): Rapid Hydrolyse Using a Hydrolase from *T. fusca*. *Macromol. Rapid Commun.* **2005**, *26*, 1400−1405.
(32) Tiso, T.; Winter, B.; Wei, R.; Hee, J.; de Witt, J.; Wierckx, N.; Quicker, P.; Bornscheuer, U. T.; Bardow, A.; Nogales, J.; Blank, L. M. The Metabolic Potential of Plastics as Biotechnological Carbon Sources − Review and Targets for the Future. *Metab. Eng.* **2021**, 1 DOI: 10.1016/j.ymben.2021.12.006.
(33) Sulaiman, S.; Yamato, S.; Kanaya, E.; Kim, J. J.; Koga, Y.; Takano, K.; Kanaya, S. Isolation of a Novel Cutinase Homolog with Polyethylene Terephthalate-Degrading Activity from Leaf-Branch Compost by Using a Metagenomic Approach. *Appl. Environ. Microbiol.* **2012**, *78*, 1556−1562.
(34) Yoshida, S.; Hiraga, K.; Takehana, T.; Taniguchi, I.; Yamaji, H.; Maeda, Y.; Toyohara, K.; Miyamoto, K.; Kimura, Y.; Oda, K. A Bacterium That Degrades and Assimilates Poly(Ethylene Terephthalate). *Science* **2016**, *351*, 1196−1199.

(35) Kan, Y.; He, L.; Luo, Y.; Bao, R. *Is*PETase Is a Novel Biocatalyst for Poly(Ethylene Terephthalate) (PET) Hydrolysis. *ChemBioChem.* **2021**, *22*, 1706−1716.
(36) Bornscheuer, U. T. Feeding on Plastic. *Science* **2016**, *351*, 1154−1155.
(37) Fujiwara, R.; Sanuki, R.; Ajiro, H.; Fukui, T.; Yoshida, S. Direct Fermentative Conversion of Poly(Ethylene Terephthalate) into Poly(Hydroxyalkanoate) by *Ideonella sakaiensis*. *Sci. Rep.* **2021**, *11*, 19991.
(38) Kawai, F.; Kawabata, T.; Oda, M. Current State and Perspectives Related to the Polyethylene Terephthalate Hydrolases Available for Biorecycling. *ACS Sustain. Chem. Eng.* **2020**, *8*, 8894−8908.
(39) Wei, Y.; Swenson, L.; Castro, C.; Derewenda, U.; Minor, W.; Arai, H.; Aoki, J.; Inoue, K.; Servin-Gonzalez, L.; Derewenda, Z. S. Structure of a Microbial Homologue of Mammalian Platelet-Activating Factor Acetylhydrolases: *Streptomyces exfoliatus* Lipase at 1.9 Å Resolution. *Structure* **1998**, *6*, 511−519.
(40) Carr, P. D.; Ollis, D. L. Alpha/Beta Hydrolase Fold: An Update. *Protein Pept. Lett.* **2009**, *16*, 1137−1148.
(41) Chen, S.; Su, L.; Chen, J.; Wu, J. Cutinase: Characteristics, Preparation, and Application. *Biotechnol. Adv.* **2013**, *31*, 1754−1767.
(42) Ronkvist, Ã. S. M.; Xie, W.; Lu, W.; Gross, R. A. Cutinase-Catalyzed Hydrolysis of Poly(Ethylene Terephthalate). *Macromolecules* **2009**, *42*, 5128−5138.
(43) de Castro, A. M.; Carniel, A.; Nicomedes Junior, J.; da Conceição Gomes, A.; Valoni, É. Screening of Commercial Enzymes for Poly(Ethylene Terephthalate) (PET) Hydrolysis and Synergy Studies on Different Substrate Sources. *J. Ind. Microbiol. Biotechnol.* **2017**, *44*, 835−844.
(44) Kaabel, S.; Therien, J. P. D.; Deschênes, C. E.; Duncan, D.; Friščić, T.; Auclair, K. Enzymatic Depolymerization of Highly Crystalline Polyethylene Terephthalate Enabled in Moist-Solid Reaction Mixtures. *Proc. Nat. Acad. Sci. U.S.A.* **2021**, *118*, No. e2026452118.
(45) Carniel, A.; Gomes, A. d. C.; Coelho, M. A. Z.; de Castro, A. M. Process Strategies to Improve Biocatalytic Depolymerization of Post-Consumer PET Packages in Bioreactors, and Investigation on Consumables Cost Reduction. *Bioprocess Biosyst. Eng.* **2021**, *44*, 507−516.
(46) Mueller, R.-J. Biological Degradation of Synthetic Polyesters–Enzymes as Potential Catalysts for Polyester Recycling. *Process Biochem.* **2006**, *41*, 2124−2128.
(47) Maurya, A.; Bhattacharya, A.; Khare, S. K. Enzymatic Remediation of Polyethylene Terephthalate (PET)−Based Polymers for Effective Management of Plastic Wastes: An Overview. *Front. Bioeng. Biotechnol.* **2020**, *8*, 602325.
(48) Takashima, S.; Ohno, M.; Hidaka, M.; Nakamura, A.; Masaki, H.; Uozumi, T. Correlation between Cellulose Binding and Activity of Cellulose-Binding Domain Mutants of *Humicola grisea* Cellobiohydrolase 1. *FEBS Lett.* **2007**, *581*, 5891−5896.
(49) Hsieh, C.-W. C.; Cannella, D.; Jørgensen, H.; Felby, C.; Thygesen, L. G. Cellulase Inhibition by High Concentrations of Monosaccharides. *J. Agric. Food Chem.* **2014**, *62*, 3800−3805.
(50) Barth, M.; Oeser, T.; Wei, R.; Then, J.; Schmidt, J.; Zimmermann, W. Effect of Hydrolysis Products on the Enzymatic Degradation of Polyethylene Terephthalate Nanoparticles by a Polyester Hydrolase from *Thermobifida fusca*. *Biochem. Eng. J.* **2015**, *93*, 222−228.
(51) Carniel, A.; Waldow, V. d. A.; Castro, A. M. d. A Comprehensive and Critical Review on Key Elements to Implement Enzymatic PET Depolymerization for Recycling Purposes. *Biotechnol. Adv.* **2021**, *52*, 107811.
(52) Sulaiman, S.; You, D. J.; Kanaya, E.; Koga, Y.; Kanaya, S. Crystal Structure and Thermodynamic and Kinetic Stability of Metagenome-Derived LC-Cutinase. *Biochemistry* **2014**, *53*, 1858−1869.
(53) Wei, R.; Breite, D.; Song, C.; Gräsing, D.; Ploss, T.; Hille, P.; Schwerdtfeger, R.; Matysik, J.; Schulze, A.; Zimmermann, W. Biocatalytic Degradation Efficiency of Postconsumer Polyethylene Terephthalate Packaging Determined by Their Polymer Microstructures. *Adv. Sci.* **2019**, *6*, 1900491.
(54) Son, H. F.; Cho, I. J.; Joo, S.; Seo, H.; Sagong, H.-Y.; Choi, S. Y.; Lee, S. Y.; Kim, K.-J. Rational Protein Engineering of Thermo-Stable PETase from *Ideonella sakaiensis* for Highly Efficient PET Degradation. *ACS Catal.* **2019**, *9*, 3519−3526.
(55) Cui, Y.; Chen, Y.; Liu, X.; Dong, S.; Tian, Y. e.; Qiao, Y.; Mitra, R.; Han, J.; Li, C.; Han, X.; Liu, W.; Chen, Q.; Wei, W.; Wang, X.; Du, W.; Tang, S.; Xiang, H.; Liu, H.; Liang, Y.; Houk, K. N.; Wu, B. Computational Redesign of a PETase for Plastic Biodegradation under Ambient Condition by the GRAPE Strategy. *ACS Catal.* **2021**, *11*, 1340−1350.
(56) Brott, S.; Pfaff, L.; Schuricht, J.; Schwarz, J.-N.; Böttcher, D.; Badenhorst, C. P. S.; Wei, R.; Bornscheuer, U. T. Engineering and Evaluation of Thermostable *Is*PETase Variants for PET Degradation. *Eng. Life Sci.* **2021**, 1 DOI: 10.1002/elsc.202100105.
(57) Witt, U.; Yamamoto, M.; Seeliger, U.; Müller, R.-J.; Warzelhan, V. Biodegradable Polymeric Materials—Not the Origin but the Chemical Structure Determines Biodegradability. *Angew. Chem., Int. Ed.* **1999**, *38*, 1438−1442.
(58) Marten, E.; Müller, R.-J.; Deckwer, W.-D. Studies on the Enzymatic Hydrolysis of Polyesters. II. Aliphatic-Aromatic Copolyesters. *Polym. Degrad. Stab.* **2005**, *88*, 371−381.
(59) Keller, A.; Lester, G. R.; Morgan, L. B. Crystallization Phenomena in Polymers. I. Preliminary Investigation of the Crystallization Characteristics of Polyethylene Terephthalate. *Philos. Trans. Royal Soc. A* **1954**, *247*, 1−12.
(60) Langevin, D.; Grenet, J.; Saiter, J. M. Moisture Sorption in PET Influence on the Thermokinetic Parameters. *Eur. Polym. J.* **1994**, *30*, 339−345.
(61) Alves, N. M.; Mano, J. F.; Balaguer, E.; Meseguer Dueñas, J. M.; Gómez Ribelles, J. L. Glass Transition and Structural Relaxation in Semi-Crystalline Poly(Ethylene Terephthalate): A DSC Study. *Polymer* **2002**, *43*, 4111−4122.
(62) Wellen, R. M. R.; Canedo, E.; Rabello, M. S. Nonisothermal Cold Crystallization of Poly(Ethylene Terephthalate). *J. Mater. Res.* **2011**, *26*, 1107−1115.
(63) Wei, R.; Oeser, T.; Barth, M.; Weigl, N.; Lübs, A.; Schulz-Siegmund, M.; Hacker, M.; Zimmermann, W. Turbidimetric Analysis of the Enzymatic Hydrolysis of Polyethylene Terephthalate Nanoparticles. *J. Mol. Catal. B-Enzym.* **2014**, *103*, 72−78.
(64) Gamerith, C.; Zartl, B.; Pellis, A.; Guillamot, F.; Marty, A.; Acero, E. H.; Guebitz, G. M. Enzymatic Recovery of Polyester Building Blocks from Polymer Blends. *Process Biochem.* **2017**, *59*, 58−64.
(65) Austin, H. P.; Allen, M. D.; Donohoe, B. S.; Rorrer, N. A.; Kearns, F. L.; Silveira, R. L.; Pollard, B. C.; Dominick, G.; Duman, R.; El Omari, K.; Mykhaylyk, V.; Wagner, A.; Michener, W. E.; Amore, A.; Skaf, M. S.; Crowley, M. F.; Thorne, A. W.; Johnson, C. W.; Woodcock, H. L.; McGeehan, J. E.; Beckham, G. T. Characterization and Engineering of a Plastic-Degrading Aromatic Polyesterase. *Proc. Nat. Acad. Sci. U.S.A.* **2018**, *115*, E4350−E4357.
(66) Ito, E.; Kobayashi, Y. Effects of Absorbed Water on Physical Properties of Polyesters. *J. Appl. Polym. Sci.* **1980**, *25*, 2145−2157.
(67) Jabarin, S. A.; Lofgren, E. A. Effects of Water Absorption on Physical Properties and Degree of Molecular Orientation of Poly (Ethylene Terephthalate). *Polym. Eng. Sci.* **1986**, *26*, 620−625.
(68) Bianchi, R.; Chiavacci, P.; Vosa, R.; Guerra, G. Effect of Moisture on the Crystallization Behavior of PET from the Quenched Amorphous Phase. *J. Appl. Polym. Sci.* **1991**, *43*, 1087−1089.
(69) Launay, A.; Thominette, F.; Verdu, J. Water Sorption in Amorphous Poly(Ethylene Terephthalate). *J. Appl. Polym. Sci.* **1999**, *73*, 1131−1137.
(70) Shinotsuka, K.; Bliznyuk, V. N.; Assender, H. E. Near-Surface Crystallization of PET. *Polymer* **2012**, *53*, 5554−5559.
(71) Zuo, B.; Liu, Y.; Liang, Y.; Kawaguchi, D.; Tanaka, K.; Wang, X. Glass Transition Behavior in Thin Polymer Films Covered with a Surface Crystalline Layer. *Macromolecules* **2017**, *50*, 2061−2068.

(72) Falkenstein, P.; Gräsing, D.; Bielytskyi, P.; Zimmermann, W.; Matysik, J.; Wei, R.; Song, C. UV Pretreatment Impairs the Enzymatic Degradation of Polyethylene Terephthalate. *Front. Microbiol.* **2020**, *11*, 1.
(73) Baker, P. J.; Poultney, C.; Liu, Z.; Gross, R.; Montclare, J. K. Identification and Comparison of Cutinases for Synthetic Polyester Degradation. *Appl. Microbiol. Biotechnol.* **2012**, *93*, 229−240.
(74) Kawai, F. The Current State of Research on PET Hydrolyzing Enzymes Available for Biorecycling. *Catalysts* **2021**, *11*, 206.
(75) Danso, D.; Schmeisser, C.; Chow, J.; Zimmermann, W.; Wei, R.; Leggewie, C.; Li, X.; Hazen, T.; Streit, W. R. New Insights into the Function and Global Distribution of Polyethylene Terephthalate (PET)-Degrading Bacteria and Enzymes in Marine and Terrestrial Metagenomes. *Appl. Environ. Microbiol.* **2018**, *84*, No. e02773-02717.
(76) Miyakawa, T.; Mizushima, H.; Ohtsuka, J.; Oda, M.; Kawai, F.; Tanokura, M. Structural Basis for the Ca^{2+}-Enhanced Thermostability and Activity of PET-Degrading Cutinase-Like Enzyme from *Saccharomonospora viridis* AHK190. *Appl. Microbiol. Biotechnol.* **2015**, *99*, 4297−4307.
(77) Then, J.; Wei, R.; Oeser, T.; Gerdts, A.; Schmidt, J.; Barth, M.; Zimmermann, W. A Disulfide Bridge in the Calcium Binding Site of a Polyester Hydrolase Increases Its Thermal Stability and Activity against Polyethylene Terephthalate. *FEBS Open Bio* **2016**, *6*, 425−432.
(78) Oda, M.; Yamagami, Y.; Inaba, S.; Oida, T.; Yamamoto, M.; Kitajima, S.; Kawai, F. Enzymatic Hydrolysis of PET: Functional Roles of Three Ca^{2+} Ions Bound to a Cutinase-Like Enzyme, Cut190*, and Its Engineering for Improved Activity. *Appl. Microbiol. Biotechnol.* **2018**, *102*, 10067−10077.
(79) Then, J.; Wei, R.; Oeser, T.; Barth, M.; Belisário-Ferrari, M. R.; Schmidt, J.; Zimmermann, W. Ca^{2+} and Mg^{2+} Binding Site Engineering Increases the Degradation of Polyethylene Terephthalate Films by Polyester Hydrolases from *Thermobifida fusca*. *Biotechnol. J.* **2015**, *10*, 592−598.
(80) Numoto, N.; Kamiya, N.; Bekker, G.-J.; Yamagami, Y.; Inaba, S.; Ishii, K.; Uchiyama, S.; Kawai, F.; Ito, N.; Oda, M. Structural Dynamics of the PET-Degrading Cutinase-Like Enzyme from *Saccharomonospora viridis* AHK190 in Substrate-Bound States Elucidates the Ca^{2+}-Driven Catalytic Cycle. *Biochemistry* **2018**, *57*, 5289−5300.
(81) Emori, M.; Numoto, N.; Senga, A.; Bekker, G.-J.; Kamiya, N.; Kobayashi, Y.; Ito, N.; Kawai, F.; Oda, M. Structural Basis of Mutants of PET-Degrading Enzyme from *Saccharomonospora viridis* AHK190 with High Activity and Thermal Stability. *Proteins* **2021**, *89*, 502−511.
(82) Baker, P.; Grossman, R. F. Properties and Reactions of Metal Terephthalates. *J. Vinyl Technol.* **1989**, *11*, 59−61.
(83) Zhong-Johnson, E. Z. L.; Voigt, C. A.; Sinskey, A. J. An Absorbance Method for Analysis of Enzymatic Degradation Kinetics of Poly(Ethylene Terephthalate) Films. *Sci. Rep.* **2021**, *11*, 928.
(84) Nakamura, A.; Kobayashi, N.; Koga, N.; Iino, R. Positive Charge Introduction on the Surface of Thermostabilized PET Hydrolase Facilitates PET Binding and Degradation. *ACS Catal.* **2021**, *11*, 8550−8564.
(85) Xi, X.; Ni, K.; Hao, H.; Shang, Y.; Zhao, B.; Qian, Z. Secretory Expression in *Bacillus subtilis* and Biochemical Characterization of a Highly Thermostable Polyethylene Terephthalate Hydrolase from Bacterium HR29. *Enzyme Microb. Technol.* **2021**, *143*, 109715.
(86) Shirke, A. N.; White, C.; Englaender, J. A.; Zwarycz, A.; Butterfoss, G. L.; Linhardt, R. J.; Gross, R. A. Stabilizing Leaf and Branch Compost Cutinase (LCC) with Glycosylation: Mechanism and Effect on PET Hydrolysis. *Biochemistry* **2018**, *57*, 1190−1200.
(87) Fecker, T.; Galaz-Davison, P.; Engelberger, F.; Narui, Y.; Sotomayor, M.; Parra, L. P.; Ramírez-Sarmiento, C. A. Active Site Flexibility as a Hallmark for Efficient PET Degradation by *I. sakaiensis*PETase. *Biophys. J.* **2018**, *114*, 1302−1312.
(88) Lu, H.; Diaz, D. J.; Czarnecki, N. J.; Zhu, C.; Kim, W.; Shroff, R.; Acosta, D. J.; Alexander, B.; Cole, H.; Zhang, Y. J.; Lynd, N.; Ellington, A. D.; Alper, H. S. Deep Learning Redesign of PETase for Practical PET Degrading Applications. *bioRxiv*, **2021**, DOI: 10.1101/2021.10.10.463845.
(89) Bell, E.; Smithson, R.; Kilbride, S.; Foster, J.; Hardy, F.; Ramachandran, S.; Tedstone, A.; Haigh, S.; Garforth, A.; Day, P.; Levy, C.; Shaver, M.; Green, A. Directed Evolution of an Efficient and Thermostable PET Depolymerase. *ChemRxiv*, **2021**, DOI: 10.26434/chemrxiv-2021-mcjh6.
(90) Erickson, E.; Shakespeare, T. J.; Bratti, F.; Buss, B. L.; Graham, R.; Hawkins, M. A.; König, G.; Michener, W. E.; Miscall, J.; Ramirez, K. J.; Rorrer, N. A.; Zahn, M.; Pickford, A. R.; McGeehan, J. E.; Beckham, G. T. Comparative Performance of PETase as a Function of Reaction Conditions, Substrate Properties, and Product Accumulation. *ChemSusChem* **2022**, *15*, No. e202101932.
(91) Meng, X.; Yang, L.; Liu, H.; Li, Q.; Xu, G.; Zhang, Y.; Guan, F.; Zhang, Y.; Zhang, W.; Wu, N.; Tian, J. Protein Engineering of Stable *Is*PETase for PET Plastic Degradation by Premuse. *Int. J. Biol. Macromol.* **2021**, *180*, 667−676.
(92) Singh, A.; Rorrer, N. A.; Nicholson, S. R.; Erickson, E.; DesVeaux, J. S.; Avelino, A. F. T.; Lamers, P.; Bhatt, A.; Zhang, Y.; Avery, G.; Tao, L.; Pickford, A. R.; Carpenter, A. C.; McGeehan, J. E.; Beckham, G. T. Techno-Economic, Life-Cycle, and Socioeconomic Impact Analysis of Enzymatic Recycling of Poly(Ethylene Terephthalate). *Joule* **2021**, *5*, 2479−2503.
(93) Woodard, L. N.; Grunlan, M. A. Hydrolytic Degradation and Erosion of Polyester Biomaterials. *ACS Macro Lett.* **2018**, *7*, 976−982.
(94) Kari, J.; Andersen, M.; Borch, K.; Westh, P. An Inverse Michaelis−Menten Approach for Interfacial Enzyme Kinetics. *ACS Catal.* **2017**, *7*, 4904−4914.
(95) Vogel, K.; Wei, R.; Pfaff, L.; Breite, D.; Al-Fathi, H.; Ortmann, C.; Estrela-Lopis, I.; Venus, T.; Schulze, A.; Harms, H.; Bornscheuer, U. T.; Maskow, T. Enzymatic Degradation of Polyethylene Terephthalate Nanoplastics Analyzed in Real Time by Isothermal Titration Calorimetry. *Sci. Total Environ.* **2021**, *773*, 145111.
(96) Bååth, J. A.; Borch, K.; Jensen, K.; Brask, J.; Westh, P. Comparative Biochemistry of Four Polyester (PET) Hydrolases. *ChemBioChem.* **2021**, *22*, 1627−1637.
(97) Silva, C.; Da, S.; Silva, N.; Matama, T.; Araujo, R.; Martins, M.; Chen, S.; Chen, J.; Wu, J.; Casal, M.; Cavaco-Paulo, A. Engineered *Thermobifida fusca* Cutinase with Increased Activity on Polyester Substrates. *Biotechnol. J.* **2011**, *6*, 1230−1239.
(98) Wei, R.; Oeser, T.; Then, J.; Kühn, N.; Barth, M.; Schmidt, J.; Zimmermann, W. Functional Characterization and Structural Modeling of Synthetic Polyester-Degrading Hydrolases from *Thermomonospora curvata*. *AMB Express* **2014**, *4*, 44.
(99) Wei, R.; Oeser, T.; Schmidt, J.; Meier, R.; Barth, M.; Then, J.; Zimmermann, W. Engineered Bacterial Polyester Hydrolases Efficiently Degrade Polyethylene Terephthalate Due to Relieved Product Inhibition. *Biotechnol. Bioeng.* **2016**, *113*, 1658−1665.
(100) Ribitsch, D.; Yebra, A. O.; Zitzenbacher, S.; Wu, J.; Nowitsch, S.; Steinkellner, G.; Greimel, K.; Doliska, A.; Oberdorfer, G.; Gruber, C. C.; Gruber, K.; Schwab, H.; Stana-Kleinschek, K.; Acero, E. H.; Guebitz, G. M. Fusion of Binding Domains to *Thermobifida cellulosilytica* Cutinase to Tune Sorption Characteristics and Enhancing PET Hydrolysis. *Biomacromolecules* **2013**, *14*, 1769−1776.
(101) Zumstein, M. T.; Kohler, H.-P. E.; McNeill, K.; Sander, M. Enzymatic Hydrolysis of Polyester Thin Films: Real-Time Analysis of Film Mass Changes and Dissipation Dynamics. *Environ. Sci. Technol.* **2016**, *50*, 197−206.
(102) Weinberger, S.; Haernvall, K.; Scaini, D.; Ghazaryan, G.; Zumstein, M. T.; Sander, M.; Pellis, A.; Guebitz, G. M. Enzymatic Surface Hydrolysis of Poly(Ethylene Furanoate) Thin Films of Various Crystallinities. *Green Chem.* **2017**, *19*, 5381−5384.
(103) Xue, R.; Chen, Y.; Rong, H.; Wei, R.; Cui, Z.; Zhou, J.; Dong, W.; Jiang, M. Fusion of Chitin-Binding Domain from *Chitinolyticbacter meiyuanensis* SYBC-H1 to the Leaf-Branch Compost Cutinase for Enhanced PET Hydrolysis. *Front. Bioeng. Biotechnol.* **2021**, *9*, 762854.
(104) Zhang, Y.; Wang, L.; Chen, J.; Wu, J. Enhanced Activity toward PET by Site-Directed Mutagenesis of *Thermobifida fusca*

Cutinase-CBM Fusion Protein. *Carbohydr. Polym.* **2013**, *97*, 124−129.
(105) Bååth, J. A.; Novy, V.; Carneiro, L. V.; Guebitz, G. M.; Olsson, L.; Westh, P.; Ribitsch, D. Structure-Function Analysis of Two Closely Related Cutinases from *Thermobifida cellulosilytica*. *Biotechnol. Bioeng.* **2022**, *119*, 470−481.
(106) Badino, S. F.; Bååth, J. A.; Borch, K.; Jensen, K.; Westh, P. Adsorption of Enzymes with Hydrolytic Activity on Polyethylene Terephthalate. *Enzyme Microb. Technol.* **2021**, *152*, 109937.
(107) Boneta, S.; Arafet, K.; Moliner, V. QM/MM Study of the Enzymatic Biodegradation Mechanism of Polyethylene Terephthalate. *J. Chem. Inf. Model.* **2021**, *61*, 3041−3051.
(108) Feng, S.; Yue, Y.; Zheng, M.; Li, Y.; Zhang, Q.; Wang, W. *Is*PETase- and *Is*MHETase-Catalyzed Cascade Degradation Mechanism toward Polyethylene Terephthalate. *ACS Sustain. Chem. Eng.* **2021**, *9*, 9823−9832.
(109) Jerves, C.; Neves, R. P. P.; Ramos, M. J.; da Silva, S.; Fernandes, P. A. Reaction Mechanism of the PET Degrading Enzyme PETase Studied with DFT/MM Molecular Dynamics Simulations. *ACS Catal.* **2021**, *11*, 11626−11638.
(110) Zheng, M.; Li, Y.; Dong, W.; Feng, S.; Zhang, Q.; Wang, W. Computational Biotransformation of Polyethylene Terephthalate by Depolymerase: A QM/MM Approach. *J. Hazard. Mater.* **2022**, *423*, 127017.
(111) Roth, C.; Wei, R.; Oeser, T.; Then, J.; Foellner, C.; Zimmermann, W.; Sträter, N. Structural and Functional Studies on a Thermostable Polyethylene Therephtalate Degrading Hydrolase from *Thermobifida fusca*. *Appl. Microbiol. Biotechnol.* **2014**, *98*, 7815−7823.
(112) Joo, S.; Cho, I. J.; Seo, H.; Son, H. F.; Sagong, H.-Y.; Shin, T. J.; Choi, S. Y.; Lee, S. Y.; Kim, K.-J. Structural Insight into Molecular Mechanism of Poly(Ethylene Terephthalate) Degradation. *Nat. Commun.* **2018**, *9*, 382.
(113) da Costa, C. H. S.; dos Santos, A. M.; Alves, C. N.; Martí, S.; Moliner, V.; Santana, K.; Lameira, J. Assessment of the PETase Conformational Changes Induced by Poly(Ethylene Terephthalate) Binding. *Proteins* **2021**, *89*, 1340−1352.
(114) Taniguchi, I.; Yoshida, S.; Hiraga, K.; Miyamoto, K.; Kimura, Y.; Oda, K. Biodegradation of PET: Current Status and Application Aspects. *ACS Catal.* **2019**, *9*, 4089−4105.
(115) Wei, R.; Song, C.; Gräsing, D.; Schneider, T.; Bielytskyi, P.; Böttcher, D.; Matysik, J.; Bornscheuer, U. T.; Zimmermann, W. Conformational Fitting of a Flexible Oligomeric Substrate Does Not Explain the Enzymatic PET Degradation. *Nat. Commun.* **2019**, *10*, 5581.
(116) Han, X.; Liu, W.; Huang, J.-W.; Ma, J.; Zheng, Y.; Ko, T.-P.; Xu, L.; Cheng, Y.-S.; Chen, C.-C.; Guo, R.-T. Structural Insight into Catalytic Mechanism of PET Hydrolase. *Nat. Commun.* **2017**, *8*, 2106.
(117) Chen, C.-C.; Han, X.; Ko, T.-P.; Liu, W.; Guo, R.-T. Structural Studies Reveal the Molecular Mechanism of PETase. *FEBS J.* **2018**, *285*, 3717−3723.
(118) Liu, B.; He, L.; Wang, L.; Li, T.; Li, C.; Liu, H.; Luo, Y.; Bao, R. Protein Crystallography and Site-Direct Mutagenesis Analysis of the Poly(Ethylene Terephthalate) Hydrolase PETase from *Ideonella sakaiensis*. *ChemBioChem.* **2018**, *19*, 1471−1475.
(119) Chen, C.-C.; Han, X.; Li, X.; Jiang, P.; Niu, D.; Ma, L.; Liu, W.; Li, S.; Qu, Y.; Hu, H.; Min, J.; Yang, Y.; Zhang, L.; Zeng, W.; Huang, J.-W.; Dai, L.; Guo, R.-T. General Features to Enhance Enzymatic Activity of Poly(Ethylene Terephthalate) Hydrolysis. *Nat. Catal.* **2021**, *4*, 425−430.
(120) Araujo, R.; Silva, C.; O'Neill, A.; Micaelo, N.; Guebitz, G.; Soares, C. M.; Casal, M.; Cavaco-Paulo, A. Tailoring Cutinase Activity Towards Polyethylene Terephthalate and Polyamide 6,6 Fibers. *J. Biotechnol.* **2007**, *128*, 849−857.
(121) Falkenstein, P.; Wei, R.; Matysik, J.; Song, C. Mechanistic Investigation of Enzymatic Degradation of Polyethylene Terephthalate by Nuclear Magnetic Resonance. In *Methods in Enzymology*, Weber, G.; Bornscheuer, U. T.; Wei, R., Eds.; Academic Press, 2021; Vol. *648*, pp 231−252.
(122) Furukawa, M.; Kawakami, N.; Tomizawa, A.; Miyamoto, K. Efficient Degradation of Poly(Ethylene Terephthalate) with *Thermobifida fusca* Cutinase Exhibiting Improved Catalytic Activity Generated Using Mutagenesis and Additive-Based Approaches. *Sci. Rep.* **2019**, *9*, 16038.
(123) Barth, M.; Honak, A.; Oeser, T.; Wei, R.; Belisário-Ferrari, M. R.; Then, J.; Schmidt, J.; Zimmermann, W. A Dual Enzyme System Composed of a Polyester Hydrolase and a Carboxylesterase Enhances the Biocatalytic Degradation of Polyethylene Terephthalate Films. *Biotechnol. J.* **2016**, *11*, 1082−1087.
(124) Eugenio, E. d. Q.; Campisano, I. S. P.; de Castro, A. M.; Coelho, M. A. Z.; Langone, M. A. P. Kinetic Modeling of the Post-Consumer Poly(Ethylene Terephthalate) Hydrolysis Catalyzed by Cutinase from *Humicola insolens*. *J. Polym. Environ.* **2021**, 1 DOI: 10.1007/s10924-021-02301-4.
(125) Knott, B. C.; Erickson, E.; Allen, M. D.; Gado, J. E.; Graham, R.; Kearns, F. L.; Pardo, I.; Topuzlu, E.; Anderson, J. J.; Austin, H. P.; Dominick, G.; Johnson, C. W.; Rorrer, N. A.; Szostkiewicz, C. J.; Copié, V.; Payne, C. M.; Woodcock, H. L.; Donohoe, B. S.; Beckham, G. T.; McGeehan, J. E. Characterization and Engineering of a Two-Enzyme System for Plastics Depolymerization. *Proc. Nat. Acad. Sci. U.S.A.* **2020**, *117*, 25476−25485.
(126) Meyer-Cifuentes, I. E.; Öztürk, B. Mle046 Is a Marine Mesophilic MHETase-Like Enzyme. *Front. Microbiol.* **2021**, *12*, 693985.
(127) Palm, G. J.; Reisky, L.; Böttcher, D.; Müller, H.; Michels, E. A. P.; Walczak, M. C.; Berndt, L.; Weiss, M. S.; Bornscheuer, U. T.; Weber, G. Structure of the Plastic-Degrading *Ideonella sakaiensis* MHETase Bound to a Substrate. *Nat. Commun.* **2019**, *10*, 1717.
(128) Dissanayake, L.; Jayakody, L. N. Engineering Microbes to Bio-Upcycle Polyethylene Terephthalate. *Front. Bioeng. Biotechnol.* **2021**, *9*, 656465.
(129) Hachisuka, S.-i.; Nishii, T.; Yoshida, S. Development of a Targeted Gene Disruption System in the Poly(Ethylene Terephthalate)-Degrading Bacterium *Ideonella sakaiensis* and Its Applications to PETase and MHETase Genes. *Appl. Environ. Microbiol.* **2021**, *87*, No. e00020.
(130) Barth, M.; Wei, R.; Oeser, T.; Then, J.; Schmidt, J.; Wohlgemuth, F.; Zimmermann, W. Enzymatic Hydrolysis of Polyethylene Terephthalate Films in an Ultrafiltration Membrane Reactor. *J. Membr. Sci.* **2015**, *494*, 182−187.
(131) Dai, L.; Qu, Y.; Huang, J.-W.; Hu, Y.; Hu, H.; Li, S.; Chen, C.-C.; Guo, R.-T. Enhancing PET Hydrolytic Enzyme Activity by Fusion of the Cellulose−Binding Domain of Cellobiohydrolase I from *Trichoderma reesei*. *J. Biotechnol.* **2021**, *334*, 47−50.
(132) Weber, J.; Petrović, D.; Strodel, B.; Smits, S. H. J.; Kolkenbrock, S.; Leggewie, C.; Jaeger, K.-E. Interaction of Carbohydrate-Binding Modules with Poly(Ethylene Terephthalate). *Appl. Microbiol. Biotechnol.* **2019**, *103*, 4801−4812.
(133) Berger, B. W.; Sallada, N. D. Hydrophobins: Multifunctional Biosurfactants for Interface Engineering. *J. Biol. Eng.* **2019**, *13*, 10.
(134) Espino-Rammer, L.; Ribitsch, D.; Przylucka, A.; Marold, A.; Greimel, K. J.; Herrero Acero, E.; Guebitz, G. M.; Kubicek, C. P.; Druzhinina, I. S. Two Novel Class II Hydrophobins from *Trichoderma* spp. Stimulate Enzymatic Hydrolysis of Poly(Ethylene Terephthalate) When Expressed as Fusion Proteins. *Appl. Environ. Microbiol.* **2013**, *79*, 4230−4238.
(135) Ribitsch, D.; Herrero Acero, E.; Przylucka, A.; Zitzenbacher, S.; Marold, A.; Gamerith, C.; Tscheliessnig, R.; Jungbauer, A.; Rennhofer, H.; Lichtenegger, H.; Amenitsch, H.; Bonazza, K.; Kubicek, C. P.; Druzhinina, I. S.; Guebitz, G. M. Enhanced Cutinase-Catalyzed Hydrolysis of Polyethylene Terephthalate by Covalent Fusion to Hydrophobins. *Appl. Environ. Microbiol.* **2015**, *81*, 3586−3592.
(136) Puspitasari, N.; Tsai, S.-L.; Lee, C.-K. Class I Hydrophobins Pretreatment Stimulates PETase for Monomers Recycling of Waste PET. *Int. J. Biol. Macromol.* **2021**, *176*, 157−164.
(137) Dai, L.; Qu, Y.; Hu, Y.; Min, J.; Yu, X.; Chen, C.-C.; Huang, J.-W.; Guo, R.-T. Catalytically Inactive Lytic Polysaccharide Mono-

oxygenase PCAA14A Enhances the Enzyme-Mediated Hydrolysis of Polyethylene Terephthalate. *Int. J. Biol. Macromol.* **2021**, *190*, 456−462.
(138) Chen, K.; Hu, Y.; Dong, X.; Sun, Y. Molecular Insights into the Enhanced Performance of EKylated PETase toward PET Degradation. *ACS Catal.* **2021**, *11*, 7358−7370.
(139) Várnai, A.; Siika-Aho, M.; Viikari, L. Carbohydrate-Binding Modules (CBMs) Revisited: Reduced Amount of Water Counterbalances the Need for CBMs. *Biotechnol. Biofuels* **2013**, *6*, 30.
(140) Kari, J.; Olsen, J. P.; Jensen, K.; Badino, S. F.; Krogh, K. B. R. M.; Borch, K.; Westh, P. Sabatier Principle for Interfacial (Heterogeneous) Enzyme Catalysis. *ACS Catal.* **2018**, *8*, 11966−11972.
(141) Herrero Acero, E.; Ribitsch, D.; Steinkellner, G.; Gruber, K.; Greimel, K.; Eiteljoerg, I.; Trotscha, E.; Wei, R.; Zimmermann, W.; Zinn, M.; Cavaco-Paulo, A.; Freddi, G.; Schwab, H.; Guebitz, G. Enzymatic Surface Hydrolysis of PET: Effect of Structural Diversity on Kinetic Properties of Cutinases from *Thermobifida*. *Macromolecules* **2011**, *44*, 4632−4640.
(142) Schmidt, J.; Wei, R.; Oeser, T.; Belisário-Ferrari, M. R.; Barth, M.; Then, J.; Zimmermann, W. Effect of Tris, MOPS, and Phosphate Buffers on the Hydrolysis of Polyethylene Terephthalate Films by Polyester Hydrolases. *FEBS Open Bio* **2016**, *6*, 919−927.
(143) Kim, H. T.; Hee Ryu, M.; Jung, Y. J.; Lim, S.; Song, H. M.; Park, J.; Hwang, S. Y.; Lee, H.-S.; Yeon, Y. J.; Sung, B. H.; Bornscheuer, U. T.; Park, S. J.; Joo, J. C.; Oh, D. X. Chemo-Biological Upcycling of Poly(Ethylene Terephthalate) to Multifunctional Coating Materials. *ChemSusChem* **2021**, *14*, 4251−4259.
(144) Rogers, B. A.; Okur, H. I.; Yan, C.; Yang, T.; Heyda, J.; Cremer, P. S. Weakly Hydrated Anions Bind to Polymers but Not Monomers in Aqueous Solutions. *Nat. Chem.* **2022**, *14*, 40−45.
(145) Sonnendecker, C.; Oeser, J.; Richter, P. K.; Hille, P.; Zhao, Z.; Fischer, C.; Lippold, H.; Blázquez-Sánchez, P.; Engelberger, F.; Ramírez-Sarmiento, C. A.; Oeser, T.; Lihanova, Y.; Frank, R.; Jahnke, H.-G.; Billig, S.; Abel, B.; Sträter, N.; Matysik, J.; Zimmermann, W. Low Carbon Footprint Recycling of Post-Consumer PET Plastic with a Metagenomic Polyester Hydrolase. *ChemSusChem* **2021**, 1 DOI: 10.1002/cssc.202101062.
(146) Gundupalli, S. P.; Hait, S.; Thakur, A. A Review on Automated Sorting of Source-Separated Municipal Solid Waste for Recycling. *Waste Manage.* **2017**, *60*, 56−74.
(147) Hahladakis, J. N.; Iacovidou, E. An Overview of the Challenges and Trade-Offs in Closing the Loop of Post-Consumer Plastic Waste (PCPW): Focus on Recycling. *J. Hazard. Mater.* **2019**, *380*, 120887.
(148) Tsochatzis, E. D.; Lopes, J. A.; Corredig, M. Chemical Testing of Mechanically Recycled Polyethylene Terephthalate for Food Packaging in the European Union. *Resour. Conserv. Recycl.* **2022**, *179*, 106096.
(149) Beckham, G. T.; Matthews, J. F.; Peters, B.; Bomble, Y. J.; Himmel, M. E.; Crowley, M. F. Molecular-Level Origins of Biomass Recalcitrance: Decrystallization Free Energies for Four Common Cellulose Polymorphs. *J. Phys. Chem. B* **2011**, *115*, 4118−4127.
(150) Hon, J.; Borko, S.; Stourac, J.; Prokop, Z.; Zendulka, J.; Bednar, D.; Martinek, T.; Damborsky, J. EnzymeMiner: Automated Mining of Soluble Enzymes with Diverse Structures, Catalytic Properties and Stabilities. *Nucleic Acids Res.* **2020**, *48*, W104−W109.
(151) Gumulya, Y.; Baek, J.-M.; Wun, S.-J.; Thomson, R. E. S.; Harris, K. L.; Hunter, D. J. B.; Behrendorff, J. B. Y. H.; Kulig, J.; Zheng, S.; Wu, X.; Wu, B.; Stok, J. E.; De Voss, J. J.; Schenk, G.; Jurva, U.; Andersson, S.; Isin, E. M.; Bodén, M.; Guddat, L.; Gillam, E. M. J. Engineering Highly Functional Thermostable Proteins Using Ancestral Sequence Reconstruction. *Nat. Catal.* **2018**, *1*, 878−888.
(152) Vanacek, P.; Sebestova, E.; Babkova, P.; Bidmanova, S.; Daniel, L.; Dvorak, P.; Stepankova, V.; Chaloupkova, R.; Brezovsky, J.; Prokop, Z.; Damborsky, J. Exploration of Enzyme Diversity by Integrating Bioinformatics with Expression Analysis and Biochemical Characterization. *ACS Catal.* **2018**, *8*, 2402−2412.
(153) Mazurenko, S.; Prokop, Z.; Damborsky, J. Machine Learning in Enzyme Engineering. *ACS Catal.* **2020**, *10*, 1210−1223.
(154) Musil, M.; Khan, R. T.; Beier, A.; Stourac, J.; Konegger, H.; Damborsky, J.; Bednar, D. FireProt^{ASR}: A Web Server for Fully Automated Ancestral Sequence Reconstruction. *Brief. Bioinformatics* **2021**, *22*, No. bbaa337.
(155) Jumper, J.; Evans, R.; Pritzel, A.; Green, T.; Figurnov, M.; Ronneberger, O.; Tunyasuvunakool, K.; Bates, R.; Žídek, A.; Potapenko, A.; Bridgland, A.; Meyer, C.; Kohl, S. A. A.; Ballard, A. J.; Cowie, A.; Romera-Paredes, B.; Nikolov, S.; Jain, R.; Adler, J.; Back, T.; Petersen, S.; Reiman, D.; Clancy, E.; Zielinski, M.; Steinegger, M.; Pacholska, M.; Berghammer, T.; Bodenstein, S.; Silver, D.; Vinyals, O.; Senior, A. W.; Kavukcuoglu, K.; Kohli, P.; Hassabis, D. Highly Accurate Protein Structure Prediction with AlphaFold. *Nature* **2021**, *596*, 583−589.
(156) Baek, M.; DiMaio, F.; Anishchenko, I.; Dauparas, J.; Ovchinnikov, S.; Lee, G. R.; Wang, J.; Cong, Q.; Kinch, L. N.; Schaeffer, R. D.; Millán, C.; Park, H.; Adams, C.; Glassman, C. R.; DeGiovanni, A.; Pereira, J. H.; Rodrigues, A. V.; Dijk, A. A. v.; Ebrecht, A. C.; Opperman, D. J.; Sagmeister, T.; Buhlheller, C.; Pavkov-Keller, T.; Rathinaswamy, M. K.; Dalwadi, U.; Yip, C. K.; Burke, J. E.; Garcia, K. C.; Grishin, N. V.; Adams, P. D.; Read, R. J.; Baker, D. Accurate Prediction of Protein Structures and Interactions Using a Three-Track Neural Network. *Science* **2021**, *373*, 871−876.
(157) Sahtoe, D. D.; Praetorius, F.; Courbet, A.; Hsia, Y.; Wicky, B. I. M.; Edman, N. I.; Miller, L. M.; Timmermans, B. J. R.; Decarreau, J.; Morris, H. M.; Kang, A.; Bera, A. K.; Baker, D. Reconfigurable Asymmetric Protein Assemblies through Implicit Negative Design. *Science* **2022**, *375*, No. eabj7662.
(158) Vermaas, J. V.; Crowley, M. F.; Beckham, G. T.; Payne, C. M. Effects of Lytic Polysaccharide Monooxygenase Oxidation on Cellulose Structure and Binding of Oxidized Cellulose Oligomers to Cellulases. *J. Phys. Chem. B* **2015**, *119*, 6129−6143.
(159) Heinz, H.; Lin, T.-J.; Kishore Mishra, R.; Emami, F. S. Thermodynamically Consistent Force Fields for the Assembly of Inorganic, Organic, and Biological Nanostructures: The Interface Force Field. *Langmuir* **2013**, *29*, 1754−1765.
(160) Tiso, T.; Narancic, T.; Wei, R.; Pollet, E.; Beagan, N.; Schröder, K.; Honak, A.; Jiang, M.; Kenny, S. T.; Wierckx, N.; Perrin, R.; Avérous, L.; Zimmermann, W.; O'Connor, K.; Blank, L. M. Towards Bio-Upcycling of Polyethylene Terephthalate. *Metab. Eng.* **2021**, *66*, 167−178.
(161) Werner, A. Z.; Clare, R.; Mand, T. D.; Pardo, I.; Ramirez, K. J.; Haugen, S. J.; Bratti, F.; Dexter, G. N.; Elmore, J. R.; Huenemann, J. D.; Peabody, G. L.; Johnson, C. W.; Rorrer, N. A.; Salvachúa, D.; Guss, A. M.; Beckham, G. T. Tandem Chemical Deconstruction and Biological Upcycling of Poly(Ethylene Terephthalate) to β-Ketoadipic Acid by *Pseudomonas putida* KT2440. *Metab. Eng.* **2021**, *67*, 250−261.
(162) Kim, H. T.; Kim, J. K.; Cha, H. G.; Kang, M. J.; Lee, H. S.; Khang, T. U.; Yun, E. J.; Lee, D.-H.; Song, B. K.; Park, S. J.; Joo, J. C.; Kim, K. H. Biological Valorization of Poly(Ethylene Terephthalate) Monomers for Upcycling Waste PET. *ACS Sustain. Chem. Eng.* **2019**, *7*, 19396−19406.
(163) Heyde, S. A. H.; Arnling Bååth, J.; Westh, P.; Nørholm, M. H. H.; Jensen, K. Surface Display as a Functional Screening Platform for Detecting Enzymes Active on PET. *Microb. Cell Fact.* **2021**, *20*, 93.
(164) Chen, Z.; Xiao, Y.; Weber, G.; Wei, R.; Wang, Z. Yeast Cell Surface Display of Bacterial PET Hydrolase as a Sustainable Biocatalyst for the Degradation of Polyethylene Terephthalate. In *Methods in Enzymology*, Weber, G.; Bornscheuer, U. T.; Wei, R., Eds.; Academic Press, 2021; Vol. *648*, pp 457−477.
(165) Yan, F.; Wei, R.; Cui, Q.; Bornscheuer, U. T.; Liu, Y.-J. Thermophilic Whole-Cell Degradation of Polyethylene Terephthalate Using Engineered *Clostridium thermocellum*. *Microb. Biotechnol.* **2021**, *14*, 374−385.
(166) Moog, D.; Schmitt, J.; Senger, J.; Zarzycki, J.; Rexer, K.-H.; Linne, U.; Erb, T.; Maier, U. G. Using a Marine Microalga as a Chassis for Polyethylene Terephthalate (PET) Degradation. *Microb. Cell Fact.* **2019**, *18*, 171.

(167) Gao, R.; Sun, C. A Marine Bacterial Community Capable of Degrading Poly(Ethylene Terephthalate) and Polyethylene. *J. Hazard. Mater.* **2021**, *416*, 125928.
(168) Oberbeckmann, S.; Labrenz, M. Marine Microbial Assemblages on Microplastics: Diversity, Adaptation, and Role in Degradation. *Annu. Rev. Mar. Sci.* **2020**, *12*, 209.
(169) Liu, J.; He, J.; Xue, R.; Xu, B.; Qian, X.; Xin, F.; Blank, L. M.; Zhou, J.; Wei, R.; Dong, W.; Jiang, M. Biodegradation and Up-Cycling of Polyurethanes: Progress, Challenges, and Prospects. *Biotechnol. Adv.* **2021**, *48*, 107730.
(170) Knyazev, V. D. Effects of Chain Length on the Rates of C-C Bond Dissociation in Linear Alkanes and Polyethylene. *J. Phys. Chem. A* **2007**, *111*, 3875−3883.
(171) Jiang, Q.; Li, Z.; Cui, Z.; Wei, R.; Nie, K.; Xu, H.; Liu, L. Quantum Mechanical Investigation of the Oxidative Cleavage of the C−C Backbone Bonds in Polyethylene Model Molecules. *Polymers* **2021**, *13*, 2730.
(172) Guzik, M. W.; Kenny, S. T.; Duane, G. F.; Casey, E.; Woods, T.; Babu, R. P.; Nikodinovic-Runic, J.; Murray, M.; O'Connor, K. E. Conversion of Post Consumer Polyethylene to the Biodegradable Polymer Polyhydroxyalkanoate. *Appl. Microbiol. Biotechnol.* **2014**, *98*, 4223−4232.
(173) Ghatge, S.; Yang, Y.; Ko, Y.; Yoon, Y.; Ahn, J.-H.; Kim, J. J.; Hur, H.-G. Degradation of Sulfonated Polyethylene by a Bio-Photo-Fenton Approach Using Glucose Oxidase Immobilized on Titanium Dioxide. *J. Hazard. Mater.* **2022**, *423*, 127067.
(174) Ballerstedt, H.; Tiso, T.; Wierckx, N.; Wei, R.; Averous, L.; Bornscheuer, U.; O'Connor, K.; Floehr, T.; Jupke, A.; Klankermayer, J.; Liu, L.; de Lorenzo, V.; Narancic, T.; Nogales, J.; Perrin, R.; Pollet, E.; Prieto, A.; Casey, W.; Haarmann, T.; Sarbu, A.; Schwaneberg, U.; Xin, F.; Dong, W.; Xing, J.; Chen, G.-Q.; Tan, T.; Jiang, M.; Blank, L. M. Mixed Plastics Biodegradation and Upcycling Using Microbial Communities: EU Horizon 2020 Project MIX-UP Started January 2020. *Environ. Sci. Europe* **2021**, *33*, 99.
(175) Shinozaki, Y.; Watanabe, T.; Nakajima-Kambe, T.; Kitamoto, H. K. Rapid and Simple Colorimetric Assay for Detecting the Enzymatic Degradation of Biodegradable Plastic Films. *J. Biosci. Bioeng.* **2013**, *115*, 111−114.
(176) Zumstein, M. T.; Kohler, H.-P. E.; McNeill, K.; Sander, M. High-Throughput Analysis of Enzymatic Hydrolysis of Biodegradable Polyesters by Monitoring Cohydrolysis of a Polyester-Embedded Fluorogenic Probe. *Environ. Sci. Technol.* **2017**, *51*, 4358−4367.
(177) Wei, R.; Oeser, T.; Billig, S.; Zimmermann, W. A High-Throughput Assay for Enzymatic Polyester Hydrolysis Activity by Fluorimetric Detection. *Biotechnol. J.* **2012**, *7*, 1517−1521.
(178) Pfaff, L.; Breite, D.; Badenhorst, C. P. S.; Bornscheuer, U. T.; Wei, R. Fluorimetric High-Throughput Screening Method for Polyester Hydrolase Activity Using Polyethylene Terephthalate Nanoparticles. In *Methods in Enzymology*, Weber, G.; Bornscheuer, U. T.; Wei, R., Eds.; Academic Press, 2021; Vol. *648*, pp 253−270.
(179) Weigert, S.; Gagsteiger, A.; Menzel, T.; Höcker, B. A Versatile Assay Platform for Enzymatic Poly(Ethylene-Terephthalate) Degradation. *Protein Eng. Des. Sel.* **2021**, *34*, No. gzab022.
(180) Molitor, R.; Bollinger, A.; Kubicki, S.; Loeschcke, A.; Jaeger, K.-E.; Thies, S. Agar Plate-Based Screening Methods for the Identification of Polyester Hydrolysis by *Pseudomonas* Species. *Microb. Biotechnol.* **2020**, *13*, 274−284.
(181) Charnock, C. A Simple and Novel Method for the Production of Polyethylene Terephthalate Containing Agar Plates for the Growth and Detection of Bacteria Able to Hydrolyze This Plastic. *J. Microbiol. Methods* **2021**, *185*, 106222.
(182) Qiao, Y.; Hu, R.; Chen, D.; Wang, L.; Wang, Z.; Yu, H.; Fu, Y.; Li, C.; Dong, Z.; Weng, Y.-X.; Du, W. Fluorescence-Activated Droplet Sorting of PET Degrading Microorganisms. *J. Hazard. Mater.* **2022**, *424*, 127417.
(183) Pardo, I.; Jha, R. K.; Bermel, R. E.; Bratti, F.; Gaddis, M.; McIntyre, E.; Michener, W.; Neidle, E. L.; Dale, T.; Beckham, G. T.; Johnson, C. W. Gene Amplification, Laboratory Evolution, and Biosensor Screening Reveal Muck as a Terephthalic Acid Transporter in *Acinetobacter baylyi* ADP1. *Metab. Eng.* **2020**, *62*, 260−274.
(184) Meyer, A.; Pellaux, R.; Potot, S.; Becker, K.; Hohmann, H.-P.; Panke, S.; Held, M. Optimization of a Whole-Cell Biocatalyst by Employing Genetically Encoded Product Sensors inside Nanolitre Reactors. *Nat. Chem.* **2015**, *7*, 673−678.
(185) Clarkson, S. M.; Giannone, R. J.; Kridelbaugh, D. M.; Elkins, J. G.; Guss, A. M.; Michener, J. K.; Vieille, C. Construction and Optimization of a Heterologous Pathway for Protocatechuate Catabolism in *Escherichia coli* Enables Bioconversion of Model Aromatic Compounds. *Appl. Environ. Microbiol.* **2017**, *83*, No. e01313.

https://doi.org/10.1021/acscatal.1c05856
ACS Catal. 2022, 12, 3382−3396

Article II

ACS Catalysis

pubs.acs.org/acscatalysis Research Article

Structural Insights into (Tere)phthalate-Ester Hydrolysis by a Carboxylesterase and Its Role in Promoting PET Depolymerization

Gerlis von Haugwitz, Xu Han, Lara Pfaff, Qian Li, Hongli Wei, Jian Gao, Karen Methling, Yufei Ao, Yannik Brack, Jan Mican, Christian G. Feiler, Manfred S. Weiss, David Bednar, Gottfried J. Palm, Michael Lalk, Michael Lammers, Jiri Damborsky, Gert Weber, Weidong Liu,* Uwe T. Bornscheuer,* and Ren Wei*

Cite This: https://doi.org/10.1021/acscatal.2c03772 Read Online

ACCESS | Metrics & More | Article Recommendations | Supporting Information

ABSTRACT: TfCa, a promiscuous carboxylesterase from *Thermobifida fusca*, was found to hydrolyze polyethylene terephthalate (PET) degradation intermediates such as bis(2-hydroxyethyl) terephthalate (BHET) and mono-(2-hydroxyethyl)-terephthalic acid (MHET). In this study, we elucidated the structures of TfCa in its apo form, as well as in complex with a PET monomer analogue and with BHET. The structure−function relationship of TfCa was investigated by comparing its hydrolytic activity on various ortho- and para-phthalate esters of different lengths. Structure-guided rational engineering of amino acid residues in the substrate-binding pocket resulted in the TfCa variant I69W/V376A (WA), which showed 2.6-fold and 3.3-fold higher hydrolytic activity on MHET and BHET, respectively, than the wild-type enzyme. TfCa or its WA variant was mixed with a mesophilic PET depolymerizing enzyme variant [*Ideonella sakaiensis* PETase (*Is*PETase) PM] to degrade PET substrates of various crystallinity. The dual enzyme system with the wild-type TfCa or its WA variant produced up to 11-fold and 14-fold more terephthalate (TPA) than the single *Is*PETase PM, respectively. In comparison to the recently published chimeric fusion protein of *Is*PETase and MHETase, our system requires 10% *Is*PETase and one-fourth of the reaction time to yield the same amount of TPA under similar PET degradation conditions. Our simple dual enzyme system reveals further advantages in terms of cost-effectiveness and catalytic efficiency since it does not require time-consuming and expensive cross-linking and immobilization approaches.

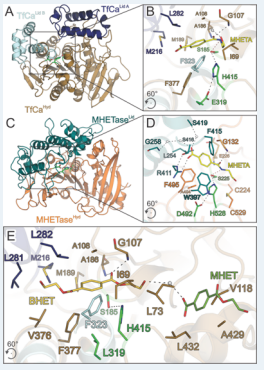

KEYWORDS: *PET hydrolysis, plastic, dual enzyme system, carboxylesterase, structure, enzyme engineering*

INTRODUCTION

In recent years, enzymatic depolymerization of polyethylene terephthalate (PET) has emerged as an alternative technology to conventional mechanical and chemical plastic recycling approaches.[1] TfH from *Thermobifida fusca* (*T. fusca*) was the first enzyme discovered in 2005 to possess PET degrading activity.[2] Since then, many new PET hydrolases (PETases) have been identified and engineered for higher PET degradation efficiency.[3−5] Enzymatic PET hydrolysis produces small-molecule degradation products, which can be recovered and used to synthesize virgin polymers.[5,6] In addition to the desired PET monomers terephthalate (TPA) and ethylene glycol (EG), bis(2-hydroxyethyl) terephthalate (BHET) and mono-(2-hydroxyethyl)-terephthalate (MHET) are also released as degradation intermediates that are known as inhibitors for selected PETases.[7]

Methods for mitigating the product inhibition during enzymatic PET hydrolysis include the continuous removal of small-molecule products using ultrafiltration membranes,[8] the use of engineered PETase variants that are less affected by the inhibitors,[9] and the introduction of a helper enzyme with a specific hydrolytic activity on the inhibitors. *Ideonella sakaiensis* (*I. sakaiensis*) is a bacterium that can degrade PET and assimilate its monomers.[10] In addition to the extracellular *I. sakaiensis* PETase (*Is*PETase) which can depolymerize PET predominantly to MHET, the intracellular MHETase has been assumed to facilitate the PET assimilation by converting MHET to TPA and EG.[10,11] This allowed for the development of a chimeric MHETase:*Is*PETase fusion protein exhibiting markedly improved PET depolymerization activity.[12] At 30 °C and pH 7.5, this chimeric system produced approximately sixfold more degradation products in 96 h than single *Is*PETase in the PET hydrolysis. TfCa is a *T. fusca* carboxylesterase with hydrolytic activity on PET oligomers, including MHET, BHET, and a cyclic PET trimer.[13,14] When TfCa was immobilized on a SulfoLink resin and then coupled with various PETases such as LC-cutinase or TfCut2 for PET

Received: August 1, 2022
Revised: October 9, 2022

degradation, the yield of degradation products was up to twofold higher than when TfCa was absent.[15] Nevertheless, both dual enzyme systems may be less feasible for industrial applications due to the need of an efficient cross-linking method or the high cost of the immobilization matrix. Therefore, a low-cost dual enzyme system with enhanced PET oligomer hydrolyzing activity is required.

While the crystal structures of MHETase have been recently solved and repeatedly reported,[11,12,16] the structural basis underlying the mechanism of TfCa-catalyzed hydrolysis of TPA esters remains elusive. In this study, we elucidated the first crystal structure of TfCa in its apo form and in complex with the MHET-like analogue 4-[(2-hydroxyethyl) carbamoyl] benzoic acid (MHETA) and BHET at atomic resolutions. By comparing its specific activity on various TPA esters and an ortho-phthalate ester (diethyl phthalate, DEP), the structural basis for substrate recognition and hydrolysis by TfCa was explored. Moreover, we rationally engineered TfCa and obtained a mutant with significantly higher MHET and BHET hydrolytic activity. This TfCa variant was applied in a simple dual enzyme system in combination with an *Is*PETase penta-mutant, *Is*PETase$^{S121E/D186H/R280A/N233C/S282C}$ (*Is*PETase PM), for enhanced degradation of a variety of PET substrates with different crystallinity.

MATERIAL AND METHODS

Materials. Chemicals and consumables were purchased from Merck KGaA (Darmstadt, Germany), Sigma-Aldrich (Steinheim, Germany), Thermo Fisher Scientific (Waltham, MA, USA), and New England Biolabs GmbH (Frankfurt am Main, Germany) unless stated otherwise. Primers were ordered from Eurofins (Ebersberg, Germany) and Thermo Fisher Scientific (Waltham, MA, USA). The amorphous PET film (GfPET, ES30-FM-0001445) and the semi-crystalline PET powder (maximum particle size: 300 μm, crystallinity >40%, product number: ES306031/1) were purchased from Goodfellow GmbH (Bad Nauheim, Germany). PET nanoparticles (PET-NPs) were prepared as described previously by Pfaff et al.,[17] bis[2-(benzoyloxy)ethyl] terephthalate was defined as 3PET and synthesized according to Fischer-Colbrie et al.,[18] MHETA was synthesized as described by Palm et al.[11]

METHODS

Crystallization, Data Collection, Structure Determination, and Refinement. All crystallization experiments were conducted at 25 °C using the sitting-drop vapor-diffusion method. In general, 1 μL TfCa solution (40 mg/mL in 25 mM Tris−HCl containing 150 mM NaCl, pH 7.5) was mixed with 1 μL reservoir solution in 48-well Cryschem Plates and equilibrated against 100 μL of the reservoir solution. The optimized crystallization conditions of TfCa and TfCa E319L were 22% (w/v) poly(acrylic acid) sodium salt 5100, 0.02 M $MgCl_2$, 0.1 M HEPES at pH 7.5. The mutant TfCa E319L was created to eliminate residue E319 of the catalytic triad to avoid the hydrolysis of the substrate during the soaking period. A detailed description of the enzyme expression for crystallization purposes is included in the Supporting Information.

Within 5−6 days, the crystals reached their final size suitable for X-ray diffraction. The TfCa and TfCa E319L crystals in complex with MHETA, BHET, or MHET plus BHET were obtained by soaking the enzyme with 10 mM of each compound for 72 h.

All the X-ray diffraction data sets were collected at the National Facility for Protein Science in Shanghai at Shanghai Synchrotron Radiation Facility at the beamlines BL10U2/BL02U1(BL17U)/BL17B/BL18U1/BL19U1, and in Berlin at the third-generation synchrotron radiation source (BESSY II) with beamline 14.1.[19] The crystals were mounted in a cryoloop and soaked with cryoprotectant solution [25% w/v poly(acrylic acid sodium salt) 5100, 0.02 M $MgCl_2$, 0.1 M HEPES pH 7.5, 10% glycerol] prior to data collection at 100 K. The diffraction images were processed using HKL2000. The crystal structure of TfCa was solved by the molecular replacement method with the Phaser program[20] from the Phenix[21] suite using the structure of the carboxylesterase from *Geobacillus stearothermophilus* (PDB-ID: 2OGT) as a search model. Further refinement was carried out using the programs phenix.refine[22] and Coot.[23] Prior to structural refinement, 5% of randomly selected reflections were used for calculating R_{free}[24] to monitor the refinement process. Data collection and refinement statistics are summarized in Table S1.

Expression and Purification of Recombinant TfCa and *Is*PETase PM. For enzymatic PET degradation, the TfCa gene was cloned into a pET20b(+) vector and the plasmid was transformed into *Escherichia coli* BL21 (DE3). Bacterial cells were grown in lysogeny broth (LB) medium at 37 °C to an optical density at 600 nm (OD_{600}) of 1 and then further incubated at 18 °C. When the OD_{600} reached 1.5, recombinant protein expression was induced by adding 1 mM isopropyl β-D-thiogalactopyranoside and cells were further grown at 18 °C until an OD_{600} of 3. Cells were harvested by centrifugation at 10,000 × *g* for 5 min. Cell pellets were re-suspended in lysis buffer containing 50 mM Na_2HPO_4, pH 8, and 150 mM NaCl, followed by disruption by ultrasonication (3 × 90 s, 50% pulse, 50% power, 2 min breaks). Cell debris was removed by centrifugation at 10,000 × *g* for 30 min. The supernatant was then applied to a Ni^{2+}-nitrilotriacetic acid column, washed with lysis buffer and a 20−90 mM imidazole gradient as described before.[14] The enzyme with an apparent molecular mass of 55 kDa was eluted with 250 mM imidazole, which was then exchanged to the assay buffer (25 mM Tris−HCl, pH 7.5, set at 45 °C) using Vivaspin (Sartorius Lab Instruments, Göttingen, Germany) with 10 kDa cutoff. The membrane of the Vivaspin was equilibrated with 5 mL Tris−HCl buffer (25 mM, pH 7.5, set at 45 °C) by centrifugation for 5 min at 5000 × *g*. Afterward, the eluted protein was added to the Vivaspin, topped with 5 mL Tris−HCl buffer, and centrifuged for 15 min at 5000 × *g* and 4 °C. After repeating this four times, the enzyme was removed from the upper compartment of the Vivaspin column. The enzyme concentration was determined using a NanoDrop 1000 device (Thermo Fisher Scientific, Waltham, MA, USA). *Is*PETase PM was expressed as described by Brott et al.[25] and purified as described here for TfCa. The model substrate para-nitrophenyl acetate (pNPA) was used for determining the enzymatic activity as described before.[14]

Site-Directed Mutagenesis. Mutation of the TfCa-encoding gene was performed using the Q5 Site-Directed Mutagenesis Kit (New England Biolabs GmbH, Frankfurt am Main, Germany) according to the supplier's protocol. Successful mutagenesis was confirmed by sequencing.

Enzymatic Production of the Substrate MHET. Similar to terephthalic acid, commercially available MHET has a benzoic acid end group and is hence almost insoluble in aqueous solutions without organic solvents. Therefore, soluble MHET with a deprotonated carboxylate end was prepared

https://doi.org/10.1021/acscatal.2c03772
ACS Catal. XXXX, XXX, XXX−XXX

from controlled enzymatic BHET degradation using TfCa as described earlier.[7] Up to 100 mM BHET was added into ethanol and sonicated in a water bath for 30 min until BHET was dissolved to form a clear solution. The production of MHET was carried out in a 50 mL reaction volume, containing 20 mM of BHET in ethanol, 550 nM of purified TfCa, and 25 mM Tris−HCl buffer (pH 7.5, set at 45 °C). The final concentration of ethanol in the reaction was 10%. The solution was incubated at room temperature for 30 min without agitation. After incubation, the sample was heated to 80 °C for 10 min to inactivate TfCa and then centrifuged (10,000 × *g*, 5 min) to remove insoluble compounds. The supernatant was analyzed using high-performance liquid chromatography (HPLC) to ensure MHET purity and then used as a substrate for further enzyme characterizations.

Enzymatic Hydrolysis of Various Substrates. Enzymatic hydrolysis of the small ester substrates 3PET, BHET, MHET, and DEP was performed in 1 mL reaction volume using 25 mM Tris−HCl buffer (pH 7.5) at 50 °C with 550 nM purified enzyme unless stated otherwise. In total, 2 mM 3PET, BHET, or MHET, or 5 mM DEP were used in the reactions. For an enhanced solubility of the substrates, the hydrolysis of 3PET, BHET, and MHET was performed in the presence of 10% ethanol and that of DEP hydrolysis in 10% dimethyl sulfoxide. Sampling at different time points during hydrolysis reactions was performed as indicated below in the Results section. The degradation products benzoic acid (BA), BHET, MHET, and TPA were confirmed by HPLC, whereas monoethyl phthalate (MEP) was confirmed by liquid chromatography coupled with mass spectrometry (LC−MS). A detailed description of the LC−MS method is included in the Supporting Information.

In a dual enzyme system, PET NPs, PET powder, or PET film were employed as substrates. PET NPs were used at a final concentration of 2, 20, and 200 μg/mL, whereas PET powder and PET film were used at a final concentration of 60 mg/mL in Tris−HCl buffer (set to pH 7.5 at 45 °C). Purified *Is*PETase PM was used at a concentration of 30 nM for PET NPs and 50 nM for PET film and PET powder as described before.[25] The amounts of the aromatic products were determined using HPLC according to Palm et al.[11] The amount of TPA, MHET, or BHET was calculated based on a TPA standard curve and the amount of MEP was calculated based on a phthalic acid (PA) standard curve. The specific activity was calculated as U/mg_{enzyme}, while one unit (U) was defined as one μmol substrate converted per min.

Determination of Melting Points. The melting points (T_m) of TfCa and its mutants were determined using nano differential scanning fluorimetry on a Prometheus NT.48 device (NanoTemper Technologies, Munich, Germany). Purified enzymes at a concentration of 300 μg/mL were used to monitor the thermal denaturation profiles from 40 to 80 °C at 1 °C/min steps. T_m was calculated based on the excitation changes at 285 nm with emission wavelengths at 330 and 350 nm.

Molecular Docking. Molecular docking of 3PET, DEP, and MEP into the active site of TfCa was performed with an AutoDock Vina v1.2.0 and Dockprep as part of Chimera v1.15.[26] The docking for 3PET was performed in a box with an edge length of 50 Å around S185, the docking for DEP and MEP was performed in a box with an edge length of 25 Å for DEP and MEP around residue A108, which includes the active site and its surroundings. The AutoDock Vina score was set to −9.9, −6.2, and −6.0 for 3PET, DEP, or MEP, respectively.

Molecular Dynamics Simulations. The crystal structures of TfCa with the ligand MHETA (PDB-ID: 7W1J, 1.92 Å) as well as the chain A structure of MHETase from *I. sakaiensis* (PDB-ID: 6QGA, 2.1 Å)[11,27] were used for molecular dynamics (MD) simulations. In total, three independent MD replicates with 20 ns long production simulation were run for each system at 310 K (37 °C) using the Langevin thermostat at a constant pressure of 1.0 bar and a pressure coupling constant of 1.0 ps. Coordinates were saved at intervals of 4 ps. In total, 60 ns of simulation time was produced for each enzyme−ligand system.

Each complex was clustered into three trajectories and the molecular mechanics/generalized Born surface area (MM/GBSA)[28,29] method was applied to calculate the binding free energy (ΔG_{bind}) of MHET in the enzymes and the respective residue-by-residue interactions.[28,30] A more detailed description of these MD simulations is included in the Supporting Information.

RESULTS

Structure of TfCa in Its Apo Form. The ligand-free wild-type TfCa (TfCa wt) was crystallized in the monoclinic space group $P2_1$ (PDB-ID: 7W1K, 1.40 Å). The enzyme is built from three domains, a hydrolase domain that adopts the fold of a canonical α/β hydrolase with a central antiparallel β-sheet surrounded by α-helices, a lid domain A and a lid domain B (Figure 1A). As predicted from sequence alignment with homologous enzymes that exhibit carboxylesterase activity, TfCa contains a strictly conserved catalytic triad consisting of the residues S185, E319, and H415. Hence, a *p*-nitrobenzyl esterase (pNB-E) from *Bacillus subtilis* (PDB-ID: 1QE3) and the carboxylesterase Est55 from *G. stearothermophilus* (PDB-ID: 2OGS) were used as templates for elucidating the backbone structure of TfCa. Within the catalytic triad of TfCa, S185 serves as the nucleophile and is located within hydrogen-bond (H-bond) distance to be polarized by the base H415, which is stabilized by the acid E319. A sequence alignment, as well as structural alignments of pNB-E, Est55, and TfCa, are shown in Figures S1 and S2.

Binding Modes to PET-Related Ligands. To explore the catalytic mechanism of TfCa, protein crystals were soaked with the substrates MHET and BHET as well as with the substrate analogue MHETA. MHETA has an amide bond in place of the ester bond in MHET and can hence not be hydrolyzed by esterolytic enzymes including TfCa. With TfCa wt, a ligand-bound structure of TfCa with MHETA (PDB-ID: 7W1J, 1.92 Å) was solved. By mutating E319 in the catalytic triad, an inactive TfCa variant E319L was generated. This variant allowed for stable substrate binding and two additional complex structures with BHET (PDB-ID: 7W1L, 2.43 Å) and with both degradation intermediates, MHET and BHET (PDB-ID: 7W1I, 1.67 Å). In the ligand-bound structures of TfCa, the ligands were located at the bottom of a deep active site cleft containing the hydrophobic residues L282, L322, and V376. The side chain of the catalytic S185 is within H-bonding distance to the ester oxygen atom of BHET (PDB-ID: 7W1I, Figure 1E) and the nitrogen atom of MHETA (PDB-ID: 7W1J, Figure 1B).

The overall structures of TfCa and MHETase and their binding modes to the ligand MEHTA are compared as shown in Figure 1A−D. While MHETase consists of one hydrolase

https://doi.org/10.1021/acscatal.2c03772
ACS Catal. XXXX, XXX, XXX−XXX

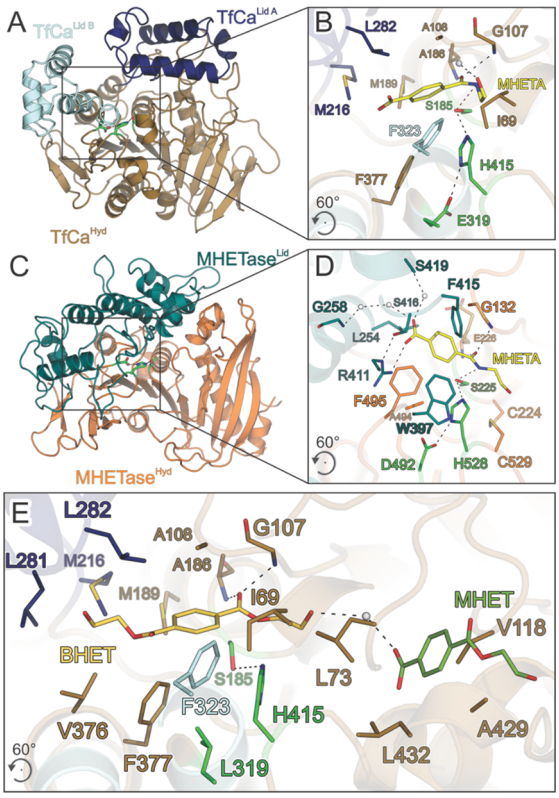

Figure 1. Ligand-free and complex structures of TfCa from *T. fusca* in comparison to MHETase from *I. sakaiensis*. (A) Crystallographic structure of TfCa reveals three subdomains: hydrolase domain ($TfCa^{Hyd}$, brown), lid domain A ($TfCa^{LidA}$, dark blue), and lid domain B ($TfCa^{LidB}$, cyan). The catalytic triad consisting of S185, E319, and H415 is shown as green sticks. (B) Close-up view of the active site of TfCa with bound MHETA (yellow) (PDB-ID: 7W1J, 1.92 Å). Residues from different domains are shown in brown ($TfCa^{Hyd}$), dark blue ($TfCa^{LidA}$), and cyan ($TfCa^{LidB}$). (C) Structure of MHETase from *I. sakaiensis* with its two domains: the hydrolase domain ($MHETase^{Hyd}$, orange) and the lid domain ($MHETase^{Lid}$, dark aquamarine) (PDB-ID: 6QGA).[11] (D) Close-up view of the active site of MHETase with bound MHETA (yellow). Residues from different domains are shown in orange ($MHETase^{Hyd}$) and dark aquamarine ($MHETase^{Lid}$). (E) Close-up view of the active site of TfCa E319L with bound BHET (yellow) and MHET (green) (PDB-ID: 7W1I, 1.67 Å). Dashed lines indicate H-bond formation, molecules and interacting residues are colored by atom types: carbon: varying colors, nitrogen: blue, oxygen: red. Residues of the catalytic triad are shown as green sticks.

domain and one lid domain, the overall structure of TfCa can be divided into one hydrolase domain and two lid domains (Lid A and Lid B). In the active site of TfCa, only three H-bonds are formed, preliminarily with the amide bond and the neighboring hydroxyl end in MHETA (Figure 1B). By comparison, five H-bonds are present in MHETase to interact with both ends of the MHETA ligand (Figure 1D). Side chains of selected phenylalanine residues (F323 and F377 for TfCa, F495 and F415 for MHETase) were found to be potentially involved in stabilizing the TPA moiety in MHETA. In MHETase, F415 and F495 are located on both sides of the benzoic ring of the soaked MHETA ligand. In contrast, F323 and F377 in TfCa are exclusively positioned on one side of MHETA. This binding mode may only permit a staggered stacking interaction of F323 and a very weak T-shaped interaction of the more distant F377 from the same direction to the TPA moiety (Figure 1B). Similar interactions between these two aromatic residues and the BHET ligand (Figure 1E) suggest that F377 plays a minor role in the substrate stabilization.

We also investigated the binding of MHET to TfCa and MHETase using MD simulations. As shown in Table S5, by clustering the snapshots during the 60 ns productive simulations, MHET has a significantly higher likelihood of staying in the substrate binding pocket of MHETase than in that of TfCa. For clustering the snapshots, the distance between the MHET ester carbonyl atom and the side chain oxygen of the catalytic serine in each enzyme is defined as the catalytic C−O distance. Those snapshots with a catalytic C−O distance less than 4.5 Å were selected to calculate the binding free energy of MHET to individual residues in the substrate binding pocket of each enzyme using MM/GBSA.[29] In MHETase we found that, in addition to the aforementioned F415 and F495, R411 and W397 considerably contribute to the interaction with MHET (Table S3 and Figure S10B). By contrast, in TfCa, certain small residues such as G106, G107, and A108 appear to play an important role in the binding to MHET, in addition to the amino acids neighboring S185 and the aromatic residues F323 and F377 discovered in the crystal structures (Figures 1B,E and S10A). In accordance with the crystal structure analysis, MD simulation results support the conclusion that MHETase has a higher overall binding affinity to MHET than TfCa.

Substrate Profile of TfCa. The substrate profile of TfCa was investigated with TPA-based oligo-esters of various lengths, such as MHET, BHET, and 3PET, as well as the ortho-phthalate ester DEP. HPLC-derived product profile allowed us to hypothesize the degradation pathways of longer substrates and estimate the specific activity of TfCa in hydrolyzing various esters at each reaction step (Figure 2). f2

MHET is the monoester of TPA and EG and also the smallest among all the investigated substrates. The specific activity of MHET hydrolysis by TfCa was 0.024 U/mg_{enzyme} as shown in Figure 2A. BHET is the diester of one TPA with two EG. The first hydrolysis of BHET will form MHET and EG, while the second hydrolysis step yields TPA and EG (Figure 2B). The specific activity of TfCa for the first BHET hydrolysis step was found to be much higher (5.12 U/mg_{enzyme}) than that of the second hydrolysis step (0.011 U/mg_{enzyme}) (Figure 2A,B). Although the second hydrolysis step of BHET is equivalent to the MHET hydrolysis, it revealed an approximately two times lower specific activity than the primary MHET hydrolysis. This can be attributed to a less-preferred binding of MHET in the presence of the competitive substrate BHET, which can be hydrolyzed nearly 500 times faster by TfCa.

Similar to BHET, DEP is a diester of ortho-phthalate and ethanol (Figure 2D). After 1 h of incubation at 50 °C, DEP was not detectable as a result of TfCa-catalyzed hydrolysis. LC−MS analysis suggested that DEP was completely converted to MEP (Figure S11), which can also be monitored as a new peak at a retention time of 11.25 min on HPLC. The specific activity of this primary hydrolysis step is 1.64 U/mg_{enzyme}, which is 3 times lower than BHET hydrolysis but 82 times higher than MHET hydrolysis. MEP was not further hydrolyzed to PA, suggesting that it is a less-preferred substrate for TfCa than MHET.

3PET is the longest oligomer investigated in this study with four ester bonds. TfCa-catalyzed hydrolysis of 3PET can yield

https://doi.org/10.1021/acscatal.2c03772
ACS Catal. XXXX, XXX, XXX−XXX

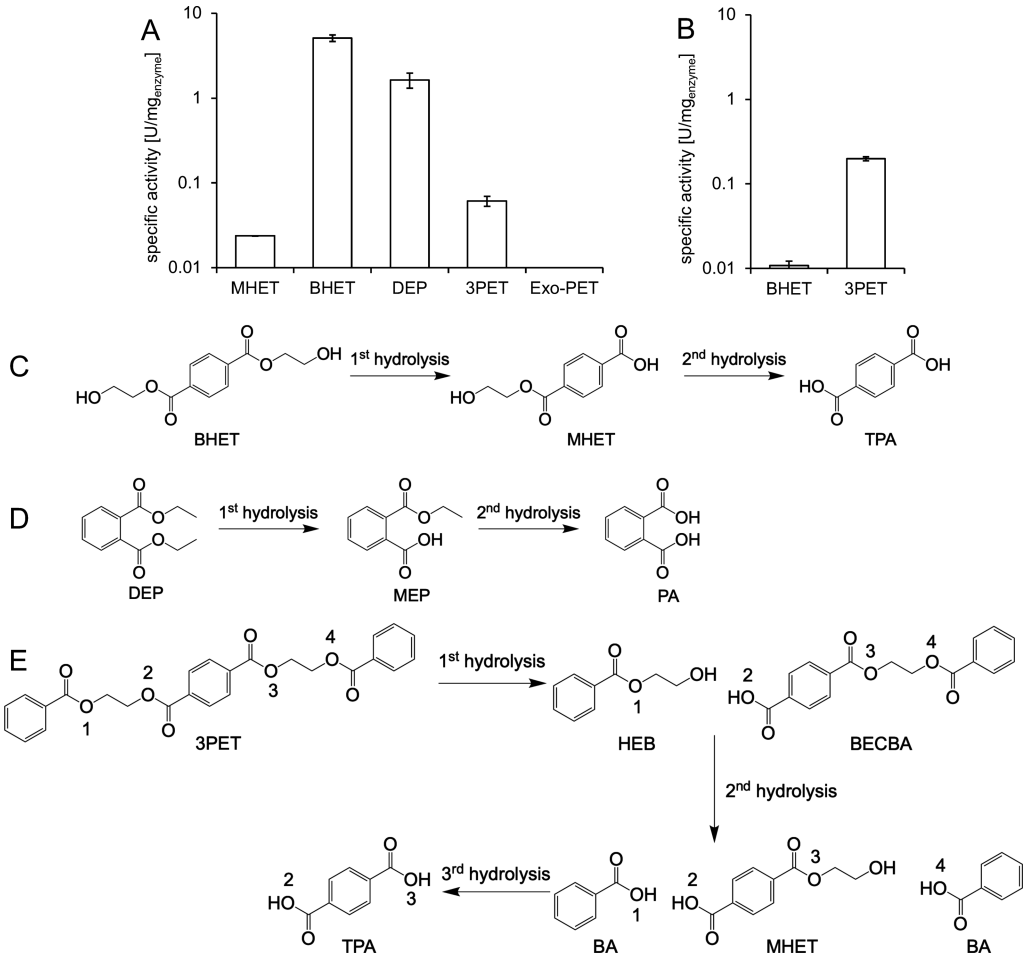

Figure 2. TfCa catalyzed hydrolysis of (tere)phthalate esters of various lengths. (A) Specific activity of TfCa for the hydrolysis of the first ester bond in each model substrate. The specific activity is shown on a logarithmic scale. (B) Specific activity of TfCa for the hydrolysis of the second ester bond in 3PET and BHET. The specific activity is shown on a logarithmic scale. Error bars indicate the standard deviations calculated from at least three replicates. Putative degradation pathways for (C) BHET, (D) DEP (TfCa can only catalyze the hydrolysis of DEP to MEP), and (E) 3PET. For simplicity, EG is not shown as a degradation product. Chemical structures and schemes were drawn with ChemDraw 21.0.0.

different product profiles depending on where the first hydrolysis step occurs (Figures S9 and 2E). After 10 min hydrolysis reaction with TfCa at 50 °C, 2-hydroxyethyl-benzoate (HEB) was detected as one product, of which the amount decreases with the reaction duration. Consequently, we suggest a preferential degradation pathway of 3PET, which releases HEB as an intermediate product from 3PET by TfCa. This degradation pattern is similar to that described by Eberl et al.[31] for 3PET hydrolysis catalyzed by a *T. fusca* cutinase. However, the other product from the first hydrolysis step, 4-{[2-(benzoyloxy)ethoxy]-carbonyl} benzoic acid (BECBA) cannot be detected by HPLC. Based on the rate of HEB formation, we determined a specific activity of 0.06 U/mg_{enzyme} for the first hydrolysis step of 3PET. This is three times higher than that for MHET but 85 times and 27 times lower than for BHET and DEP, respectively. The lower specific activity for 3PET is probably due to the size of the substrate. The high specific activity observed for BHET and DEP suggests that (tere)phthalate diesters may have the ideal size for the substrate binding pocket of TfCa. In the second hydrolysis step of 3PET, both HEB and BECBA are further hydrolyzed. This can be verified by the decreasing concentration of HEB and the increasing amounts of BA and MHET in the samples at the later reaction stage. The estimated specific activity of this reaction step is lower than the first step hydrolysis of 3PET but slightly higher than MHET (Figure 2A). HEB is a monoester comparable to MHET, whereas BECBA is a diester with two aromatic moieties. The markedly lower specific activity observed for BECBA compared to BHET suggests that the additional aromatic ring may hinder the TfCa hydrolysis efficiency. This is consistent with a previous study demonstrating that TfCa can hydrolyze BHET faster than 1,2-ethanediyl bis(4-methylbenzoate).[32] Similar to BECBA, the latter model substrate is a diester with two aromatic moieties and is also commonly used to resemble PET repeating units. The final reaction step of 3PET hydrolysis is MHET hydrolysis, which releases TPA and EG. After a 6 h reaction, MHET was the major product measured by HPLC, followed by BA and TPA (Figure S6).

A previous study has shown that MHETase possesses an exo-PETase activity allowing for the hydrolysis of the terminal ester groups of PET polymers.[16] Accordingly, we tested TfCa for its capacity to hydrolyze PET end groups but were unable to demonstrate its exo-PETase activity (Figures 2A and S7).

Structure-Based Enzyme Engineering of TfCa. To improve the activity of TfCa on MHET and BHET, amino acid residues within 5 Å of the soaked ligands (Figures 1B,E and S3) were selected for rational engineering. Among the 29

https://doi.org/10.1021/acscatal.2c03772
ACS Catal. XXXX, XXX, XXX−XXX

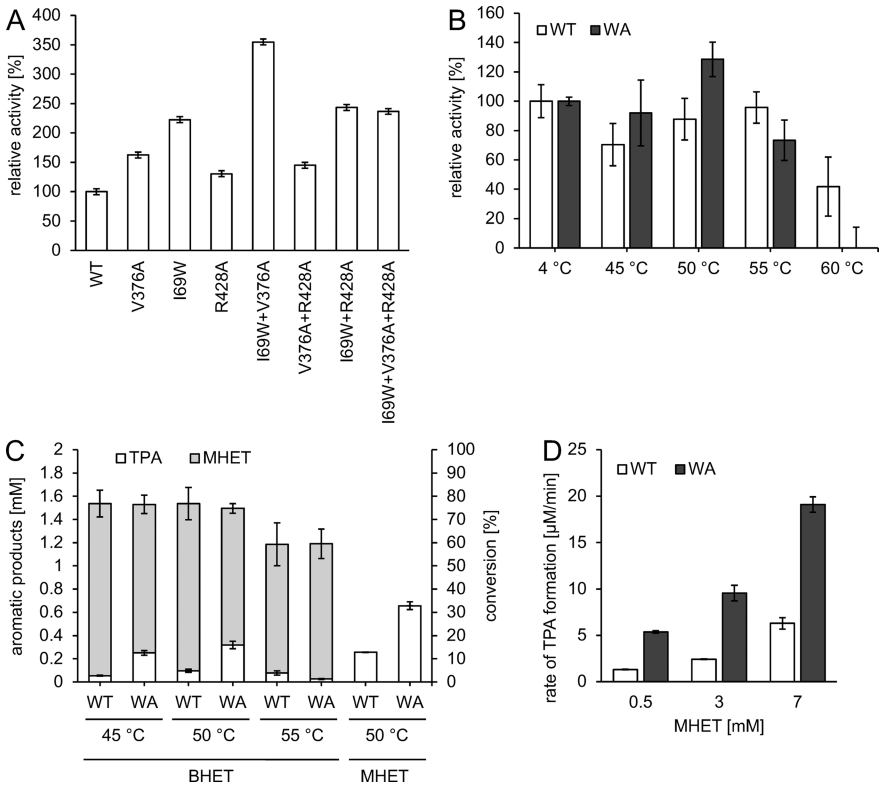

Figure 3. Semi-rational enzyme engineering of TfCa and characterization of the most active TfCa$^{I69W+V376A}$ (WA) mutant. (A) Relative activity of mutants compared to TfCa wt based on the hydrolysis of 2 mM BHET into TPA at 45 °C in 25 mM Tris-buffer (pH 7.5, set at 45 °C). The amount of the degradation product TPA was determined by HPLC analysis. (B) Relative residual activity determined at 25 °C after 1 h incubation at various temperatures. The hydrolytic activity was determined with the model substrate pNPA in 25 mM Tris−HCl buffer (pH 7.5, set at 25 °C). The data determined at 4 °C were used as reference values to define 100% residual activity. (C) 2 mM BHET or MHET were degraded with TfCa wt or TfCa WA at various temperatures in 25 mM Tris−HCl buffer (pH 7.5) for 6 h. The amount of the degradation products MHET and TPA were determined by HPLC. (D) The rates of TPA yield from MHET were determined with 0.55 μM TfCa wt or the variant WA at various substrate concentrations ranging from 0.5 to 7 mM. Reaction supernatants were taken after 30 min of incubation at 50 °C in 25 mM Tris-buffer (pH 7.5, set at 50 °C) and subjected to HPLC analysis. Error bars indicate the standard deviations calculated from at least three replicates.

amino acids identified, all alanine, glycine, and proline residues, and those in the catalytic triad as well as the conserved GxSxG motif were excluded from mutagenesis. The remaining 14 residues were individually substituted with alanine (alanine scan). The resulting mutants were first evaluated for BHET hydrolysis activity (Figure S4). Two variants, R428A and V376A, showed ≥1.2-fold higher activity than TfCa wt and were thus selected for further investigations (Figures 3A and S4). R428 and V376 have rather bulky side-chains, which are assumed to affect the substrate binding. As a result, an alanine substitution may possibly provide additional space to accommodate larger substrates like BHET. By contrast, the I69A and M189A variants were completely inactive. These two residues were then subjected to site saturation mutagenesis. The variant I69W was found to be more than twofold active than that of TfCa wt (Figure 3A), whereas none of the M189 site-saturated mutants was significantly more active with the model substrate pNPA (Figure S5). Based on the complex structures shown in Figures 1 and S3, we hypothesize that the mutation I69W, similar to the residues F323 and F377, may facilitate to interact with the aromatic moiety in the substrate.

All three variants with significantly increased activity, namely, TfCa^{R428A}, TfCa^{V376A}, and TfCa^{I69W}, were combined in all possible variations (Figure 3A). The highest activity was achieved with the mutant TfCa$^{I69W+V376A}$, which had a 3.3-fold higher activity on BHET than TfCa wt at 45 °C and is designated as TfCa WA in the following descriptions.

We further investigated the thermostability of TfCa wt and WA. Although TfCa WA has a lower T_m (60.3 °C) than TfCa wt (64.5 °C) (Table S2), its relative residual activities after 1 h incubation at 45, 50, and 55 °C were comparable to those of TfCa wt (Figure 3B). In contrast, TfCa WA became inactive after 1 h at 60 °C whereas TfCa wt had still 40% of its initial activity. Based on these results, we determined the temperature profile of both enzymes for BHET hydrolysis in the temperature range of 45−55 °C (Figure 3C). Although a substrate conversion at a similar level of approximately 80% was obtained with both enzymes after a 6 h reaction at 45 and 50 °C, an overall lower BHET conversion of nearly 60% was determined at 55 °C (Figure 3C). At reaction temperatures up to 50 °C, TfCa WA-catalyzed BHET hydrolysis yielded higher amounts of TPA than TfCa wt. Because the biocatalytic conversion of BHET to TPA requires two ester bond cleavages, this suggested a superior hydrolytic activity of TfCa WA over wt at up to 50 °C. Although TfCa wt showed a marginally higher yield of TPA from BHET hydrolysis at 55 °C, the considerably lower total substrate conversion levels with both enzymes exclude this temperature as the ideal reaction condition. Thus, 50 °C appeared to be the optimal temperature for BHET hydrolysis by both enzymes. Next, we performed the enzymatic hydrolysis of MHET at 50 °C. At the

https://doi.org/10.1021/acscatal.2c03772
ACS Catal. XXXX, XXX, XXX−XXX

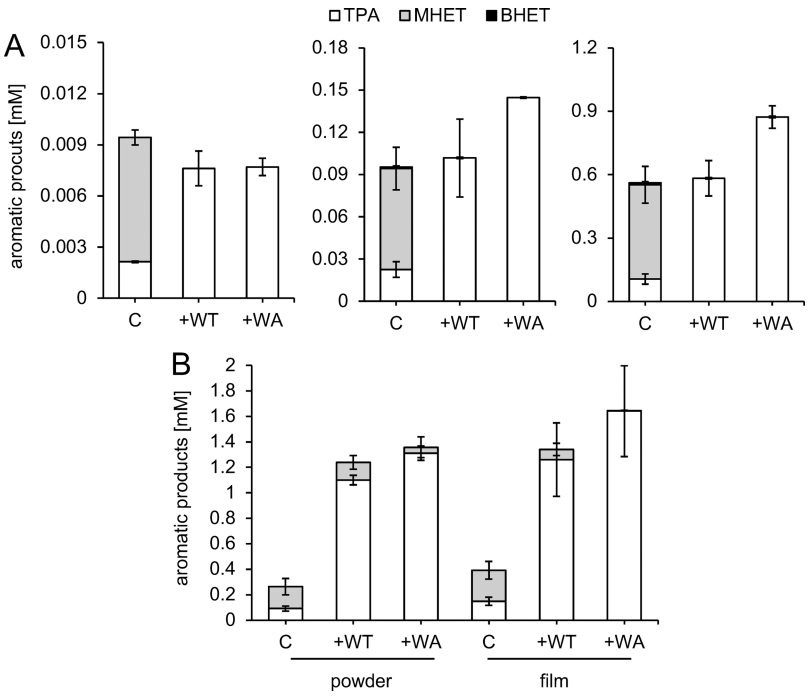

Figure 4. Degradation of various PET materials using a dual enzyme system. *Is*PETase PM is present in all samples, C: control without TfCa, wt: with 0.55 μM TfCa wt, and WA with 0.55 μM TfCa WA. The experiments were performed in 25 mM Tris−HCl buffer (pH 7.5, set at 45 °C). (A) Varying amounts of PET-NP (left: 2 μg/mL, middle: 20 μg/mL, and right: 200 μg/mL) were degraded using 30 nM of *Is*PETase PM and 0.55 μM of the indicated TfCa variant. The concentration of aromatic products was determined after 24 h of incubation at 45 °C. Aromatic products detected by HPLC include BHET, MHET, and TPA. (B) In the same set-up as shown in (A) with high-crystallinity GfPET powder (60 mg/mL) and amorphous PET film (60 mg/mL) as substrates in the presence of 50 nM *Is*PETase PM and 0.55 μM of the indicated TfCa variant. Error bars indicate the standard deviations calculated from at least three replicates.

same substrate concentration of 2 mM, more than twofold TPA was released from MHET compared to BHET with both enzymes. TfCa WA yielded 3.3-fold and 2.6-fold more TPA from the hydrolysis of BHET and MHET than TfCa wt, respectively.

Finally, we compared the rates of TPA release as a result of the enzymatic hydrolysis of MHET at various concentrations ranging from 0.5 to 7 mM (Figure 3D). In agreement with the other experiments described here, TfCa WA hydrolyzed MHET at least three times faster than TfCa wt. The superior activity of TfCa WA is more pronounced at higher substrate concentrations up to 7 mM.

Degradation of PET Polymers Using a Dual Enzyme System. We further used free TfCa in a dual enzyme system in combination with a recently published variant of *Is*PETase PM to degrade PET.[25] Based on its temperature profile determined previously,[25] the degradation reaction was performed at 45 °C. At this condition, neither TfCa wt nor TfCa WA can solely degrade PET-NP to release detectable aromatic products (data not shown). First, varying amounts of PET-NP (2, 20, and 200 μg/mL) were degraded using the dual enzyme system consisting of TfCa and *Is*PETase PM (Figure 4A). When only *Is*PETase PM was present, the main soluble product was MHET independent of the substrate amount used. By adding TfCa wt or its WA variant, TPA was the only detectable product released from PET-NP. With 2 μg/mL of PET-NP, slightly decreased overall product yields were obtained when TfCa enzymes are present. At higher substrate concentrations, the overall product yield was up to 1.6-fold higher with the TfCa WA based dual enzyme system than with TfCa wt. The latter enzyme appeared to only convert the MHET and BHET intermediates to TPA but did not further boost the polymer degradation extent.

Next, we used the dual enzyme system to degrade the high-crystalline GfPET powder and the amorphous GfPET film (Figure 4B). These materials are less degradable for PETases than PET-NP because of higher crystallinity and lower relative surface area.[33] Therefore, we used higher substrate and enzyme concentrations to simplify the detection of degradation products. As shown in Figure 4B, the addition of TPA-ester hydrolyzing enzymes has resulted in a markedly increased overall yield of aromatic products with both GfPET film and GfPET powder. When GfPET film was used as the substrate, the overall yield is 3.4- and 4.2-fold higher, respectively, in the presence of TfCa WA and TfCa wt compared to the reaction with solely *Is*PETase PM. Accordingly, the overall product yield improvements with GfPET powder were 4.7- and 5.2-fold with TfCa wt and TfCa WA, respectively. Additionally, as already observed in reactions with PET-NP, the addition of TfCa enzymes eliminated almost completely the MHET fraction in the degradation products. Overall, the TPA yield was increased by 8.3-fold with PET-NP, 14-fold with PET powder, and 11-fold with GfPET film as substrates using the dual enzyme system with TfCa WA as a helper enzyme for *Is*PETase PM.

DISCUSSION

In this work, we elucidated the apo form as well as ligand-soaked structures of the carboxylesterase TfCa and characterized its enzymatic activity on (tere)phthalate-based oligoesters of various lengths. We found that BHET, an aromatic para-diester, is the most easily hydrolysable substrate for TfCa.

https://doi.org/10.1021/acscatal.2c03772
ACS Catal. XXXX, XXX, XXX−XXX

When the diesters are ortho-positioned, like in DEP, or with two aromatic moieties (BECBA), the specific activity becomes lower but is still higher than the hydrolysis of MHET and other monoesters (Figure 2). The aromatic monoester MEP has an ortho-positioned carboxylic acid end group, and it cannot be further hydrolyzed to PA by TfCa. Molecular docking of DEP into the apo form of TfCa suggests that when MEP reenters the active site, it cannot be further hydrolyzed due to its unproductive positioning in the substrate-binding pocket (Figure 5A,B). For the substrate 3PET, we suggest a

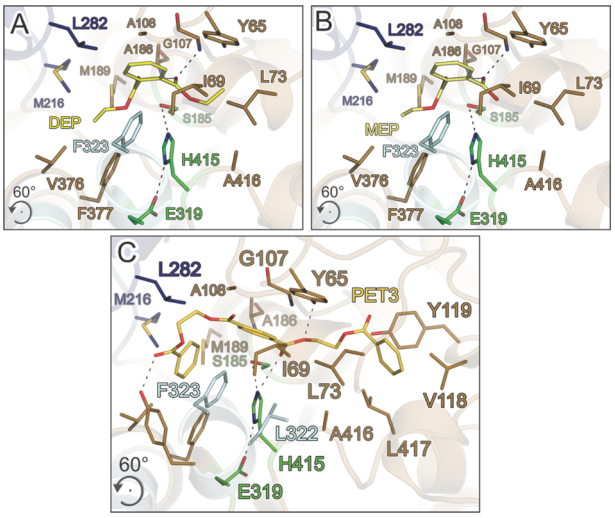

Figure 5. Docking results of various substrates to the TfCa apo structure. (A) Positioning of DEP in the active site of TfCa according to docking experiments. The ester closest to S185 will be cleaved, allowing EG and MEP to leave the active site. (B) The most favorable docking pose of MEP in the active site of TfCa is analogous to that after the hydrolysis event of DEP. In this manner, the ester bond in MEP cannot be hydrolyzed by the enzyme. (C) Positioning of 3PET, the largest substrate investigated, in the active site of TfCa supports the suggested degradation pathway. Residues from different domains are shown in brown ($TfCa^{Hyd}$), dark blue ($TfCa^{LidA}$), and cyan ($TfCa^{LidB}$). Ligands are shown as yellow sticks.

degradation pathway based on the analysis of the hydrolysis products. The first hydrolysis step of 3PET forms HEB and BECBA, which is confirmed by docking results shown in Figure 5C. The positioning of the oligo-ester in the substrate-binding pocket of TfCa suggests a preferential hydrolysis of the second ester bond (Figure 2) in 3PET, releasing the products HEB and BECBA. While HEB should leave the binding site earlier in the hydrolysis event, BECBA could presumably bind the same enzyme molecule more easily, allowing it to undergo pseudo-processive hydrolysis to release MHET and BA. This hypothesis is supported by the change of the product profile determined by HPLC during the TfCa-catalyzed hydrolysis of 3PET (Figure S6).

We engineered TfCa toward higher oligo-ester hydrolyzing activity based on crystal structures of TfCa with different ligands. The mutant TfCa WA possesses a 3.3-fold higher activity in converting BHET to TPA compared to TfCa wt.

We used the variant TfCa WA in a dual enzyme system to depolymerize PET together with a recently published variant of *Is*PETase.[25] The addition of the carboxylesterase increased the TPA yield in the reaction by up to 14-fold. Similar to MHETase from *I. sakaiensis*, TfCa alone is not active on PET but can promote the conversion of MHET, which is the major product of enzymatic PET depolymerization by many PET hydrolases,[34] in a dual enzyme system with *Is*PETase PM. This conversion will not only help to offset the inhibitory effect of MHET on PET hydrolases, but it will furthermore aid in the recovery of extremely pure TPA, which can be directly used for the polymer synthesis.[4,5] In the presence of immobilized TfCa, an increased yield of TPA from PET film has been reported with a dual enzyme system containing the PET hydrolases LC-cutinase or TfCut2.[15] The authors immobilized TfCa using a SulfoLink matrix. This dual enzyme system resulted in an increased overall product yield by 91% for TfCut2 and 104% for LCC. Using another dual enzyme system containing chimeric *I. sakaiensis* PETase and MHETase, Knott et al. degraded the amorphous PET film (2−3% crystallinity, Goodfellow, UK) at 30 °C for 96 h using 0.25 mg PETase and 0.5 mg MHETase per gram PET.[12] *Is*PETase alone produced approximately 0.2 mM TPA at this condition, whereas the addition of free MHETase resulted in a twofold higher TPA yield. The chimeric proteins of MHETase and *Is*PETase constructed in the same study showed further increased activity by up to sevenfold in comparison to the dual free enzyme system.[12] In this study, we used a recently published variant of *Is*PETase[25] in combination with TfCa wt and WA. Compared to the results reported by Knott et al., we yielded the same amount of TPA from the same substrate (GfPET amorphous film) using 10% *Is*PETase (0.024 mg/g PET) within one-fourth of the reaction time (24 h) at 45 °C.

In general, carboxylesterases such as TfCa are known to exhibit similar functions and contain highly conserved regions. We constructed a phylogenetic tree showing the relationship between the different homologous sequences to TfCa (Figure S8). Some of the strains we found in the phylogenetic tree, for example, *Thermobifida alba*, *Thermobifida halotolerans*, and *Actinomadura hallensis*, contain enzymes known to potentially catalyze the PET polymer degradation.[35−37] Furthermore, the strains *Actinomadura rubrobrunea*, *Actinomadura nitritigenes*, and *Thermobifida cellulosilytica* were mentioned in a phylogenetic study on the characterization and isolation of polyester degrading bacteria.[38] These findings lead to the question of whether polyester depolymerases and oligomer hydrolases co-exist in bacteria. Since both the PETase and the MHETase were found in *I. sakaiensis*, the emergence of natural dual enzyme systems appears to be a logical conclusion. Additionally, *I. sakaiensis* was found to metabolize TPA and possess a specific TPA translocation system.[39] However, the lack of a specific transporter machinery for MHET in *I. sakaiensis* invalidates the assumption that the extracellular PETase and intracellular MHETase can work synergistically during the bacterial assimilation of PET. Similarly, TfCa and TfCut2, the artificially synergistic enzymes in PET depolymerization, are derived from the same species of *T. fusca*.[15] Unlike *I. sakaiensis*, the genome of *T. fusca*[40] does not encode any potential TPA metabolic pathway. Kleeberg et al. have grown a *T. fusca* strain on mineral salt agar using a TPA-containing aliphatic-aromatic co-polyester as the sole carbon source.[41] Although the polyesters depolymerized rapidly during the culturing process, only poor bacterial growth was observed. This is in line with the aforementioned genome analysis, which suggests *T. fusca* cannot effectively metabolize PET degradation products, including MHET. As *T. fusca* is extremely unlikely to be able to translocate MHET into the cytosol, similar to *I. sakaiensis*, the role of TfCa in PET depolymerization in the natural environment remains elusive.

https://doi.org/10.1021/acscatal.2c03772
ACS Catal. XXXX, XXX, XXX−XXX

The ability of TfCa to degrade the ortho-phthalate ester DEP broadens its substrate specificity. DEP is not only an ortho-phthalate ester but also one of the widely used plasticizers, which are produced annually on a million-ton scale. Plasticizers are added to various polymer materials to alter their properties for easier raw material handling or to meet the application demands required for the end products.[42] However, phthalate-ester-based plasticizers like DEP are known to have endocrine-disrupting, carcinogenic, teratogenic, and mutagenic effects on humans and wildlife.[43] As a result, an efficient decontamination of phthalic esters is a global concern. PA can be assimilated by various microbes and used as a carbon source.[44−46] PA-ring opening enzymes, such as dioxygenases and carboxylesterases, are needed by the PA assimilating species like *Rhodococcus*, *Sphingomonas*, or *Arthrobacter* and others. Nonetheless, our phylogenetic analysis (Figure S8) indicates that these strains are unlikely to express TfCa homologous enzymes. Although the promiscuous hydrolytic activity of TfCa on aromatic oligo-esters in nature is still unknown, the recombinant form of this enzyme has the potential to find ideal application scenarios in the area of environmental biocatalysis and remediation.

In conclusion, the apo and complex crystal structures of TfCa solved in this study shed light on the mechanistic aspects of this enzyme in the hydrolysis of aromatic oligo-esters. These findings allow us to rationally engineer TfCa and applied its most active WA variant in a simple dual enzyme system to relieve product inhibition during enzymatic PET depolymerization. In comparison to previous efforts that employed cross-linked MHETase and *Is*PETase or immobilized TfCa, our simplified dual enzyme system provides a more efficient and less costly solution, which may hold greater promise for industrial-scale applications.[47]

■ ASSOCIATED CONTENT

Supporting Information

The Supporting Information is available free of charge at https://pubs.acs.org/doi/10.1021/acscatal.2c03772.

Materials and methods; data collection of crystal structures; melting temperature of TfCa mutants with increased activity towards BHET; individual contributions of amino acid residues to ligand binding for TfCa and MHETase; ligand binding and unbinding events defined by the catalytic C−O distance for individual protein−ligand complexes with MHET as the ligand; number of snapshots clustered based on the catalytic distance; sequence alignment of TfCa with *p*-nitrobenzyl esterase (pNB-E) and a carboxylesterase; structural alignment of TfCa with *p*-nitrobenzyl esterase and a carboxylesterase; ligand-soaked structure of TfCa with ligand BHET as well as apo form of TfCa docked with DEP and MEP; alanine scan of the substrate binding pocket of TfCa; semi-rational enzyme engineering of TfCa based on the elucidated structure; hydrolysis of 3PET by TfCa over a time course of 6 h; exo-PETase function of TfCa; relation of TfCa to enzymes with similar sequences; putative degradation pathways for 3PET; comparison of residues contributing to the binding of MHET in TfCa and MHETase; confirming MEP as the product of DEP degradation by TfCa; and nucleotide and protein sequence of TfCa wt (PDF)

■ AUTHOR INFORMATION

Corresponding Authors

Weidong Liu − *Tianjin Institute of Industrial Biotechnology, Chinese Academy of Sciences, Tianjin 300308, China; National Technology Innovation Center of Synthetic Biology, Tianjin 300308, China; University of Chinese Academy of Sciences, Beijing 100049, China;* orcid.org/0000-0001-7954-7700; Email: liu_wd@tib.cas.cn

Uwe T. Bornscheuer − *Department of Biotechnology and Enzyme Catalysis, Institute of Biochemistry, University of Greifswald, 17487 Greifswald, Germany;* orcid.org/0000-0003-0685-2696; Email: uwe.bornscheuer@uni-greifswald.de

Ren Wei − *Department of Biotechnology and Enzyme Catalysis, Institute of Biochemistry, University of Greifswald, 17487 Greifswald, Germany;* orcid.org/0000-0003-3876-1350; Email: ren.wei@uni-greifswald.de

Authors

Gerlis von Haugwitz − *Department of Biotechnology and Enzyme Catalysis, Institute of Biochemistry, University of Greifswald, 17487 Greifswald, Germany*

Xu Han − *Tianjin Institute of Industrial Biotechnology, Chinese Academy of Sciences, Tianjin 300308, China; National Technology Innovation Center of Synthetic Biology, Tianjin 300308, China*

Lara Pfaff − *Department of Biotechnology and Enzyme Catalysis, Institute of Biochemistry, University of Greifswald, 17487 Greifswald, Germany;* orcid.org/0000-0002-1529-8917

Qian Li − *Tianjin Institute of Industrial Biotechnology, Chinese Academy of Sciences, Tianjin 300308, China; National Technology Innovation Center of Synthetic Biology, Tianjin 300308, China*

Hongli Wei − *Tianjin Institute of Industrial Biotechnology, Chinese Academy of Sciences, Tianjin 300308, China; National Technology Innovation Center of Synthetic Biology, Tianjin 300308, China*

Jian Gao − *Tianjin Institute of Industrial Biotechnology, Chinese Academy of Sciences, Tianjin 300308, China; National Technology Innovation Center of Synthetic Biology, Tianjin 300308, China*

Karen Methling − *Department of Cellular Biochemistry and Metabolomics, Institute of Biochemistry, University of Greifswald, 17487 Greifswald, Germany*

Yufei Ao − *Department of Biotechnology and Enzyme Catalysis, Institute of Biochemistry, University of Greifswald, 17487 Greifswald, Germany; University of Chinese Academy of Sciences, Beijing 100049, China*

Yannik Brack − *Department of Biotechnology and Enzyme Catalysis, Institute of Biochemistry, University of Greifswald, 17487 Greifswald, Germany*

Jan Mican − *Loschmidt Laboratories, Department of Experimental Biology and RECETOX, Faculty of Science, Masaryk University, 625 00 Brno, Czech Republic; International Clinical Research Center, St. Anne's University Hospital, 656 91 Brno, Czech Republic;* orcid.org/0000-0002-8877-163X

Christian G. Feiler − *Macromolecular Crystallography, Helmholtz-Zentrum Berlin, 12489 Berlin, Germany*

Manfred S. Weiss − *Macromolecular Crystallography, Helmholtz-Zentrum Berlin, 12489 Berlin, Germany*

https://doi.org/10.1021/acscatal.2c03772
ACS Catal. XXXX, XXX, XXX−XXX

David Bednar − *Loschmidt Laboratories, Department of Experimental Biology and RECETOX, Faculty of Science, Masaryk University, 625 00 Brno, Czech Republic; International Clinical Research Center, St. Anne's University Hospital, 656 91 Brno, Czech Republic*

Gottfried J. Palm − *Department of Synthetic and Structural Biochemistry, Institute of Biochemistry, University of Greifswald, 17487 Greifswald, Germany;* orcid.org/0000-0003-0329-0413

Michael Lalk − *Department of Cellular Biochemistry and Metabolomics, Institute of Biochemistry, University of Greifswald, 17487 Greifswald, Germany*

Michael Lammers − *Department of Synthetic and Structural Biochemistry, Institute of Biochemistry, University of Greifswald, 17487 Greifswald, Germany*

Jiri Damborsky − *Loschmidt Laboratories, Department of Experimental Biology and RECETOX, Faculty of Science, Masaryk University, 625 00 Brno, Czech Republic; International Clinical Research Center, St. Anne's University Hospital, 656 91 Brno, Czech Republic*

Gert Weber − *Macromolecular Crystallography, Helmholtz-Zentrum Berlin, 12489 Berlin, Germany;* orcid.org/0000-0003-3624-1060

Complete contact information is available at: https://pubs.acs.org/10.1021/acscatal.2c03772

Author Contributions

Conceptualization, R.W., W.L., and U.T.B.; protein crystallographic studies, J.G., X.H., C.G.F., Q.L., G.J.P., M.L., and W.L.; computational simulations, G.W., J.M., D.B., J.D., and W.L.; protein engineering and characterization, G.H.; substrate generation and characterization, Y.A. and L.P.; product identification, G.H., K.M., M.L., and R.W.; generation of the phylogenetic tree, Y.B.; writing—original draft, G.H., J.M., W.L., and R.W.; writing, review and editing, all authors; supervision and funding acquisition, J.D., W.L., U.T.B., and R.W.

Funding

The authors W.L., J.G., X.H., Q.L., and H.W. acknowledge the financial support provided by the National Key Research and Development Program of China (2018YFA0901201, 2021YFA0910200, and 2021YFC2103600). The authors U.B., R.W., G.H., D.B., J.M., and J.D., gratefully acknowledge the financial support received from the European Union's Horizon 2020 research and innovation program (MIX-UP, Grant number 870294; CETOCOEN Excellence, Grant number 857560) and the Czech Ministry of Education (CZ.02.1.01/0.0/0.0/16_026/0008451). The authors J.G., X.H., and W.L. also thank the Tianjin Synthetic Biotechnology Innovation Capacity Improvement Project (TSBICIP-PTJJ-008, TSBICIP-IJCP-003, TSBICIP-KJGG-009-01, and TSBICIP-KJGG-002-06), the Youth Innovation Promotion Association CAS and the China Scholarship Council for financial support. Computational resources were supplied by the project "e-Infrastruktura CZ" (e-INFRA CZ LM2018140) supported by the Ministry of Education, Youth and Sports of the Czech Republic and by the ELIXIR-CZ project (LM2018131), part of the international ELIXIR infrastructure.

Notes

The authors declare no competing financial interest.

ACKNOWLEDGMENTS

We thank the staff from the BL10U2/BL02U1(BL17U)/BL17B/BL18U1/BL19U1 beamlines of the National Facility for Protein Science in Shanghai (NFPS) at Shanghai Synchrotron Radiation Facility (SSRF) and the staff from the Beamline 14.1 at BESSY for assistance during data collection.

ABBREVIATIONS

BA	benzoic acid
BECBA	4-{[2-(benzoyloxy)ethoxy]-carbonyl} benzoic acid
BHET	bis(2-hydroxyethyl) terephthalate
DEP	diethyl phthalate
DMSO	dimethyl sulfoxide
DSF	differential scanning fluorimetry
EG	ethylene glycol
GfPET	amorphous PET film purchased from Goodfellow Ltd.
HEB	2-hydroxyethyl-benzoate
HPLC	high-performance liquid chromatography
IPTG	isopropyl β-D-thiogalactopyranoside
*Is*PETase PM	a variant of PETase from *Ideonella sakaiensis*
LC−MS	liquid chromatography coupled with mass spectrometry
MEP	monoethyl phthalate
MD	molecular dynamics
MHET	mono(2-hydroxyethyl) terephthalate
MHETA	4-[(2-hydroxyethyl) carbamoyl] benzoic acid
MR	molecular replacement
Ni-NTA	Ni^{2+}-nitrilotriacetic acid
OD_{600}	optical density measured at 600 nm
NP	nanoparticle
PA	phthalic acid
PET	polyethylene terephthalate
PETase	PET hydrolase
pNPA	para-nitrophenyl acetate
p-NP-E	*p*-nitrobenzyl esterase
T. fusca	*Thermobifida fusca*
TfCa	carboxylesterase from *T. fusca*
T_g	glass transition temperature
T_m	melting temperature
TPA	terephthalate
WA	TfCa variant$^{I69W/V376A}$
3PET	bis[2-(benzoyloxy)ethyl] terephthalate

REFERENCES

(1) Wei, R.; Tiso, T.; Bertling, J.; O'Connor, K.; Blank, L. M.; Bornscheuer, U. T. Possibilities and limitations of biotechnological plastic degradation and recycling. *Nat. Catal.* **2020**, *3*, 867−871.

(2) Müller, R.-J.; Schrader, H.; Profe, J.; Dresler, K.; Deckwer, W.-D. Enzymatic degradation of poly(ethylene terephthalate): Rapid hydrolyse using a hydrolase from *T. fusca*. *Macromol. Rapid Commun.* **2005**, *26*, 1400−1405.

(3) Lu, H.; Diaz, D. J.; Czarnecki, N. J.; Zhu, C.; Kim, W.; Shroff, R.; Acosta, D. J.; Alexander, B. R.; Cole, H. O.; Zhang, Y.; Lynd, N. A.; Ellington, A. D.; Alper, H. S. Machine learning-aided engineering of hydrolases for PET depolymerization. *Nature* **2022**, *604*, 662−667.

(4) Wei, R.; von Haugwitz, G.; Pfaff, L.; Mican, J.; Badenhorst, C. P. S.; Liu, W.; Weber, G.; Austin, H. P.; Bednar, D.; Damborsky, J.; Bornscheuer, U. T. Mechanism-based design of efficient PET hydrolases. *ACS Catal.* **2022**, *12*, 3382−3396.

(5) Tournier, V.; Topham, C. M.; Gilles, A.; David, B.; Folgoas, C.; Moya-Leclair, E.; Kamionka, E.; Desrousseaux, M.-L.; Texier, H.; Gavalda, S.; Cot, M.; Guémard, E.; Dalibey, M.; Nomme, J.; Cioci, G.;

(6) Wei, R.; Zimmermann, W. Microbial enzymes for the recycling of recalcitrant petroleum-based plastics: how far are we? *Microb. Biotechnol.* **2017**, *10*, 1308−1322.
(7) Barth, M.; Oeser, T.; Wei, R.; Then, J.; Schmidt, J.; Zimmermann, W. Effect of hydrolysis products on the enzymatic degradation of polyethylene terephthalate nanoparticles by a polyester Hydrolase from *Thermobifida fusca*. *Biochem. Eng. J.* **2015**, *93*, 222−228.
(8) Barth, M.; Wei, R.; Oeser, T.; Then, J.; Schmidt, J.; Wohlgemuth, F.; Zimmermann, W. Enzymatic hydrolysis of polyethylene terephthalate films in an ultrafiltration membrane reactor. *J. Membr. Sci.* **2015**, *494*, 182−187.
(9) Wei, R.; Oeser, T.; Schmidt, J.; Meier, R.; Barth, M.; Then, J.; Zimmermann, W. Engineered bacterial polyester hydrolases efficiently degrade polyethylene terephthalate due to relieved product inhibition. *Biotechnol. Bioeng.* **2016**, *113*, 1658−1665.
(10) Yoshida, S.; Hiraga, K.; Takehana, T.; Taniguchi, I.; Yamaji, H.; Maeda, Y.; Toyohara, K.; Miyamoto, K.; Kimura, Y.; Oda, K. A bacterium that degrades and assimilates poly(ethylene terephthalate). *Science* **2016**, *351*, 1196−1199.
(11) Palm, G. J.; Reisky, L.; Böttcher, D.; Müller, H.; Michels, E. A. P.; Walczak, M. C.; Berndt, L.; Weiss, M. S.; Bornscheuer, U. T.; Weber, G. Structure of the plastic-degrading *Ideonella sakaiensis* MHETase bound to a substrate. *Nat. Commun.* **2019**, *10*, 1717.
(12) Knott, B. C.; Erickson, E.; Allen, M. D.; Gado, J. E.; Graham, R.; Kearns, F. L.; Pardo, I.; Topuzlu, E.; Anderson, J. J.; Austin, H. P.; Dominick, G.; Johnson, C. W.; Rorrer, N. A.; Szostkiewicz, C. J.; Copié, V.; Payne, C. M.; Woodcock, H. L.; Donohoe, B. S.; Beckham, G. T.; McGeehan, J. E. Characterization and engineering of a two-enzyme system for plastics depolymerization. *Proc. Natl. Acad. Sci. U. S. A.* **2020**, *117*, 25476−25485.
(13) Billig, S.; Oeser, T.; Birkemeyer, C.; Zimmermann, W. Hydrolysis of cyclic poly(ethylene terephthalate) trimers by a carboxylesterase from *Thermobifida fusca* KW3. *Appl. Microbiol. Biotechnol.* **2010**, *87*, 1753−1764.
(14) Oeser, T.; Wei, R.; Baumgarten, T.; Billig, S.; Föllner, C.; Zimmermann, W. High level expression of a hydrophobic poly(ethylene terephthalate)-hydrolyzing carboxylesterase from *Thermobifida fusca* KW3 in *Escherichia coli* BL21(DE3). *J. Biotechnol.* **2010**, *146*, 100−104.
(15) Barth, M.; Honak, A.; Oeser, T.; Wei, R.; Belisário-Ferrari, M. R.; Then, J.; Schmidt, J.; Zimmermann, W. A dual enzyme system composed of a polyester hydrolase and a carboxylesterase enhances the biocatalytic degradation of polyethylene terephthalate films. *Biotechnol. J.* **2016**, *11*, 1082−1087.
(16) Sagong, H.-Y.; Seo, H.; Kim, T.; Son, H. F.; Joo, S.; Lee, S. H.; Kim, S.; Woo, J.-S.; Hwang, S. Y.; Kim, K.-J. Decomposition of the PET film by MHETase using exo-PETase function. *ACS Catal.* **2020**, *10*, 4805−4812.
(17) Pfaff, L.; Breite, D.; Badenhorst, C. P. S.; Bornscheuer, U.; Wei, R. Fluorimetric high-throughput screening method for polyester hydrolase activity using polyethylene terephthalate nanoparticles. *Methods Enzymol.* **2021**, *648*, 253−270.
(18) Fischer-Colbrie, G.; Heumann, S.; Liebminger, S.; Almansa, E.; Cavaco-Paulo, A.; Guebitz, G. M. New enzymes with potential for PET surface modification. *Biocatal. Biotransform.* **2004**, *22*, 341−346.
(19) Mueller, U.; Förster, R.; Hellmig, M.; Huschmann, F. U.; Kastner, A.; Malecki, P.; Pühringer, S.; Röwer, M.; Sparta, K.; Steffien, M.; Ühlein, M.; Wilk, P.; Weiss, M. S. The macromolecular crystallography beamlines at BESSY II of the Helmholtz-Zentrum Berlin: Current status and perspectives. *Eur. Phys. J. Plus* **2015**, *130*, 141.
(20) McCoy, A. J.; Grosse-Kunstleve, R. W.; Adams, P. D.; Winn, M. D.; Storoni, L. C.; Read, R. J. Phaser crystallographic software. *J. Appl. Crystallogr.* **2007**, *40*, 658−674.
(21) Liebschner, D.; Afonine, P. V.; Baker, M. L.; Bunkóczi, G.; Chen, V. B.; Croll, T. I.; Hintze, B.; Hung, L.-W.; Jain, S.; McCoy, A. J.; Moriarty, N. W.; Oeffner, R. D.; Poon, B. K.; Prisant, M. G.; Read, R. J.; Richardson, J. S.; Richardson, D. C.; Sammito, M. D.; Sobolev, O. V.; Stockwell, D. H.; Terwilliger, T. C.; Urzhumtsev, A. G.; Videau, L. L.; Williams, C. J.; Adams, P. D. Macromolecular structure determination using X-rays, neutrons and electrons: recent developments in Phenix. *Acta Crystallogr. D Struct. Biol.* **2019**, *75*, 861−877.
(22) Afonine, P. V.; Grosse-Kunstleve, R. W.; Echols, N.; Headd, J. J.; Moriarty, N. W.; Mustyakimov, M.; Terwilliger, T. C.; Urzhumtsev, A.; Zwart, P. H.; Adams, P. D. Towards automated crystallographic structure refinement with phenix.refine. *Acta Crystallogr. D Biol. Crystallogr.* **2012**, *68*, 352−367.
(23) Emsley, P.; Cowtan, K. Coot: model-building tools for molecular graphics. *Acta Crystallogr. D Biol. Crystallogr.* **2004**, *60*, 2126−2132.
(24) Brünger, A. T. Assessment of phase accuracy by cross validation: the free R value. Methods and applications. *Acta Crystallogr. D Biol. Crystallogr.* **1993**, *49*, 24−36.
(25) Brott, S.; Pfaff, L.; Schuricht, J.; Schwarz, J.-N.; Böttcher, D.; Badenhorst, C. P. S.; Wei, R.; Bornscheuer, U. T. Engineering and evaluation of thermostable IsPETase variants for PET degradation. *Eng. Life Sci.* **2022**, *22*, 192−203.
(26) Trott, O.; Olson, A. J. AutoDock Vina: improving the speed and accuracy of docking with a new scoring function, efficient optimization, and multithreading. *J. Comput. Chem.* **2010**, *31*, 455−461.
(27) Berman, H. M.; Westbrook, J.; Feng, Z.; Gilliland, G.; Bhat, T. N.; Weissig, H.; Shindyalov, I. N.; Bourne, P. E. The Protein Data Bank. *Nucleic Acids Res.* **2000**, *28*, 235−242.
(28) Miller, B. R.; McGee, T. D.; Swails, J. M.; Homeyer, N.; Gohlke, H.; Roitberg, A. E. MMPBSA.py: An efficient program for end-state free energy calculations. *J. Chem. Theory Comput.* **2012**, *8*, 3314−3321.
(29) Genheden, S.; Ryde, U. The MM/PBSA and MM/GBSA methods to estimate ligand-binding affinities. *Expert Opin. Drug Discov.* **2015**, *10*, 449−461.
(30) Weiser, J.; Shenkin, P. S.; Still, W. C. Approximate atomic surfaces from linear combinations of pairwise overlaps (LCPO). *J. Comput. Chem.* **1999**, *20*, 217−230.
(31) Eberl, A.; Heumann, S.; Brückner, T.; Araujo, R.; Cavaco-Paulo, A.; Kaufmann, F.; Kroutil, W.; Guebitz, G. M. Enzymatic surface hydrolysis of poly(ethylene terephthalate) and bis-(benzoyloxyethyl) terephthalate by lipase and cutinase in the presence of surface active molecules. *J. Biotechnol.* **2009**, *143*, 207−212.
(32) Belisário-Ferrari, M. R.; Wei, R.; Schneider, T.; Honak, A.; Zimmermann, W. Fast turbidimetric assay for analyzing the enzymatic hydrolysis of polyethylene terephthalate model substrates. *Biotechnol. J.* **2019**, *14*, No. 1800272.
(33) Vogel, K.; Wei, R.; Pfaff, L.; Breite, D.; Al-Fathi, H.; Ortmann, C.; Estrela-Lopis, I.; Venus, T.; Schulze, A.; Harms, H.; Bornscheuer, U. T.; Maskow, T. Enzymatic degradation of polyethylene terephthalate nanoplastics analyzed in real time by isothermal titration calorimetry. *Sci. Total Environ.* **2021**, *773*, No. 145111.
(34) Pfaff, L.; Gao, J.; Li, Z.; Jäckering, A.; Weber, G.; Mican, J.; Chen, Y.; Dong, W.; Han, X.; Feiler, C. G.; Ao, Y.-F.; Badenhorst, C. P. S.; Bednar, D.; Palm, G. J.; Lammers, M.; Damborsky, J.; Strodel, B.; Liu, W.; Bornscheuer, U. T.; Wei, R. Multiple substrate binding mode-guided engineering of a thermophilic PET hydrolase. *ACS Catal.* **2022**, *12*, 9790−9800.
(35) Ribitsch, D.; Herrero Acero, E.; Greimel, K.; Dellacher, A.; Zitzenbacher, S.; Marold, A.; Rodriguez, R. D.; Steinkellner, G.; Gruber, K.; Schwab, H.; Guebitz, G. M. A New esterase from *Thermobifida halotolerans* hydrolyses polyethylene terephthalate (PET) and polylactic acid (PLA). *Polymer* **2012**, *4*, 617−629.
(36) Samak, N. A.; Jia, Y.; Sharshar, M. M.; Mu, T.; Yang, M.; Peh, S.; Xing, J. Recent advances in biocatalysts engineering for polyethylene terephthalate plastic waste green recycling. *Environ. Int.* **2020**, *145*, No. 106144.

https://doi.org/10.1021/acscatal.2c03772
ACS Catal. XXXX, XXX, XXX−XXX

(37) Sonnendecker, C.; Oeser, J.; Richter, P. K.; Hille, P.; Zhao, Z.; Fischer, C.; Lippold, H.; Blázquez-Sánchez, P.; Engelberger, F.; Ramírez-Sarmiento, C. A.; Oeser, T.; Lihanova, Y.; Frank, R.; Jahnke, H.-G.; Billig, S.; Abel, B.; Sträter, N.; Matysik, J.; Zimmermann, W. Low carbon footprint recycling of post-consumer PET plastic with a metagenomic polyester hydrolase. *ChemSusChem* **2022**, *15*, No. e202101062.
(38) Sriyapai, P.; Chansiri, K.; Sriyapai, T. Isolation and characterization of polyester-based plastics-degrading bacteria from compost soils. *Microbiology* **2018**, *87*, 290−300.
(39) Gautom, T.; Dheeman, D.; Levy, C.; Butterfield, T.; Alvarez Gonzalez, G.; Le Roy, P.; Caiger, L.; Fisher, K.; Johannissen, L.; Dixon, N. Structural basis of terephthalate recognition by solute binding protein TphC. *Nat. Commun.* **2021**, *12*, 6244.
(40) Lykidis, A.; Mavromatis, K.; Ivanova, N.; Anderson, I.; Land, M.; DiBartolo, G.; Martinez, M.; Lapidus, A.; Lucas, S.; Copeland, A.; Richardson, P.; Wilson, D. B.; Kyrpides, N. Genome sequence and analysis of the soil cellulolytic actinomycete *Thermobifida fusca* YX. *J. Bacteriol.* **2007**, *189*, 2477−2486.
(41) Kleeberg, I.; Hetz, C.; Kroppenstedt, R. M.; Müller, R.-J.; Deckwer, W.-D. Biodegradation of aliphatic-aromatic copolyesters by *Thermomonospora fusca* and other thermophilic compost isolates. *Appl. Environ. Microbiol.* **1998**, *64*, 1731−1735.
(42) Giam, C. S.; Atlas, E.; Powers, M. A.; Leonard, J. E. Phthalic acid esters. In *Anthropogenic Compounds*; Springer: Berlin, Heidelberg, 1984; pp. 67−142.
(43) Baloyi, N. D.; Tekere, M.; Maphangwa, K. W.; Masindi, V. Insights into the prevalence and impacts of phthalate esters in aquatic ecosystems. *Front. Environ. Sci.* **2021**, *9*, No. 684190.
(44) Boll, M.; Geiger, R.; Junghare, M.; Schink, B. Microbial degradation of phthalates: biochemistry and environmental implications. *Environ. Microbiol. Rep.* **2020**, *12*, 3−15.
(45) Gao, D.-W.; Wen, Z.-D. Phthalate esters in the environment: A critical review of their occurrence, biodegradation, and removal during wastewater treatment processes. *Sci. Total Environ.* **2016**, *541*, 986−1001.
(46) Vamsee-Krishna, C.; Phale, P. S. Bacterial degradation of phthalate isomers and their esters. *Indian J. Microbiol.* **2008**, *48*, 19−34.
(47) Singh, A.; Rorrer, N. A.; Nicholson, S. R.; Erickson, E.; DesVeaux, J. S.; Avelino, A. F. T.; Lamers, P.; Bhatt, A.; Zhang, Y.; Avery, G.; Tao, L.; Pickford, A. R.; Carpenter, A. C.; McGeehan, J. E.; Beckham, G. T. Techno-economic, life-cycle, and socioeconomic impact analysis of enzymatic recycling of poly(ethylene terephthalate). *Joule* **2021**, *5*, 2479−2503.

https://doi.org/10.1021/acscatal.2c03772
ACS Catal. XXXX, XXX, XXX−XXX

SUPPORTING INFORMATION

Structural Insights into (Tere)phthalate-ester Hydrolysis by a Carboxylesterase and its Role in Promoting PET Depolymerization

Gerlis von Haugwitz[1], Xu Han[2,3], Lara Pfaff[1], Qian Li[2,3], Hongli Wei[2,3], Jian Gao[2,3], Karen Methling[4], Yufei Ao[1,5], Yannik Brack[1], Jan Mican[6,7], Christian G. Feiler[8], Manfred S. Weiss[8], David Bednar[6,7], Gottfried J. Palm[9], Michael Lalk[4], Michael Lammers[9], Jiri Damborsky[6,7], Gert Weber[8], Weidong Liu[2,3,5,], Uwe T. Bornscheuer[1,*], Ren Wei[1,*]*

[1]Department of Biotechnology & Enzyme Catalysis, Institute of Biochemistry, University of Greifswald, Felix-Hausdorff-Str. 4, 17487 Greifswald, Germany

[2]Tianjin Institute of Industrial Biotechnology, Chinese Academy of Sciences, 32 West 7th Avenue, Tianjin Airport Economic Area, Tianjin 300308, China

[3]National Technology Innovation Center of Synthetic Biology, 32 West 7th Avenue, Tianjin Airport Economic Area, Tianjin 300308, China

[4]Department of Cellular Biochemistry & Metabolomics, Institute of Biochemistry, University of Greifswald, Felix-Hausdorff-Str. 4, 17487 Greifswald, Germany

[5]University of Chinese Academy of Sciences, 19A Yuquan Road, Beijing, 100049 China

[6]Loschmidt Laboratories, Department of Experimental Biology and RECETOX, Faculty of Science, Masaryk University, Kamenice 5/C13, 625 00 Brno, Czech Republic

[7]International Clinical Research Center, St. Anne's University Hospital, Pekarska 53, 656 91 Brno, Czech Republic

[8]Macromolecular Crystallography, Helmholtz-Zentrum Berlin, Alber-Einstein-Straße 15, 12489 Berlin, Germany

[9]Department Synthetic and Structural Biochemistry, Institute of Biochemistry, University of Greifswald, Felix-Hausdorff-Str. 4, 17487 Greifswald, Germany

*Email: liu_wd@tib.cas.cn; uwe.bornscheuer@uni-greifswald.de; ren.wei@uni-greifswald.de

Methods

Cloning and site-directed mutagenesis for crystallography

The gene encoding TfCa (GenBank accession number: GAZ65068.1) from *Thermobifida fusca* KW3 was chemically synthesized by GENE ray Biotech Co. (Shanghai, China) and ligated into the pET32a vector. TfCa E319L mutant was prepared by using the QuikChange site-directed mutagenesis kit (Agilent Technologies, Santa Clara, CA, USA) with the TfCa-encoding plasmid as the template. The PCR products were incubated with DpnI (New England Biolabs, Hitchin, UK) to digest the original DNA template and then separately transformed into the *Escherichia coli* strain XL1-Blue. The mutations were confirmed by sequencing.

Protein expression and purification for crystallography

The TfCa-gene harboring plasmid was transformed into *E. coli* BL21trxB(DE3) cells which were grown in lysogeny broth (LB) medium at 37°C to an optical density (OD_{600}) of approximately 0.8 and then induced with 0.6 mM isopropyl β-D-thiogalactopyranoside (IPTG) at 16°C for 20 h. Cells were harvested by centrifugation at 5,000 x g for 15 min and then re-suspended in lysis buffer containing 25 mM Tris-HCl, pH 7.5, 150 mM NaCl and 20 mM imidazole, followed by disruption with a French Press (800-1200 bar, 2-5 cycles until homogenization). Cell debris was removed by centrifugation at 17,000 x g for 1 h. The supernatant was then applied to a Ni^{2+}-NTA column with FPLC system (GE Healthcare, Chicago, USA). The target proteins were eluted at approximately 100 mM imidazole when using a 20-

250 mM imidazole gradient. Each protein was dialyzed against a buffer containing 25 mM Tris-HCl, pH 7.5, 150 mM NaCl, and subjected to tobacco etch virus (TEV) protease digestion overnight to remove the hexa-histidine (6×His) tag. The mixture was then passed through another Ni-NTA column. The untagged protein was eluted with 25 mM Tris-HCl, pH 7.5, 150 mM NaCl. The purity of each protein (> 95%) was checked by sodium dodecyl sulfate polyacrylamide gel electrophoresis (SDS-PAGE) analysis. Each of the purified proteins was concentrated to 40 mg/mL for crystallization screening.

Solid phase extraction and product identification with mass spectrometry

Prior to liquid chromatography mass spectrometry (LC-MS), solid phase extraction (SPE) was performed. For that purpose, the SPE cartridge (C18e) was conditioned 2× with 1 mL acetonitrile and equilibrated with 1 mL distilled water. The sample was applied to the cartridge and washed with 1 mL distilled water. The compounds were then eluted using 2×0.5 mL 1:4 (v/v) acetonitrile:water solution and afterwards the solvent was removed from the sample using TurboVap® (Biotage, Upsala, Sweden). Finally, the residues were dissolved in 100 µL of 1:4 (v/v) acetonitrile:water solution.

For the determination of the mass of the degradation products obtained from TfCa-catalyzed conversion of diethyl phthalate (DEP), the sample was injected without column into an Agilent 6460 Triple Quadrupole LC/MS system. The product ion scan was carried out in the negative mode in a range of mass to charge ratio (m/z) 70-300 with a collision energy of 6 V.

Molecular dynamics simulations

The crystal structure of TfCa with the ligand MHETA (PDB-ID: 7W1J, 1.92 Å) as well as the chain A structure of MHETase from *I. sakaiensis* (PDB-ID: 6QGA, 2.1 Å)[5,6] were used for molecular dynamics (MD) simulations. Residues of the enzymes were numbered according to UniProt (UniProt IDs: TfCa: P86325 and MHETase: A0A0K8P8E7). All proteins were minimized[7] and hydrogen atoms were added at pH 7.0.[8,9] The three-dimensional structure of MHET was prepared in Avogadro[10] and the

geometry was optimized using steepest descent algorithm until convergence using the MMFF94 molecular mechanics force field level of theory.[11] The optimized structure of MHET was parametrized for molecular dynamics using the R.E.D. server with default settings.[12]

The input topologies and coordinates of the enzyme and the ligand were prepared[13,14] for MD simulation. Crystallographic waters were added to the systems and an octahedral set of water molecules[15] was added leaving all atoms of the protein in a distance of at least 10 Å to the octahedron's surface. The average volumes of the equilibrated systems were used to add ions for a final NaCl concentration of 0.1 mol/L and the masses of the hydrogen atom-containing groups were repartitioned.[16]

Energy minimization was performed by 500 steps of steepest descent followed by 500 steps of conjugate gradient over five rounds with decreasing harmonic restraints. The subsequent MD simulations employed periodic boundary conditions, with treated electrostatic interactions[17], a 10 Å cut-off for nonbonded interactions, and a 4-fs time step to fix all bonds containing hydrogens.[18] Equilibration simulations consisted of two steps: (I) 40 ps of gradual heating from 0 to the final temperature of 310 K (37 °C) at constant volume using a Langevin thermostat with a collision frequency of 1.0 1/ps, and with harmonic restraints of 200.0 kcal/(mol·Å) on the positions of all solute atoms, and (II) 8,800 ps at the final temperature using the Langevin thermostat at a constant pressure of 1.0 bar using a pressure coupling constant of 1.0 ps. A production phase of the simulation was run with the same settings as in equilibration phase II for 20 ns. In total, three separate 20 ns long MD replicates were run for each system using the same settings as the second step of MD equilibration. Coordinates were saved at intervals of 4 ps. In total, 60 ns of simulation time was produced for each enzyme-ligand system.

Each enzyme-substrate complex was clustered into three trajectories and the molecular mechanics/generalized Born surface area (MM/GBSA)[19,20] method was applied to calculate the binding free energy (ΔG_{bind}) of MHET in the enzymes and the respective residue-by-residue interactions. Solvents and ions were removed from the original topology files of each system[21] to generate the corresponding topology files for the complex, receptor, and ligand. The ΔG_{bind} of the ligand in each structure was calculated.[19,22]

Phylogenetic analysis of homologous enzymes to TfCa

A phylogenetic tree was built to identify homologous enzymes to TfCa. For this purpose, a blastp[1] search was conducted on the NCBI server (https://blast.ncbi.nlm.nih.gov/Blast.cgi) with the sequence of TfCa as the template. 53 sequences with an amino acid identity of 55 % or higher were extracted, and redundant sequences (CD-HIT, a cut-off with 0.99)[2] were discarded. The resulting 42 amino acids sequences were aligned using MUSCLE[3] and the best model was determined based on ModelFinder (LG+F+I+G4).[4] This model was then used for the tree-building process performed by IQTree.[23] The final tree was then visualized by FigTree (http://tree.bio.ed.ac.uk/software/figtree/) and edited with iTOL (https://itol.embl.de)

TABLES

Table S1: Data collection and refinement statistics of TfCa crystals.

	TfCa E319L with MHET and BHET	TfCa-apo	TfCa E319L with BHET	TfCa with MHETA
Beamline	SSRF-BL17B	SSRF-BL17U	SSRF-BL18U	SSRF-BL18U
Date	2021-07-04	2019-10-24	2021-07-11	2ß21-10-31
Exposure time/ frame	10 seconds (s)	0.1 s	0.5 s	0.3 s
Frame width	1	1	1	1
Total frames	400	360	400	600
Wavelength	1.0079	0.9792	0.9197	1.0331
Space group	$P2_1$	$P2_1$	$P2_1$	$P2_12_12_1$
a, b, c [Å]	44.74/110.24/ 53.42	45.27/112.96/54.7 8	44.52/109.93/53.2 4	55.43/79.94/113.0 7
α /ß /γ (°)	90/106.42/90	90/106.04/90	90 /106.27/90	90/90 /90
Resolution (Å)	25.00 - 1.67 (1.73 - 1.67)	25.00 - 1.40 (1.45 - 1.40)	25.00 - 2.43 (2.52 - 2.43)	25.00 - 1.92 (2.03 - 1.92)
Unique reflections	56837 (5459)	103778 (10365)	18029 (1787)	38958 (2283)
Redundancy	7.4 (6.3)	6.6 (6.5)	7.2 (7.1)	13.2 (13.1)
Completeness (%)	98.7 (95.4)	99.4 (99.5)	99.7 (99.9)	99.3 (95.6)
Average I/σ(I)	17 (2.8)	27.2 (2.3)	11.7 (3.1)	15.1 (2.1)
CC 1/2	0.99 (0.84)	0.99 (0.86)	0.97 (0.89)	0.99 (0.82)
No. of reflections	56551 (5432)	103747 (9884)	17991 (1557)	38923 (3694)
No. of reflections (free set)	2832 (272)	5188 (494)	901 (78)	1946 (184)
R_{work} (95% data)	0.180 (0.223)	0.169 (0.225)	0.166 (0.216)	0.181 (0.293)
R_{free} (5% data)	0.208 (0.266)	0.186 (0.249)	0.224 (0.251)	0.218 (0.320)
Rmsd bonds (Å)	0.009	0.006	0.009	0.008
Rmsd angles (°)	1.13	0.94	1.01	0.91
Most favored (%)	96.77	96.56	95.96	97.15
Allowed (%)	3.23	3.44	4.04	2.85

Disallowed (%)	0.00	0.00	0.00	0.00
	Average B-factor/ Number of non-hydrogen atoms			
Protein	15.4 / 3743	17.2 / 3735	28. 1 / 3743	30.3 / 3720
Ligands	26.5 / 33		36.6 / 18	41.7 / 15
solvent	26.3 / 689	30.2 / 730	29.2 / 210	36.9 / 444
PDB-ID	7W1I	7W1K	7W1L	7W1J

Values in parentheses are for the outermost resolution shells.

Table S2: Melting temperature of TfCa mutants with increased activity towards BHET. The melting temperature was determined using NanoDSF.

TfCa variant	melting temperature [°C]
wt	64.5
V376A	61.5
I69W	62.9
R428A	64.3
I69W+V376A	60.3
V376A+R428A	60.8
I69W+R428A	62.2
I69W+V376A+R428A	59.4

Table S3: Individual contributions of amino acid residues to the ligand binding for TfCa and MHETase. Only amino acid residues of which the contribution to the binding energy is more than 1 kcal·mol^{-1} in the catalytic pocket are included. The standard error reflects different interacting energy in individual snapshots from the MD simulations.

System	Residue	Pocket (<4.5 Å) [kcal·mol^{-1}]
TfCa	I 69	-0.1 ± 0.1
	G 106	-1.4 ± 0.7
	G 107	-2.4 ± 0.9
	A 108	-3.6 ± 0.6
	E 184	-2.0 ± 1.7
	S 185	-2.5 ± 0.7
	A 186	-2.4 ± 0.8
	Q 263	-0.5 ± 0.7
	L 281	-0.7 ± 0.4
	L 282	-2.2 ± 0.4
	E 319	-0.1 ± 0.4
	Y 320	-1.2 ± 0.4
	F 323	-2.7 ± 0.6
	V 376	-0.7 ± 0.3
	F 377	-1.6 ± 0.4
	H 415	-1.5 ± 0.6
MHETase	S 131	-2.5 ± 0.6
	G 132	-2.8 ± 0.6
	S 225	-2.8 ± 1.1
	E 226	-2.0 ± 0.5
	L 254	-1.2 ± 0.4
	W 397	-3.2 ± 0.9
	Q 410	-0.2 ± 0.1
	R 411	-3.7 ± 0.8
	F 415	-1.8 ± 0.8

	S 416	-1.5 ± 1.0
	A 494	-0.9 ± 0.4
	F 495	-1.9 ± 0.4
	H 528	-1.5 ± 1.0

Table S4: Ligand binding and unbinding events defined by the catalytic C-O distance for individual protein-ligand complexes with MHET as the ligand.

System	Leave (>4.5 Å)	Return (<4.5 Å)	In-between (4.5–10.0 Å)	Out (>10.0 Å)
TfCa wt	2	0	6	3
MHETase	2	0	2	0

Table S5: Number of snapshots clustered based on the catalytic distance. The snapshots were clustered for the catalytic distance: (i) up to 4.5 Å, (ii) 4.5 – 10.0 Å, and (iii) above 10.0 Å. Listed are numbers of snapshots in each cluster and their percentages. MHET was used as the ligand.

System	Pocket (<4.5 Å)	In-between (4.5-10.0 Å)	Out (>10.0 Å)	Pocket [%]	In-between [%]	Out [%]
TfCa wt	13485	15578	937	45	52	3
MHETase	22688	7312	0	76	24	0

Figures

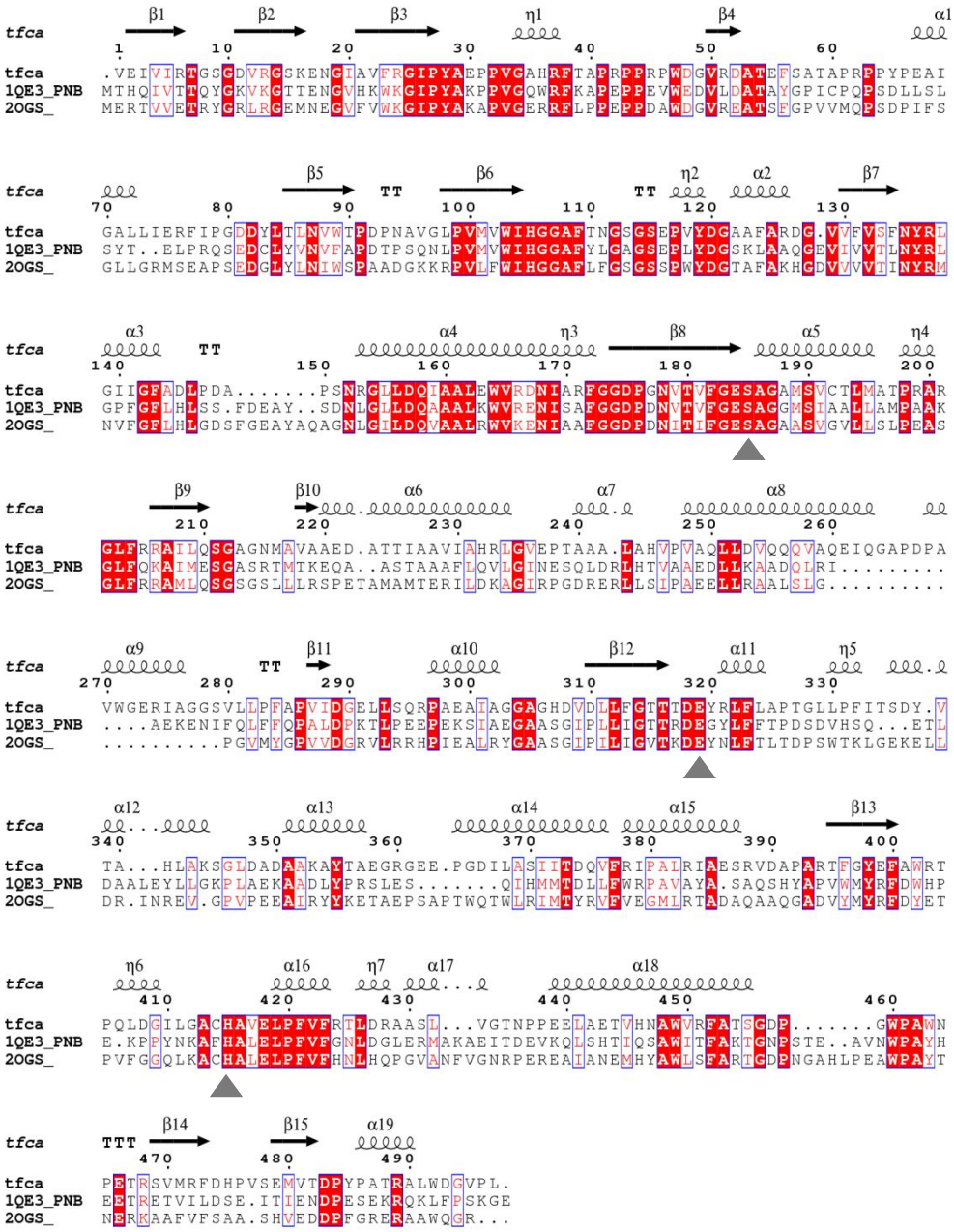

Figure S1: Sequence alignment of TfCa with *p*-nitrobenzyl esterase (pNB-E) and a carboxylesterase. The sequence as well as the structural alignment of TfCa were carried out with an pNB-E from *Bacillus subtilis* (PDB-ID: 1QE3) and a carboxylesterase from *Geobacillus stearothermophilus* (PDB-ID: 2OGS). The residues building the catalytic triad are labeled with a grey triangle.

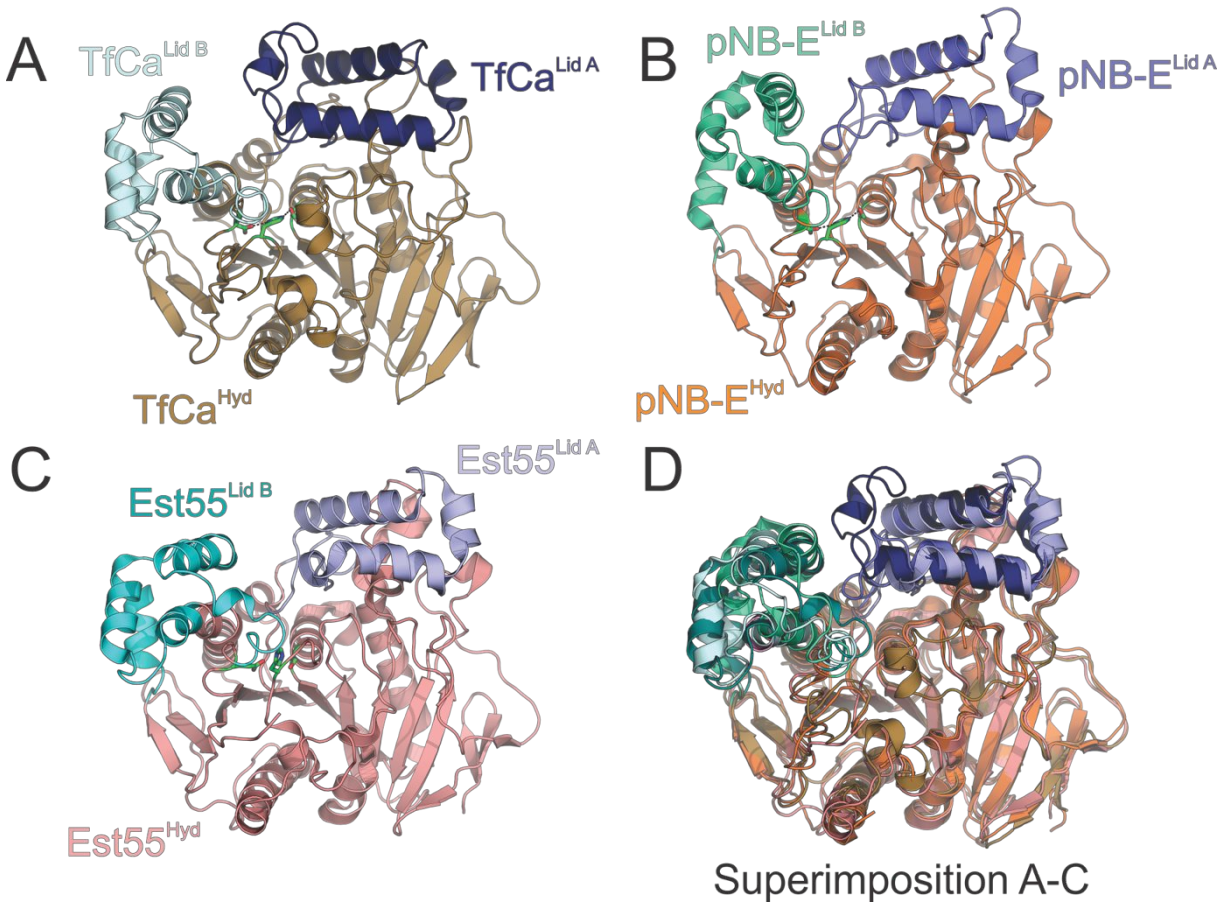

Figure S2: Structural alignment of TfCa with *p*-nitrobenzyl (pNB-E) esterase and Est55. The apo-form of TfCa was structurally aligned to pNB-E from *B. subtilis* (PDB-ID: 1QE3) and the carboxylesterase Est55 from *G. stearothermophilus* (PDB-ID: 6OGS). **A-C** show the structures of the three enzymes with their domains whereas **D** shows the superimposition of A-C.

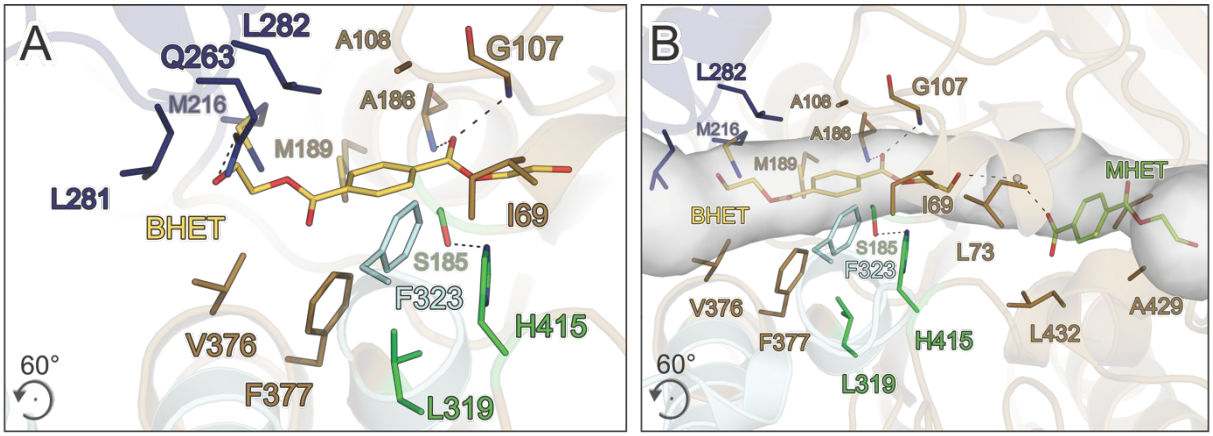

Figure S3: Ligand-soaked structure of TfCa with ligand BHET as well as apo-form of TfCa docked with DEP and MEP. A) Close-up view onto the active site of TfCa soaked with BHET (PDB-ID: 7W1L, 2.43 Å). **B)** Close-up view on the active site of TfCa E319L soaked with BHET and MHET (PDB-ID: 7W1I, 1.67 Å) in the solvent channel.

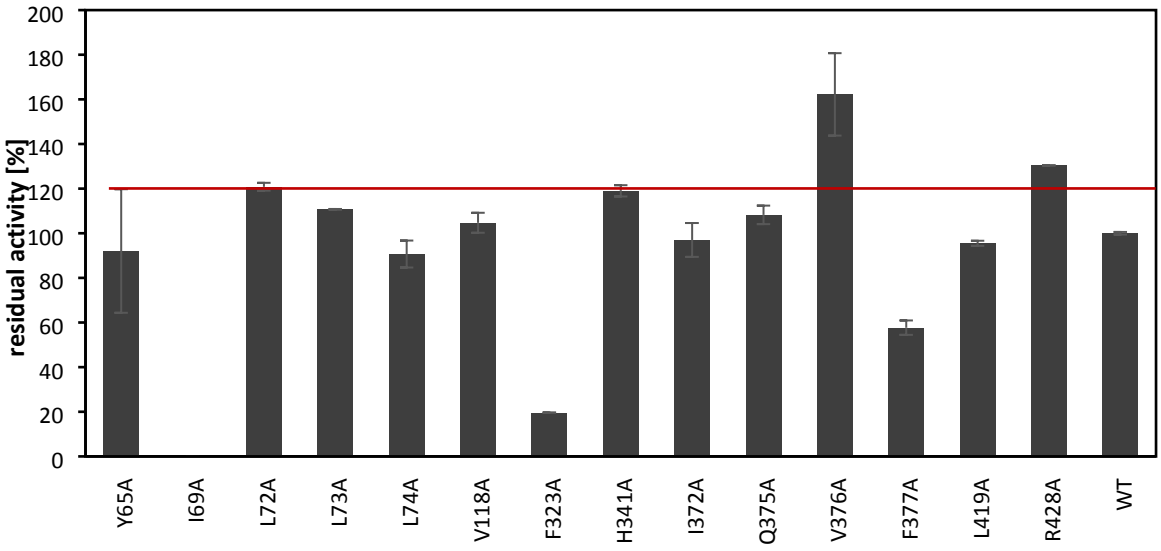

Figure S4: Alanine scan of the substrate binding pocket of TfCa. Using the substrate BHET, the residual activity of 15 mutants, obtained from the alanine scan of the substrate binding pocket, was determined. Mutants with a residual activity above 120 % were chosen for further characterization. Mutant I69A completely lost its enzymatic activity. Error bars indicate the standard deviation calculated from at least three replicates.

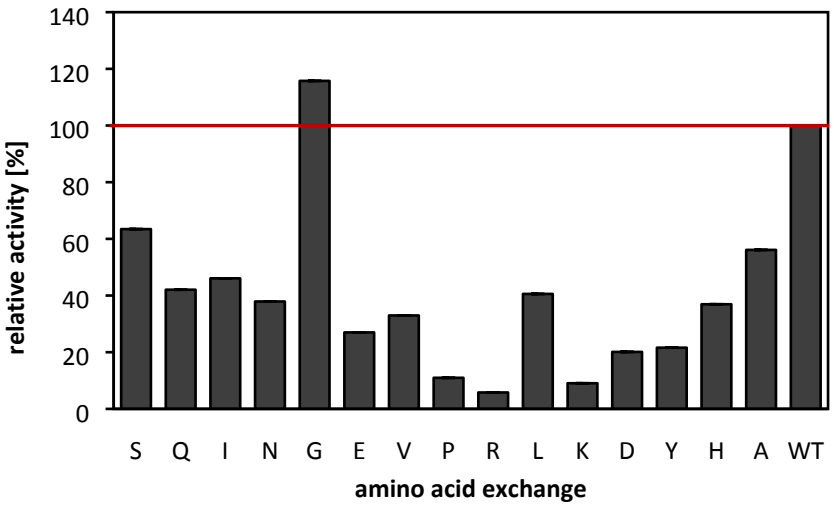

Figure S5: Semi-rational enzyme engineering of TfCa based on the elucidated structures. Residue M189 was mutated using site-saturation mutagenesis (SSM). The activity of mutants was determined using the model substrate pNPA. The amino acid substitutions to C, F, T and W were not obtained by the SSM method. None of the mutants exerted a significant increase in activity over 120 % compared to TfCa wt.

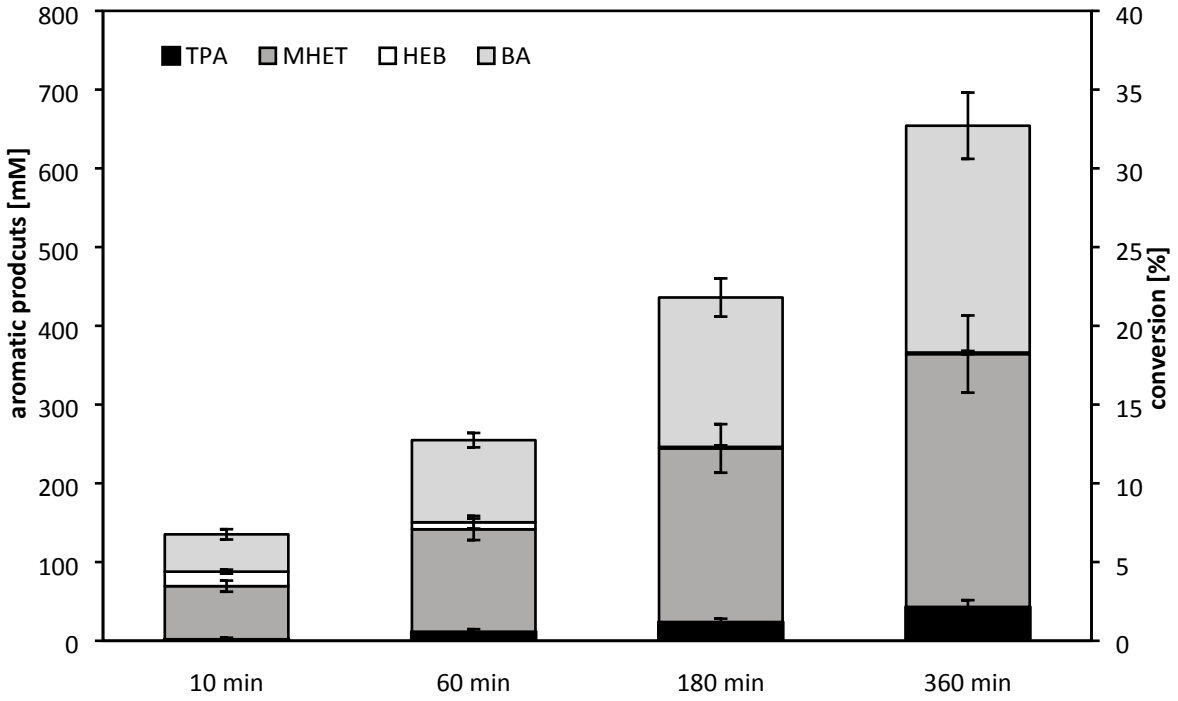

Figure S6: Hydrolysis of 3PET by TfCa over a time course of 6 h. The release of products from hydrolysis of 2 mM 3PET by TfCa is plotted. Time-course samples were taken at the indicated times and analyzed by uHPLC.

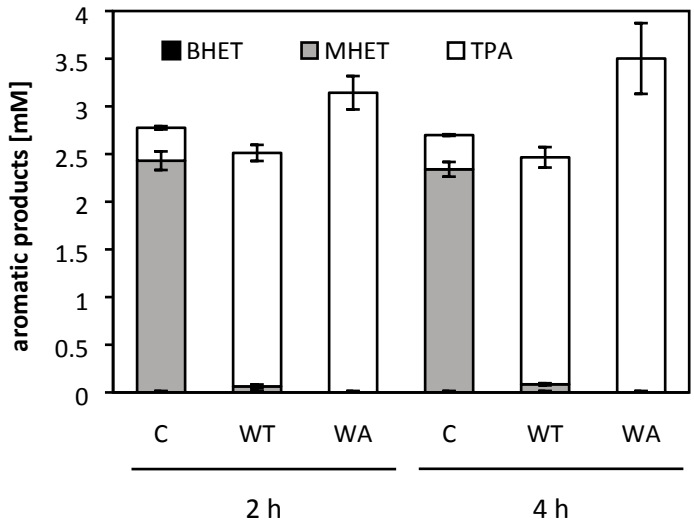

Figure S7: Exo-PETase function of the carboxylesterase TfCa. PET-NP were pre-treated using *Is*PETase PM for 2 or 4 h. After inactivation of *Is*PETase PM, TfCa wt or WA were added, and the reactions incubated for another 24 h. The aromatic degradation products BHET, MHET and TPA were analyzed by HPLC. Error bars indicate the standard deviation calculated from at least three replicates.

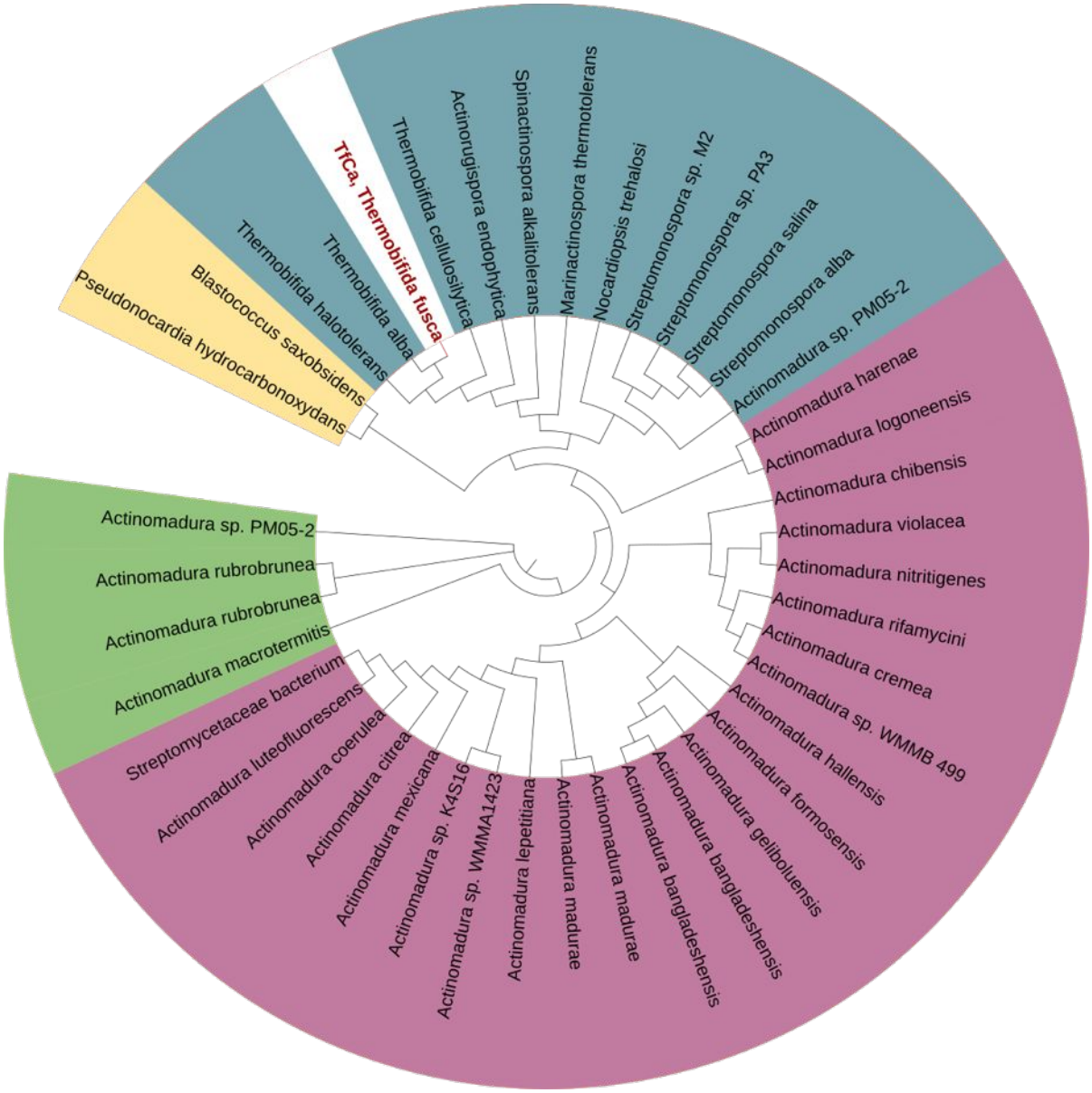

Figure S8: Relation of TfCa to enzymes with similar sequences. A phylogenetic tree was built from sequences with 55 % identity to TfCa. Four clades are shown in green, purple, blue and yellow.

A

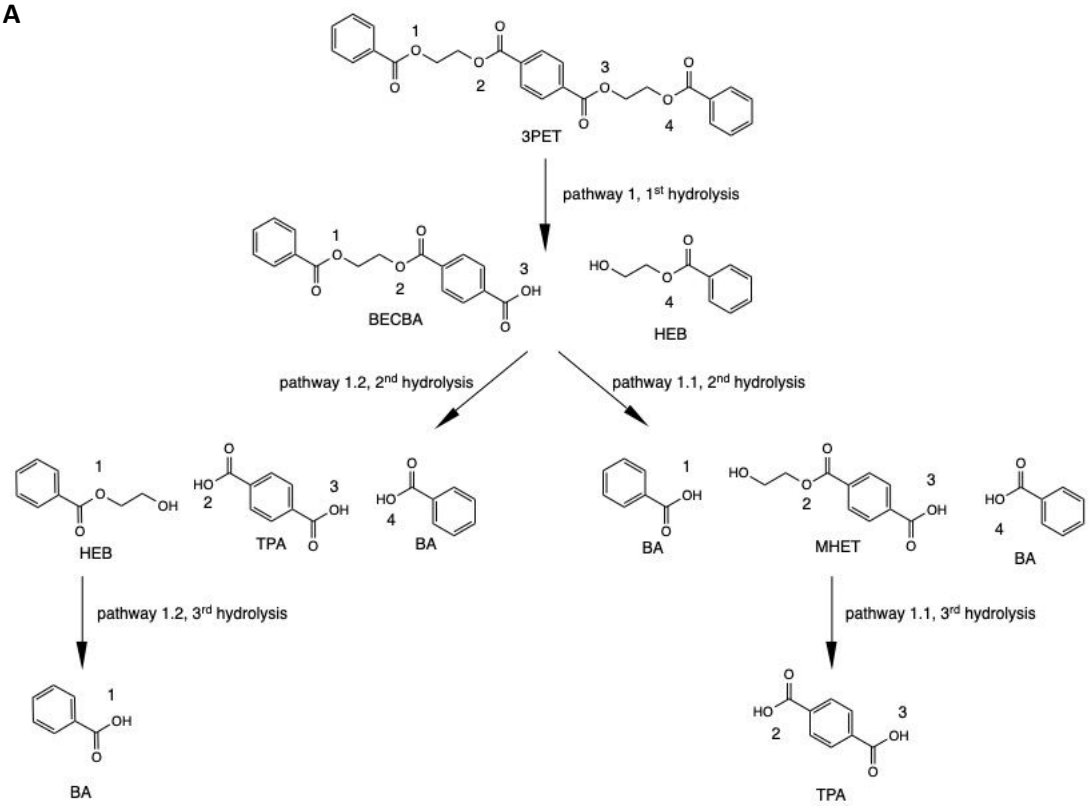
3PET
pathway 1, 1st hydrolysis
BECBA
HEB
pathway 1.2, 2nd hydrolysis
pathway 1.1, 2nd hydrolysis
HEB
TPA
BA
BA
MHET
BA
pathway 1.2, 3rd hydrolysis
pathway 1.1, 3rd hydrolysis
BA
TPA

B

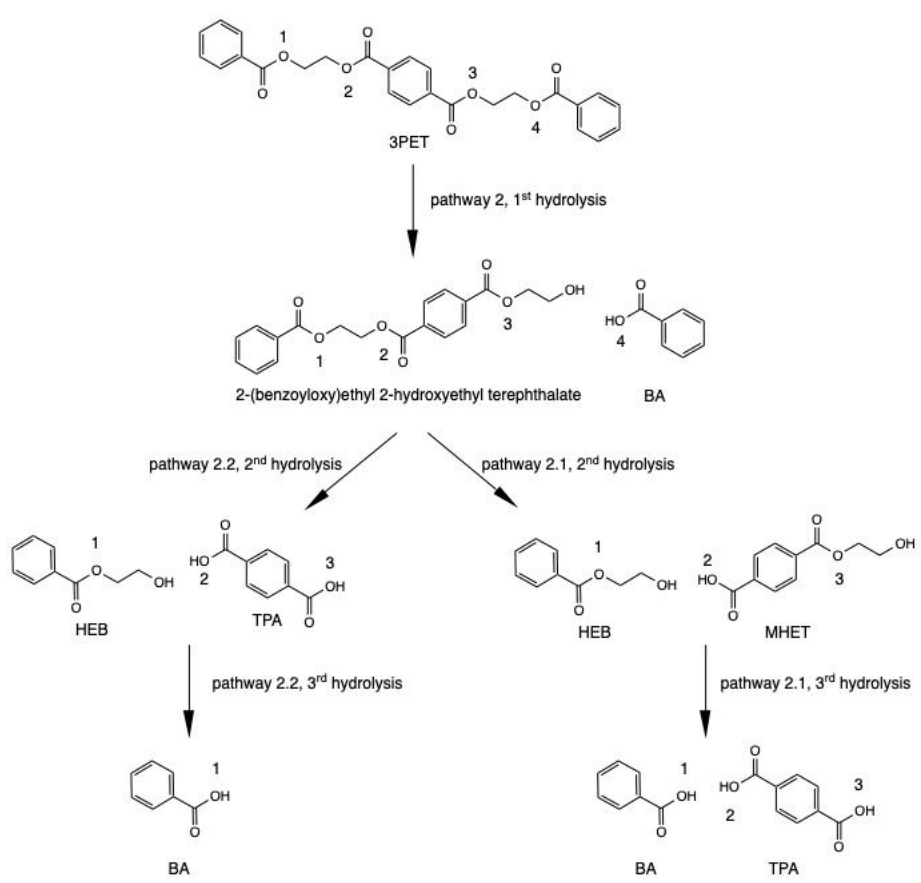
3PET
pathway 2, 1st hydrolysis
2-(benzoyloxy)ethyl 2-hydroxyethyl terephthalate
BA
pathway 2.2, 2nd hydrolysis
pathway 2.1, 2nd hydrolysis
HEB
TPA
HEB
MHET
pathway 2.2, 3rd hydrolysis
pathway 2.1, 3rd hydrolysis
BA
BA
TPA

Figure S9: Putative biocatalytic degradation pathways of 3PET. Based on which of the four ester bonds in 3PET is firstly hydrolyzed, different degradation pathways are possible. We proposed the most likely pathway in Figure 2 according to our experimental results. Here, other possible degradation pathways are shown. **A)** Pathways resulting when 3PET is firstly hydrolyzed into HEB and BECBA. **B)** Pathways resulting when 3PET is firstly cleaved into 2-(benzoyloxy)ethyl 2-hydroxyethyl terephthalate and BA. The ester bonds are numbered from one to four.

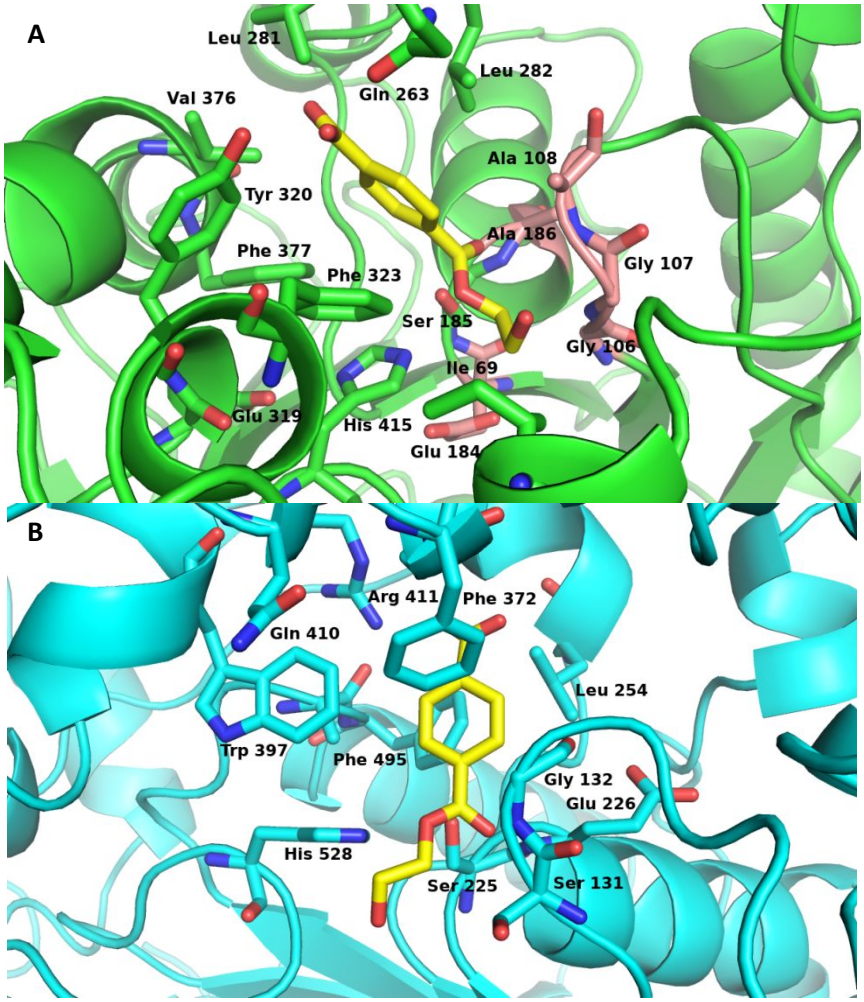

Figure S10: Comparison of residues contributing to binding of MHET in TfCa and MHETase. A) The residues contributing by more than 1 kcal/mol to the binding of MHET in TfCa are labeled and shown as sticks. **B)** The residues contributing by more than 1 kcal/mol to the binding of MHET in MHETase are labeled and shown as sticks. The MHET ligand is shown in yellow.

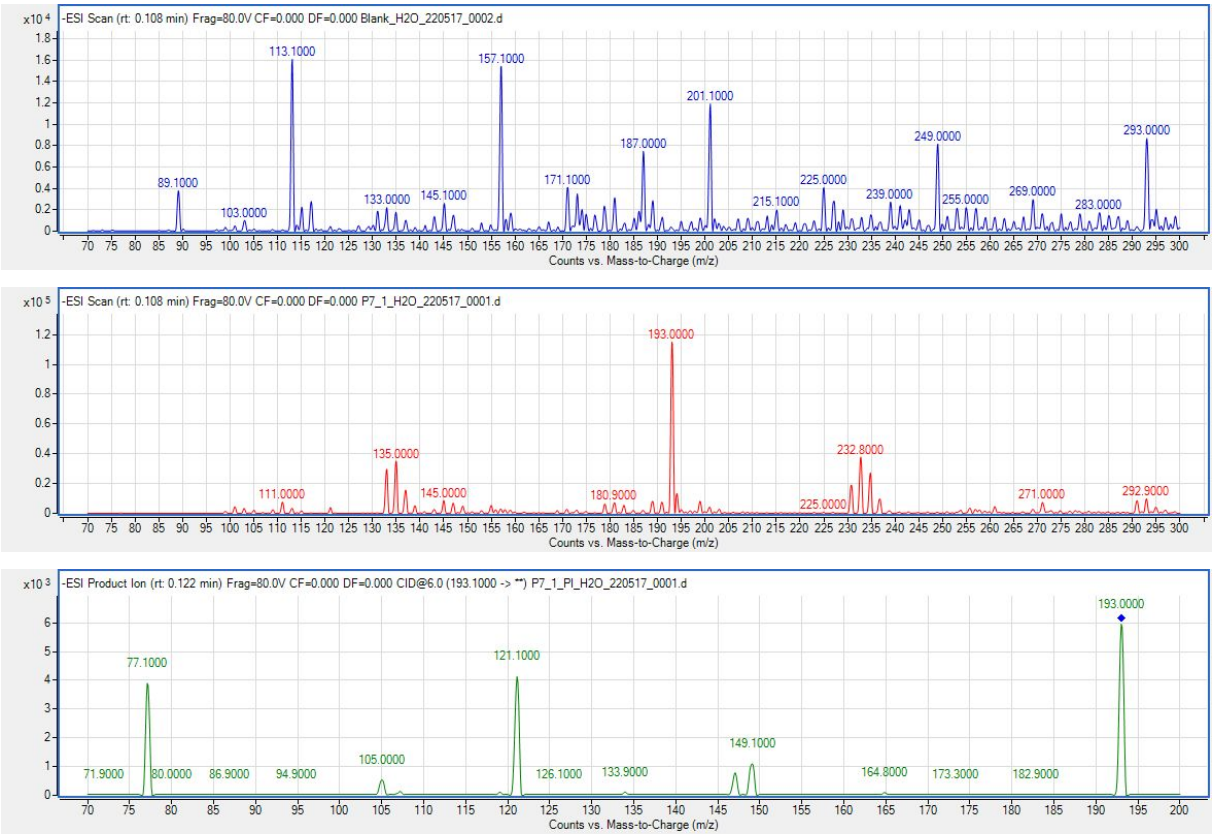

Figure S11: Confirming MEP as the product of DEP degradation by TfCa. The mass peaks resulting from LC-MS are shown for negative control measurement (blue), degradation sample (red) and the product ion scan for the degradation sample (green). The product ions were compared to Mass Bank (https://massbank.eu/MassBank/RecordDisplay?id=UF420553&dsn=UFZ) and were confirmed to be congruent with the product ions of MEP.

Nucleotide Sequence of TfCa wt including His-tag (yellow), TEV-protease cleavage site (gray) and linker region (green)

atgcatcatcatcatcatcatgaaaatctgtattttcaggggcgcaggcgcaggcgcaggtgcaggtgcaggc

gtggaaattgttattcgtaccggtagcggtgatgttcgtggtagcaaagaaaatggcattgccgtgtttcgtg

gtattccgtatgcagaacctccggttggtgcacatcgttttacagctcctcgccctcctcgtccgtgggatggtg

ttcgtgatgcaaccgaatttagcgcaaccgctccgcgtcctccgtatccggaagcaattggtgcactgctgattg

aacgttttattccgggtgatgattatctgaccctgaatgtttggacaccggatccgaatgcagttggtctgccgg

ttatggtttggattcatggtggtgcatttaccaatggtagcggtagcgaaccggtttatgatggtgcagcatttg

cacgtgatggtgttgtttttgtgagctttaattatcgcctgggcattattggttttgcagatctgccggatgcac

cgagcaatcgtggtctgctggatcagattgcagcactggaatgggttcgtgataatattgcacgtttcggtggcg

atccgggtaatgttaccgtttttggtgaaagcgcaggtgcaatgagcgtttgtaccctgatggcaacaccgcgtg

cacgtggtctgtttcgtcgtgcaattctgcagagcggtgcaggtaatatggcagttgcagcagaagatgcaaccca

ccattgcagcagttattgcacatcgtctgggtgttgaaccgaccgcagcagcactggcccatgttccggttgcac

agctgctggatgttcagcagcaggttgcacaggaaattcagggagcacctgatccggcagtttggggtgaacgta

ttgcaggtggtagcgttctgctgcctttcgcaccggttattgatggtgaactgctgtctcagcgtccggcagaag

caattgccggaggcgcaggtcatgatgttgatctgctgtttggcaccaccaccgatgaatatcgtctgtttctgg

ctccgaccggcctgctgccgtttattaccagcgattatgttaccgcacatctggctaaaagcggtctggatgcag

atgcagcaaaagcatataccgcagaaggtcgcggcgaagaaccgggtgatattctggccagcattattaccgatc

aggtgtttcgtattccggcactgcgtattgcagaaagccgtgttgatgcaccggcacgcacctttggttatgaat

ttgcatggcgtacaccgcagctggatggtattctgggtgcatgtcatgcagttgaactgccgtttgtttttcgta

ccctggatcgtgcagcaagcctggttggcaccaatccgccggaagaactggccgaaaccgttcataatgcatggg

ttcgttttgcaaccagcggtgatccgggttggccggcatggaatccggaaacccgtagcgttatgcgttttgatc

atccggttagcgaaatggttaccgatccgtatccggcaacacgtgcactgtgggatggcgttccgctgtga

Protein Sequence of TfCa wt including His-tag (yellow), TEV-protease cleavage site (gray) and linker region (green)

MHHHHHHENLYFQGAGAGAGAGAGVEIVIRTGSGDVRGSKENGIAVFRGIPYAEPPVGAHRFTAPRPPRPWDG
VRDATEFSATAPRPPYPEAIGALLIERFIPGDDYLTLNVWTPDPNAVGLPVMVWIHGGAFTNGSGSEPVYDGAAF
ARDGVVFVSFNYRLGIIGFADLPDAPSNRGLLDQIAALEWVRDNIARFGGDPGNVTVFGESAGAMSVCTLMATPR
ARGLFRRAILQSGAGNMAVAAEDATTIAAVIAHRLGVEPTAAALAHVPVAQLLDVQQQVAQEIQGAPDPAVWGER
IAGGSVLLPFAPVIDGELLSQRPAEAIAGGAGHDVDLLFGTTTDEYRLFLAPTGLLPFITSDYVTAHLAKSGLDA
DAAKAYTAEGRGEEPGDILASIITDQVFRIPALRIAESRVDAPARTFGYEFAWRTPQLDGILGACHAVELPFVFR
TLDRAASLVGTNPPEELAETVHNAWVRFATSGDPGWPAWNPETRSVMRFDHPVSEMVTDPYPATRALWDGVPL

REFERENCES

1. Altschul, S. F.; Gish, W.; Miller, W.; Myers, E. W..; Lipman, D. J. Basic local alignment search tool. J. Mol. Biol. 1990, 215, 403–410.

2. Huang, Y.; Niu, B.; Gao, Y.; Fu, L..; Li, W. CD-HIT Suite: a web server for clustering and comparing biological sequences. Bioinforma. Oxf. Engl. 2010, 26, 680–682.

3. Edgar, R. C. MUSCLE: multiple sequence alignment with high accuracy and high throughput. Nucleic Acids Res. 2004, 32, 1792–1797.

4. Kalyaanamoorthy, S.; Minh, B. Q.; Wong, T. K. F.; von Haeseler, A..; Jermiin, L. S. ModelFinder: fast model selection for accurate phylogenetic estimates. Nat. Methods 2017, 14, 587–589.

5. Palm, G. J.; Reisky, L.; Böttcher, D.; Müller, H.; Michels, E. A. P.; Walczak, M. C.; Berndt, L.; Weiss, M. S.; Bornscheuer, U. T..; Weber, G. Structure of the plastic-degrading Ideonella sakaiensis MHETase bound to a substrate. Nat. Commun. 2019, 10, 1717.

6. Berman, H. M.; Westbrook, J.; Feng, Z.; Gilliland, G.; Bhat, T. N.; Weissig, H.; Shindyalov, I. N..; Bourne, P. E. The Protein Data Bank. Nucleic Acids Res. 28, 235–242 (2000).

7. Schymkowitz, J.; Borg, J.; Stricher, F.; Nys, R.; Rousseau, F..; Serrano, L. The FoldX web server: an online force field. Nucleic Acids Res. 2005, 33, W382-388.

8. Olsson, M. H. M.; Søndergaard, C. R.; Rostkowski, M..; Jensen, J. H. PROPKA3: Consistent treatment of internal and surface residues in empirical pKa predictions. J. Chem. Theory Comput. 2011, 7, 525–537.

9. Dolinsky, T. J.; Czodrowski, P.; Li, H.; Nielsen, J. E.; Jensen, J. H.; Klebe, G..; Baker, N. A. PDB2PQR: expanding and upgrading automated preparation of biomolecular structures for molecular simulations. Nucleic Acids Res. 2007, 35, W522-525.

10. Hanwell, M. D.; Curtis, D. E.; Lonie, D. C.; Vandermeersch, T.; Zurek, E..; Hutchison, G. R. Avogadro: an advanced semantic chemical editor, visualization, and analysis platform. J. Cheminformatics 2012, 4, 17.

11. Halgren, T. A. Merck molecular force field. I. Basis, form, scope, parameterization, and performance of MMFF94. J. Comput. Chem. 1996, 17, 490–519.

12. Vanquelef, E.; Simon, S.; Marquant, G.; Garcia, E.; Klimerak, G.; Delepine, J. C.; Cieplak, P..; Dupradeau, F.-Y. R.E.D. Server: a web service for deriving RESP and ESP charges and building force field libraries for new molecules and molecular fragments. Nucleic Acids Res. 2011, 39, W511-517.

13. Maier, J. A.; Martinez, C.; Kasavajhala, K.; Wickstrom, L.; Hauser, K. E..; Simmerling, C. ff14SB: Improving the accuracy of protein side chain and backbone parameters from ff99SB. J. Chem. Theory Comput. 2015, 11, 3696–3713.

14. Case, D.; Betz, R.; Cerutti, D. S.; Cheatham, T.; Darden, T.; Duke, R.; Giese, T. J.; Gohlke, H.; Götz, A.; Homeyer, N.; Izadi, S.; Janowski, P.; Kaus, J.; Kovalenko, A.; Lee, T.-S.; LeGrand, S.; Li, P.; Lin, C.; Luchko, T..; Kollman, P. Amber 16, University of California, San Francisco. 2016. https://ambermd.org/index.php (accessed 2022-03-23)

15. Izadi, S..; Onufriev, A. V. Accuracy limit of rigid 3-point water models. J. Chem. Phys. 2016, 145, 074501.

16. Hopkins, C. W.; Le Grand, S.; Walker, R. C..; Roitberg, A. E. Long-time-step molecular dynamics through hydrogen mass repartitioning. J. Chem. Theory Comput. 2015, 11, 1864–1874.

17. Cerutti, D. S..; Case, D. A. Multi-Level Ewald: A hybrid multigrid / Fast Fourier Transform approach to the electrostatic particle—mesh problem. J. Chem. Theory Comput. 2010, 6, 443–458.

18. Ryckaert, J.-P.; Ciccotti, G..; Berendsen, H. J. C. Numerical integration of the cartesian equations of motion of a system with constraints: molecular dynamics of n-alkanes. J. Comput. Phys. 1997, 23, 327–341.

19. Miller, B. R.; McGee, T. D.; Swails, J. M.; Homeyer, N.; Gohlke, H..; Roitberg, A. E. MMPBSA.py: An efficient program for end-state free energy calculations. J. Chem. Theory Comput. 2012, 8, 3314–3321.

20. Genheden, S..; Ryde, U. The MM/PBSA and MM/GBSA methods to estimate ligand-binding affinities. Expert Opin. Drug Discov. 2015, 10, 449–461.

21. Case, D. A.; Babin, V.; Berryman, J.; Betz, R. M.; Cai, Q.; Cerutti, D. S.; Cheatham III, T. E.; Darden, T. A.; Duke, R. E.; Gohlke, H.; Goetz, A. W.; Gusarov, S.; Homeyer, N.; Janowski, P.; Kaus, J.; Kolossváry, I.; Kovalenko, A.; Lee, T. S.; LeGrand, S.; Luchko, T.; Luo, R.; Madej, B.; Merz, K. M.; Paesani, F.; Roe, D. R.; Roitberg, A.; Sagui, C.; Salomon-Ferrer, R.; Seabra, G.; Simmerling, C. L.; Smith, W.; Swails, J.; Walker, R. C.; Wang, J.; Wolf, R. M.; Wu, X..; Kollman, P. A. Amber 14. 2014. https://ambermd.org/index.php (accessed 2022-03-23)

22. Weiser, J.; Shenkin, P. S..; Still, W. C. Approximate atomic surfaces from linear combinations of pairwise overlaps (LCPO). J. Comput. Chem. 1999, 20, 217–230.

23. Nguyen, L.-T.; Schmidt, H. A.; von Haeseler, A..; Minh, B. Q. IQ-TREE: a fast and effective stochastic algorithm for estimating maximum-likelihood phylogenies. Mol. Biol. Evol. 2015, 32, 268–274.

Article III

Synthesis of Modified Polyvinyl Alcohols and their Degradation Using an Enzymatic Cascade

Gerlis von Haugwitz[a], Kian Donnelly[b], Mara Di Filippo[b], Daniel Breite[c], Max Phippard[d], Agnes Schulze[c], Ren Wei[a], Marcus Baumann[b] and Uwe T. Bornscheuer*[a]

[a] Prof. Dr. U. T., Bornscheuer, Dr. R. Wei, M.Sc. G. von Haugwitz
Dept. of Biotechnology & Enzyme Catalysis
University of Greifswald
Felix-Hausdorff-Str. 4, 17489 Greifswald, Germany
E-mail: uwe.bornscheuer@uni-greifswald.de

[b] B. Sc. K. Donnelly, M. Sc. M. Di Filippo, Dr. M. Baumann
School of Chemistry, Science Centre South
University College Dublin
Belfield Dublin 4, Ireland

[c] Dr. D. Breite, Dr. A. Schulze
Surfaces of Porous Membrane Filters
Leibniz Institute of Surface Engineering (IOM)
Permoserstraße 15, 04318 Leipzig, Deutschland

[d] M. Chem. M. Phippard
Aquapak Polymers Ltd
Hollymoor Point, Hollymoor Way, Rubery, Birmingham B31 5HE, United Kingdom

Supporting information for this article is given via a link at the end of the document.

Abstract: Polyvinyl alcohol (PVA) is a water-soluble synthetic vinyl polymer with remarkable physical properties including thermostability and viscosity. Its biodegradability, however, is low even though a large amount of PVA is released into the environment. Established physical-chemical degradation methods for PVA have several disadvantages such as high price, low efficiency, and secondary pollution. Biodegradation of PVA by microorganisms is slow and frequently involves pyrroloquinoline quinone (PQQ)-dependent enzymes, making it expensive due to the costly cofactor and hence unattractive for industrial applications. In this study, we present a modified PVA film with improved properties as well as a PQQ-independent novel enzymatic cascade for the degradation of modified and unmodified PVA. The cascade consists of four steps catalyzed by three enzymes with *in situ* cofactor recycling technology making this cascade suitable for industrial applications.

Polyvinyl alcohol (PVA) is a water-soluble synthetic vinyl polymer consisting of a carbon-carbon backbone and repeating 1,3-diols. Due to its versatile properties, PVA is used in many industrial applications such as fabric and paper sizing, fiber coating, film for packaging and more.[1] Although PVA was considered a biodegradable polymer, it has become a major pollutant of industrial wastewater.[2] The printing and dyeing industries, in particular, are major PVA emitters. Treatment of PVA wastewater via chemical or physical methods such as adsorption, filtration, ultrasonic degradation or the Fenton reaction are cost intensive, inefficient and can cause secondary pollution. Hence, alternative approaches (e.g., via microorganisms or enzymes) are required for the remediation of wastewater contaminated by PVA.[1] Additionally, in comparison to conventional desizing methods, enzymatic PVA degradation can be carried out under mild conditions.[3] Microbial degradation of PVA was already reported for bacterial strains such as *Pseudomonas putida* VM15C and VM15A and *Spingomonas* sp. SA3 and SA2[4] and has been proposed as a two-step process, (i) oxidation of one or two adjacent hydroxyl groups and (ii) subsequent cleavage of the resulting mono- or di-ketone structure. Step one was found to be carried out by a PVA oxidase or a pyrroloquinoline quinone (PQQ)-dependent PVA dehydrogenase (PVA-DH) while an aldolase or a diketone hydrolase catalyze the second step.[5] Kawai and Hu[5b] hypothesized that the polymer is cleaved extracellularly by PVA oxidases which results in fragments small enough to enter the periplasmic space. They base their suggestion on two observations: (i) PVA oxidases were found extracellularly whereas PVA-DHs were discovered membrane bound or periplasmatic[6] and (ii) oxidized PVA can be hydrolyzed by enzymes[7] but can also undergo spontaneous oxidation.[8] In the periplasm, the smaller PVA fragments are further oxidized by the PQQ-dependent PVA-DH. Aldolases or diketone hydrolases subsequently degrade the PVA further until it can be taken up by the organism through the inner membrane.[5b] However, some organisms express only PVA-DH and no PVA oxidases, which suggests that extracellular PVA degradation plays a secondary role.[5b]

Despite the fact that the microbial mechanism for PVA degradation has been known for a long time, research on degradation of PVA with isolated enzymes has been scarce. Further investigation of PVA-DH from *Sphingopyxis* sp. 113 has failed to corroborate initial findings because the recombinantly expressed enzyme formed largely insoluble inclusion bodies.[9] Wei *et al.*, however, further investigated *Stenotrophomonas rhizophila* QL-P4 and were able to efficiently express a novel PVA oxidase.[10] Nonetheless, current literature suggests that PQQ-dependent enzymes are needed for a complete degradation of Main Text Paragraph. PVA. Since PQQ is an expensive cofactor, this method is unattractive for industrial purposes.

In this work, we demonstrate a PQQ-independent enzyme cascade for the degradation of PVA which can act on modified

and unmodified PVA. To improve the properties of the PVA polymer, we firstly generated PVA bearing succinylated hydroxyl groups. Specifically, starting from a partially acetylated PVA material was desirable to study new hybrid materials that may find future applications in the packaging industries. Introducing succinate groups on the free hydroxyl groups via simple ester forming reactions was deemed attractive in altering the lipophilicity and mechanical properties in a substrate dependent manner. Succinic anhydride was identified as a desirable modifier that is biorenewable and biodegradable, readily available at low cost and non-toxic.[11] A further advantage is that this protocol avoids the formation of harmful by-products and uses water as the sole solvent. Films modified with different amounts of succinic acid were synthesized after establishing a general protocol for the creation of succinate-modified PVA samples (Scheme 1).

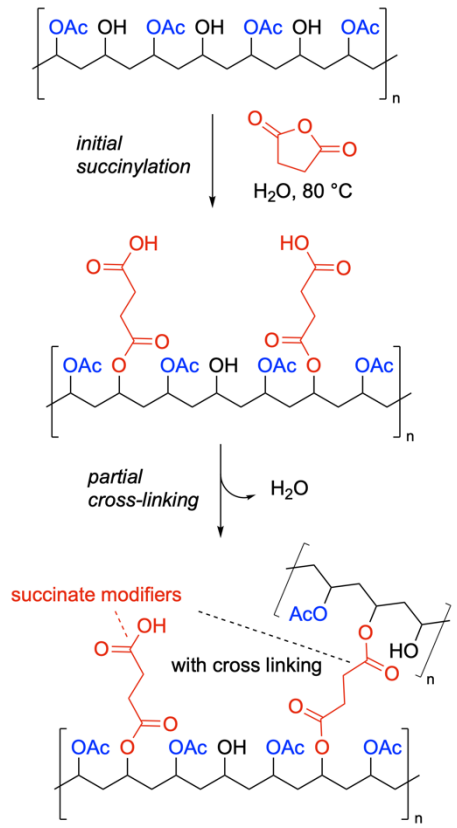

Scheme 1. Synthetic process for the preparation of succinylated PVA. The initial succinylation is carried out in water at 80 °C. Different amounts of succinic anhydride were added to the PVA suspension to yield water-soluble polymers with varying properties. After cooling and evaporation of water, the modified PVA was subsequently partially cross-linked.

Prior reports on the succinylation of (bio)polymers include cellulose as well as secondary derivatization of the resulting succinate hybrids.[12] This process was exploited using varying amounts of succinic anhydride (2, 4 and 6 g per 30 g PVA) and yielded reproducibly the desired PVA blends. In the following the modified PVA will be referred to as PVA-2 (2 g succinic anhydride), PVA-4 (4 g succinic anhydride) and PVA-6 (6 g succinic anhydride).

Though the focus was on developing a straightforward batch process, initial studies indicated that a continuous flow process is viable which may have advantages when scaling this to the multi-kg scale with regards to reproducibility, automation, safety, and efficiency. Upon casting the aqueous hybrid materials into plastic boxes and slow evaporation of water in a fume hood, thin polymer films were obtained that could be easily peeled and used for further analysis. Infrared spectroscopy was used as a technique of choice indicating a distinct change in the carbonyl stretching region (i.e., 1600-1800 cm^{-1}) which is in agreement with the introduction of succinate moieties; i.e., 1714 cm^{-1} for unmodified PVA vs. 1703 cm^{-1} for the succinate hybrid (Supporting Information (SI), Figure S1).

Further and more comprehensive testing was performed externally and indicated that key parameters can be altered effectively and in dependence of the amount of succinic anhydride used (SI, Table S1). As such, all succinate hybrids were characterized by excellent mechanical properties and retained the water solubility/dispersibility of the original PVA. These parameters are critical for future use as packaging materials, and the ability to dissolve in aqueous environments is expected to expedite biodegradation which is also supported by a slow onset of disintegration in soil (SI, Table S1).

Next, we developed an enzymatic cascade for the degradation of the modified PVA using three biocatalysts. This cascade can be performed as a one pot reaction including an *in situ* cofactor recycling. All enzymes used are well characterized and either easily recombinantly expressible in *Escherichia coli* or commercially available.[13] The enzyme cascade consists of four steps (Scheme 2) for modified PVA but can also be applied for unmodified PVA, starting at step 2. In step 1, ester bonds in the derivatized side chains are hydrolyzed by the commercially available lipase TL-IM resulting in unmodified PVA. The lipase is described to be 1,3-specific and originates from *Thermomyces lanuginosus*. Additionally, the immobilized enzyme accepts substrates with bulky side chains, making it an ideal candidate for the PVA degrading enzyme cascade.

After cleaving the ester bonds, the hydroxyl groups are oxidized to ketones by an alcohol dehydrogenase from *Lactobacillus kefir* (LK-ADH) utilizing the cofactor $NADP^+$ with formation of NADPH (Scheme 2, step 2).[13a] These ketones are then further oxidized to esters by the cyclohexanone monooxygenase (CHMO) variant M15 originally from the organism *Acinetobacter calcoaceticus*. CHMO M15 is utilizing the cofactor NADPH with formation of $NADP^+$.[13b] This, in principle, leads to an advantageous *in situ* cofactor recycling. Finally, the newly formed ester bond can be cleaved by lipase TL-IM through hydrolysis which results in smaller fragments of the polymer. Hence, a total of three enzymes in a one pot cascade can cleave PVA to release oligomers that are more accessible to further degradation by e.g., microorganisms or may serve as building blocks for upcycling of the resulting material.

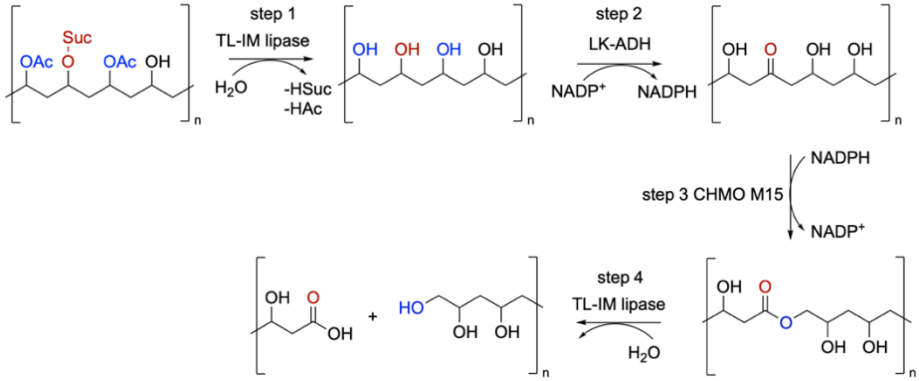

Scheme 2. Enzyme cascade for the degradation of modified and unmodified PVA. In step 1, the commercial lipase TL-IM removes the esters (HAc and HSuc) from the PVA via hydrolysis which results in unmodified PVA with 1,3-diol functional groups. These diols are then oxidized into ketones by LK-ADH, using $NADP^+$ as the cofactor and converting it into NADPH. NADPH is the cofactor for the subsequent enzymatic Baeyer-Villiger oxidation of ketones into ester-bonds which is performed by CHMO M15. In the last step, the ester bond is cleaved, which results in smaller PVA fragments. For PVA without modification, the same cascade can be applied, starting then from step 2. For simplicity, only one distinct example cascade pathway is shown, of course, steps 2-4 can also occur at further functional groups.

Degradation of PVA can be measured by staining the polymer using iodide. According to the Finley method, PVA forms a green complex with iodide in the presence of boric acid with an absorption maximum at 500 nm.[14] Changes in the staining of PVA due to degradation of the polymer can thus be detected by absorbance measurements. PVA was incubated with crude cell lysates containing LK-ADH and CHMO M15 as well as the immobilized TL-IM in a one pot reaction. As negative control, cell lysate without overexpressed enzyme was used to exclude an influence of the lysate on the polymer.

The enzyme cascade caused a decrease in absorbance of the derivatized PVA film solution at 500 nm compared to the negative control when investigated with the Finley method. The degradation performance of PVA-4 film was evaluated at a wide range of pH, temperatures, reaction times, enzyme ratios and amounts of cofactor (Figure 1). To investigate the temperature range of the enzymes used for the cascade, each enzyme was incubated for one hour at varying temperatures (4–50 °C). Subsequently, the residual activity of each enzyme was measured and plotted (SI, Figure S2**)**. It was found that LK-ADH and CHMO M15 are less stable in comparison to the immobilized TL-IM. These results are in agreement with the enzyme description for the TL-IM provided by the manufacturer Novozymes. According to the manufacturer, TL-IM has a temperature optimum of 50–75 °C. Thus, steps 2 and 3 of the PVA degradation (Scheme 2) are considered the crucial steps in the enzyme cascade.

Next, the pH of the reaction was varied in a range from 7 to 9 and, based on the results shown in Figure S2, different temperatures for the cascade reaction were studied in a range from 20 to 35 °C. It was found that the enzymatic degradation of PVA-4 ideally takes place at pH 8.5 and 20 °C under the tested conditions (Figure 1). The time dependent stability of LK-ADH and CHMO M15 was investigated at 20 °C and pH 8.5 over 24 h by following the increase or decrease of NADPH using the substrates (*R*)-1-phenyl ethanol (LK-ADH) or cyclohexanone (CHMO M15) (Figure 3). While CHMO M15 retained 80 % of its activity for the duration of the experiment, the activity of LK-ADH decreased by 20 % in 24 h at 20 °C. Hence, the degradation of PVA by the enzyme cascade can be performed at 20 °C over 24 h without a major loss of enzymatic activity. Furthermore, the optimal amount of cofactor for the reaction was investigated. Since the reaction contains an *in situ* cofactor recycling system and in step 2 $NADP^+$ is firstly required by LK-ADH for the formation of ketones, only $NADP^+$ was added to the reaction. It was found that the efficiency of the reaction increases with increasing amounts of $NADP^+$ up to 4 mM. However, the reaction efficiency did not improve when more than 4 mM $NADP^+$ were added to the enzyme cascade.

Lastly, for a sufficient cofactor recycling system, the optimal ratio of LK-ADH to CHMO M15 was investigated for the degradation of PVA film PVA-4. From the Finley method we found that enzyme ratios of 1:1 or 2:1 were most favorable for the enzymatic reaction (Figure 1). It should be mentioned at this point that the enzyme ratio and the amount of cofactor are most likely interdependent. The investigation of the enzyme ratio was performed with 4 mM $NADP^+$ whereas the investigation of the optimal amount of cofactor was carried out with a 1:1 LK-ADH to CHMO M15 ratio. In the stability testing of the enzymes, shown in Figure 1, LK-ADH performed with a higher activity (0.053 U per µL) compared to CHMO M15 (0.009 U per µL) which could lead to the conclusion that LK-ADH will convert $NADP^+$ faster into NADPH than CHMO M15 converts NADPH into $NADP^+$. However, the activity assay was carried out with the substrates (*R*)-1-phenylethanol and cyclohexanone and the activity for those substrates cannot be directly transferred to PVA. However, the enzyme ratios for PVA degradation were investigated with 2 mM $NADP^+$ (data not shown) and 4 mM $NADP^+$ which led to similar conclusions regarding the optimal enzyme ratio.

Thus, the improved degradation reaction of PVA-4 with the proposed enzyme cascade contained 4 mM $NADP^+$, LK-ADH and CHMO M15 in a ratio of either 1:1 or 2:1 carried out at pH 8.5 and 20 °C over 24 h.

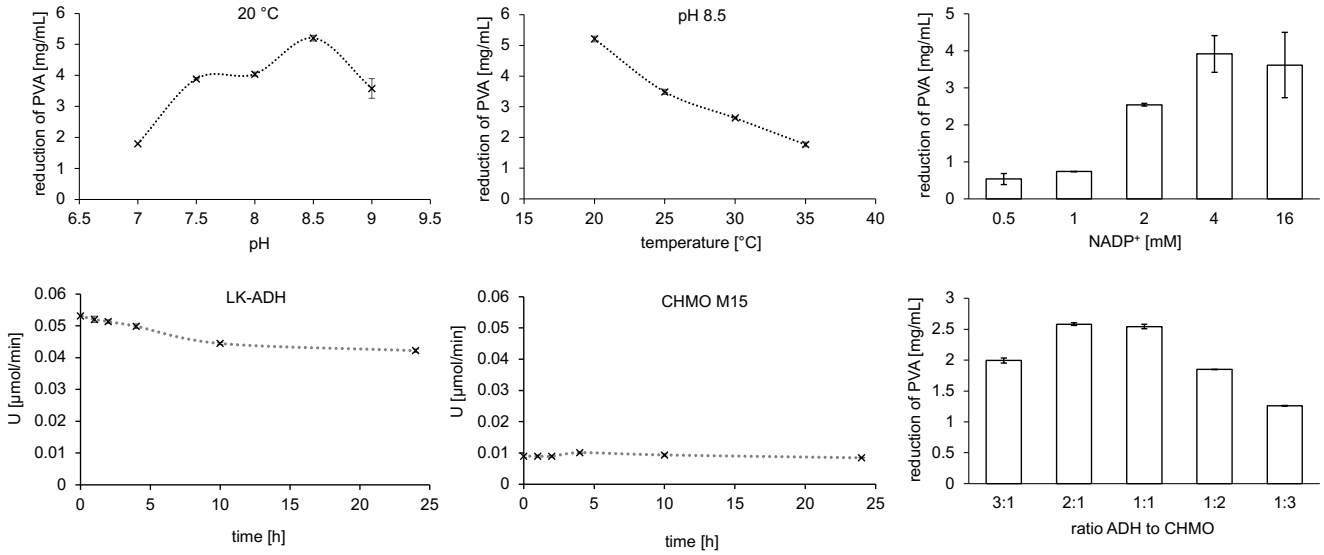

Figure 1. Investigation of the effect of various conditions on the enzymatic degradation of film PVA-4. The reaction conditions were optimized regarding pH, temperature, reaction time, the ratio of ADH to CHMO and the amount of cofactor. The best conditions were found to be pH 8.5, 20 °C, 24 h with 4 mM cofactor $NADP^+$. The activity of LK-ADH was measured by following the increase of NADPH when converting (*R*)-1-phenyl ethanol. The activity of CHMO M15 was measured by following the decrease of NADPH when converting cyclohexanone. One Unit (U) was defined as the amount of substrate converted per minute by one µL of enzyme lysate.

Table 1. Average M_n and M_w of PVA-films unmodified PVA, PVA-2, PVA-4 and PVA-6 degraded by the enzyme cascade. The average and the standard deviations were calculated from three replicates.

LK-ADH to CHMO ratio	Film	Treatment	M_n [g/mol]	M_w [g/mol]	PDI
1:1	Unmodified PVA	Enzyme cascade	37850 ± 144	161767 ± 2970	4.27
		Negative control	40667 ± 230	168167 ± 2702	4.14
	PVA-2	Enzyme cascade	33407 ± 190	98373 ± 410	2.94
		Negative control	35607 ± 163	101433 ± 814	2.85
	PVA-4	Enzyme cascade	35719 ± 663	105867 ± 2581	2.96
		Negative control	39527 ± 215	111367 ± 1380	2.82
	PVA-6	Enzyme cascade	34823 ± 704	106600 ± 800	3.06
		Negative control	38533 ± 135	110467± 3044	2.87
2:1	Unmodified PVA	Enzyme cascade	36147 ± 1809	145267 ± 424	4.02
		Negative control	39823 ± 351	161200 ± 2425	4.05
	PVA-2	Enzyme cascade	34030 ± 177	97460 ± 438	2.86
		Negative control	35683 ± 121	101267 ± 473	2.84
	PVA-4	Enzyme cascade	35177 ± 232	103120 ± 3201	2.93
		Negative control	39060 ± 170	110500 ± 2252	2.83
	PVA-6	Enzyme cascade	34197 ± 770	104200 ± 2128	3.05
		Negative control	37541 ± 1293	109133 ± 2011	2.91

Using gel permeation chromatography (GPC) the molecular mass of PVA before and after enzymatic treatment was also explored. Here, in addition to PVA-4, unmodified PVA as well as PVA-2 and PVA-6 were investigated as well for degradation with the enzyme cascade under the above-mentioned conditions. The polydispersity index (PDI), the number average molecular weight

(M_n) and the weight average molecular weight (M_w) were calculated from the measurements (Table 1). PDI increased in most conditions tested when the PVA film was treated with enzymes, indicating a broadening of the molecular weight distribution in comparison to the untreated films which in turn is an indicator for degradation of the polymer. Additionally, a decrease in M_n and M_w was observed in samples containing the enzyme cascade in comparison to the negative control. When PVA samples were treated with the enzyme cascade, both, M_n and M_w decreased in comparison to untreated PVA. As already observed with the Finley method, the GPC measurements confirmed that the enzyme ratio 1:1 or 2:1 result in a similar reduction of M_n and M_w and hence, that changing the ratio of enzyme from 1:1 to 2:1 does not influence the reaction significantly. The largest decrease in M_n was observed in degradation reactions with film PVA-4. Independently of the LK-ADH to CHMO ratio, M_n decreased by 10 % when PVA-4 was treated with enzyme. The largest decrease in M_w, however, was measured for unmodified PVA. When using a 2:1 LK-ADH to CHMO ratio, M_w decreased by 10 % for unmodified PVA whereas for PVA-4 it only decreased by 7 %. In general, the proportional decrease of M_w was lower in comparison to M_n in most cases. The exception to this is the PVA film without modification. Using an enzyme ratio of 2:1, M_w was reduced by 10 % and M_n by 9 % when the film was incubated with the enzyme cascade. In comparison to that, an enzyme ratio of 1:1 reduced M_w by only 4 % and M_n by 7 % indicating that the enzyme ratio of LK-ADH to CHMO M15 has a higher impact on PVA without modification in comparison to modified PVA. This could be due to the additional step in the reaction of modified PVA for hydrolyzing the ester bonds in the derivatized side chains of the polymer which delays the subsequent reactions of ADH and CHMO in comparison to unmodified PVA. Enhancement of enzyme stability of ADH and CHMO as well as prolonged reaction time could hence potentially lead to similar yields for modified PVA as were gained for unmodified PVA. Furthermore, from a larger decrease of M_w in comparison to M_n it can be concluded that larger molecules were more readily degraded when an enzyme ratio of 2:1 was used for unmodified PVA. M_w is taking the weight of each polymer chain into account and hence the value is less influenced than M_n when smaller molecules are preferentially degraded. This in turn leads to the conclusion that larger amounts of LK-ADH are needed for the degradation of unmodified, larger weight PVA molecules. Even though LK-ADH was proven to tolerate a wide variety of substrates and to also accept bulky side chains[15], the polymer is most likely challenging for the enzyme and an increase of the enzyme amount could hence help with degrading larger molecules. Enzyme engineering of LK-ADH towards acceptance of larger side changes could further improve the degradation rate of PVA.

In summary, a modification of PVA was achieved with succinic anhydride. This was realized via a simple chemical process using water as solvent at elevated temperature rendering succinylated PVA films through wet casting techniques. Most importantly, the here described novel enzyme cascade consisting of four steps carried out by three enzymes that can break down the modified PVA with improved properties as well as PVA without modification. The *in situ* recycling of the cofactor NADP(H) makes this enzyme cascade self-sufficient, more versatile, and applicable in comparison to published (microbial) systems for PVA degradation.

Acknowledgements

R.W., G.H. and U.T.B gratefully acknowledge the financial support received from the European Union's Horizon 2020 research and innovation program (MIX-UP, grant number 870294). The School of Chemistry at UCD is acknowledged for financial support in the form of Sir Walter Hartley scholarships to K.D. and M.D.F. Science Foundation Ireland is acknowledged for support via a Frontiers for the Future award to M. B. (20/FFP-P/8712). Furthermore, we would like to thank Dr. Elizabeth Smith, former team member of Aquapak Polymers Ltd and Dr. John Williams, current team member of Aquapak Polymers Ltd, for the material supply. Marco Went from the IOM team is acknowledged for his support with GPC measurements.

Keywords: degradation • enzyme catalysis • enzyme cascade • plastic • polyvinyl alcohol • synthesis

[1] N. B. Halima, *RSC Adv.* **2016**, *6*, 39823–39832.
[2] C. Rolsky, V. Kelkar, *Int. J. Environ. Res. Public. Health* **2021**, *18*, 6027.
[3] Y. Zhang, Q. Wang, J. Yuan, *Adv. Textile Biotechnol.* **2019**, *2,* 21–36.
[4] a) C. Sakazawa, M. Shimao, Y. Taniguchi, N. Kato, *Appl. Environ. Microbiol.* **1981**, *41*, 261–267; b) M. Shimao, I. Fukuta, N. Kato, C. Sakazawa, *Appl. Environ. Microbiol.* **1984**, *48*, 751–754.
[5] a) H. F. Wu, L. Z. Yue, S. L. Jiang, Y. Q. Lu, Y. X. Wu, Z. Y. Wan, *Water Sci. Technol.* **2019**, *79*, 2005–2012; b) F. Kawai, X. Hu, *Appl. Microbiol. Biotechnol.* **2009**, *84*, 227–237; c) S. Matsumura, N. Tomizawa, A. Toki, K. Nishikawa, K. Toshima, *Macromolecules* **1999**, *32*, 7753–7761.
[6] M. Shimao, Y. Taniguchi, S. Shikata, N. Kato, C. Sakazawa, *Appl. Environ. Microbiol.* **1982**, *44*, 28–32.
[7] W. Klomklang, A. Tani, K. Kimbara, M. Rie, U. Takashi, M. Shimao, F. Kawai *Microbiology* **2005**, *151*, 1255–1262.
[8] K. Sakai, N. Hamada, Y. Watanabe, *Agric. Biol. Chem.* **1984,** *48*, 1093–1095.
[9] D. Jia, Y. Yang, Z. Peng, D. Zhang, J. Li, L. Liu, G. Du, J. Chen, *Appl. Biochem. Biotechnol.* **2014**, *172*, 2540–2551.
[10] Y. Wei, J. Fu, J. Wu, X. Jia, Y. Zhou, C. Li, M. Dong, S. Wang, J. Zhang, F. Chen, *Appl. Environ. Microbiol.* **2017**, *84*, e01898-17.
[11] a) R. Dickson, E. Mancini, N. Garg, J. M. Woodley, K. V. Gernaey, M. Pinelo, J. Liu, S. S. Mansouri, *Energy Environ. Sci.* **2021**, *14*, 3542–3558; b) M. Morales, M. Ataman, S. Badr, S. Linster, I. Kourlimpinis, S. Papadokonstantakis, V. Hatzimanikatis, K. Hungerbühler, *Energy Environ. Sci.* **2016**, *9*, 2794–2805.
[12] Z. Söyler, K. N. Onwukamike, S. Grelier, E. Grau, H. Cramail, M. A. R. Meier, *Green Chem.* **2018**, *20*, 214–224.
[13] a) A. Becker, D. Böttcher, W. Katzer, K. Siems, L. Müller-Kuhrt, U. T. Bornscheuer, *Appl. Microbiol. Biotechnol.* **2021**, *105*, 4189–4197; b) J. Engel, K. S. Mthethwa, D. J. Opperman, S. Kara, *Mol. Catal.* **2019**, *468*, 44–51.
[14] J. H. Finley, *Anal. Chem.* **1961**, *33*, 1925–1927.
[15] C. W. Bradshaw, W. Hummel, C. H. Wong, *J. Org. Chem.* **1992**, *57*, 1532–1536.

Entry for the Table of Contents

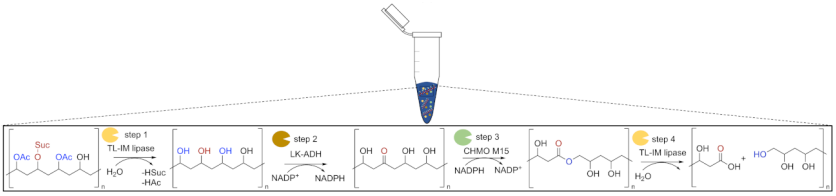

Enzymatic degradation of polyvinyl alcohol (PVA). Biodegradation of the water-soluble PVA by microorganisms is slow and frequently involves pyrroloquinoline quinone (PQQ)-dependent enzymes. In this study, we present a modified PVA film with improved properties as well as a PQQ-independent novel enzymatic cascade consisting of a lipase (TL-IM), an alcohol dehydrogenase (LK-ADH) and a Baeyer-Villiger monooxygenase (CHMO M15) for the degradation of modified and unmodified PVA.

Supporting Information

69451 Weinheim, Germany

Synthesis of Modified Polyvinyl Alcohols and their Degradation Using an Enzymatic Cascade

Gerlis von Haugwitz, Kian Donnelly, Mara Di Filippo, Daniel Breite, Max Phippard, Agnes Schulze, Ren Wei, Marcus Baumann and Uwe T. Bornscheuer*

Abstract: Polyvinyl alcohol (PVA) is a water-soluble synthetic vinyl polymer with remarkable physical properties including thermostability and viscosity. Its biodegradability, however, is low even though a large amount of PVA is released into the environment. Established physical-chemical degradation methods for PVA have several disadvantages such as high price, low efficiency, and secondary pollution. Biodegradation of PVA by microorganisms is slow and frequently involves pyrroloquinoline quinone (PQQ)-dependent enzymes, making it expensive due to the costly cofactor and hence unattractive for industrial applications. In this study, we present a modified PVA film with improved properties as well as a PQQ-independent novel enzymatic cascade for the degradation of modified and unmodified PVA. The cascade consists of four steps catalyzed by three enzymes with in situ cofactor recycling technology making this cascade suitable for industrial applications.

DOI: 10.1002/anie.2021XXXXX

Table of Contents

Experimental Procedures

Materials

Polyvinyl alcohol (PVA) standards were purchased from PSS Polymer Standards Service GmbH (Mainz, Germany). Chemicals and consumables were purchased from Merck KGaA (Darmstadt, Germany), Sigma-Aldrich (Steinheim, Germany) and Thermo Fisher Scientific (Waltham, MA, USA) unless stated otherwise. Lipase *Thermomyces lanuginosus* immobilized on silica gel (Lipozyme TL-IM) was purchased from Novozymes (Bagsværd, Denmark). PVOH-418 was purchased from Sekisui Specialty Chemicals (Dallas, Texas, United States).

Synthesis of succinate-PVOH-418 hybrids and generation of thin films

A general synthetic protocol was established whereby solid succinic anhydride (2 g, 4 g or 6 g) was added to a solution/suspension of PVOH-418 (30 g in ca. 300 mL deionised water) and vigorously stirred at 80 °C for 5 h. The set-up thereby comprised of a Schott glass bottle (500 mL volume containing a 2 cm magnetic stir bar) and an IKA hotplate with magnetic stirring. Within 1 h a clear solution was obtained. This material was then poured without prior cooling into plastic storage boxes (ca. 40 x 20 cm) aiming for 25% of solution per box (usually 3 on this scale). After two days of evaporation in a ventilated space (i.e., a fume hood), films were peeled off and stored between paper to avoid curling.

Production of enzymes

The alcohol dehydrogenase from *Lactobacillus kefir* (LK-ADH) as well as the cyclohexanone monooxygenase (CHMO) variant M15, originally from *Acinetobacter calcoaceticus*, were recombinantly expressed in *Escherichia coli* (*E. coli*) BL21. For that purpose, cells were grown in lysogeny broth medium including 50 µg/L ampicillin (Amp) overnight at 37 °C and 220 rpm. The main culture was grown in terrific broth medium including 50 µg/L Amp and in the case of LK-ADH addition of 1 mM $MgCl_2$. Inoculation was done with 1 % of the main culture. Cells containing the plasmids for CHMO M15 were induced by autoinduction by adding 0.2 % lactose and 0.05 % glucose to the culture medium. The main culture was incubated for 3 h at 37 °C and afterwards for 21 h at 21 °C. Cells containing the plasmid for LK-ADH were grown at 37 °C until an OD600 of 0.5 and afterwards the enzyme expression was induced by adding 1 mM IPTG to the culture. The subsequent incubation took place at 21 °C for 21 h.

Cells were harvested by centrifugation at 10,000 ×g for 5 min, pellets were washed with 10 mM sodium phosphate buffer (pH 8.5). The pellet from a 50 mL main culture was resuspended in 10 mL 10 mM sodium phosphate buffer (pH 8.5) and lysed by sonication (3x1.5 min, 50 % pulse) with SONOPULS HD 2070 (BANDELIN electronic GmbH & Co. KG, Berlin, DE). The soluble fraction from the crude cell lysate was separated by centrifugation at 10,000 ×g for 30 min followed by filtration through a 0.2 µm membrane before usage.

Degradation of PVA by the enzymatic cascade

PVA was dissolved at 50 °C in 10 mM sodium phosphate buffer with a concentration of 40 mg/mL and the pH was adjusted to 8.5. 100 µL LK-ADH-lysate, 100 µL CHMO M15-lysate, 2 mg of immobilized lipase TL-IM and 4 mM $NADP^+$ were added to 250 µL of the PVA stock solution and filled up to 500 µL with 10 mM sodium phosphate buffer (pH 8.5). As negative control *E. coli* BL21 lysate with an empty vector was used. Reactions were incubated for 24 h at 20 °C and 1000 rpm. Reactions were performed in triplicates unless stated otherwise. The analysis of samples regarding concentration of PVA was done by a modified Finley method. Analysis regarding the molecular weight of the remaining PVA after degradation was done by gel permeation chromatography (GPC). For GPC measurements the reactions were scaled up to a total volume of 2 mL.

Determining PVA concentration by a modified Finley method

For the determination of the PVA concentration, a modified Finley method according to Mohamed *et. al*.[1] was used, which can colorimetrically quantify the green complex formed by PVA with iodide in the presence of boric acid.[1b] A potassium iodide solution was prepared from 2.5 g/L KI and 12.7 g/L I_2. 40 µL of potassium iodide solution were mixed with 60 µL of boric acid (4 g/L) and 40 µL of sample. Using a microplate reader (Infinite® M200 pro, Tecan Group Ltd. (Männedorf, Switzerland)) the absorbance of every sample was measured at 500 nm.

Gel permeation chromatography

Determination of the molecular weight was carried out using gel permeation chromatography (Tosoh EcoSEC, HLC-8320GPC, equipped with a pre-column (PSS Suprema Pre-column 10 µ, 8x50 mm) and three columns (PSS Suprema 10 µ, 1000 Å/100 Å/30 Å, 8x300 mm). The eluent flux and temperature were set to 1 mL/min and 45 °C, respectively. Mn, and Mw were then determined using the instrument's software.

Characterization of enzymes regarding temperature stability

Enzymes were incubated at different temperatures in the range of 4–50 °C for one hour. Afterwards, the residual activity was determined at 25 °C and pH 7. The activity of all enzymes was determined spectrophotometrically using different substrates. In the case of the lipase TL-IM, the formation of *p*-nitrophenol (pNP) from *p*-nitrophenyl acetate (pNPA) was monitored. For this purpose, 2 mg of TL-IM were added to 900 µL of 50 mM sodium phosphate buffer (pH 7), followed by adding 100 µL pNPA (10 mM in dimethyl sulfoxide (DMSO)) to start the reaction with a final substrate concentration of 1 mM. After one minute of reaction, the amount of pNP (extinction coefficient: ε = 17,500 $M^{-1}cm^{-1}$) was determined at 410 nm in a microplate reader.

For LK-ADH and CHMO M15 the increase or decrease of the co-factor NADPH was followed at 340 nm. Reactions were performed in a similar way as described for LK-ADH by Becker *et al.*[2] Prior to the reaction, LK-ADH lysate was diluted 1:40 and CHMO M15 was diluted 1:5. (*R*)-1-phenylethanol (LK-ADH) and cyclohexanone (CHMO M15) were used as substrates for the enzymes. 20 µL of (diluted) lysate were added to 0.5 mM NADP(H) and 1 mM of the respective substrate in a total volume of 200 µL.

Results and Discussion

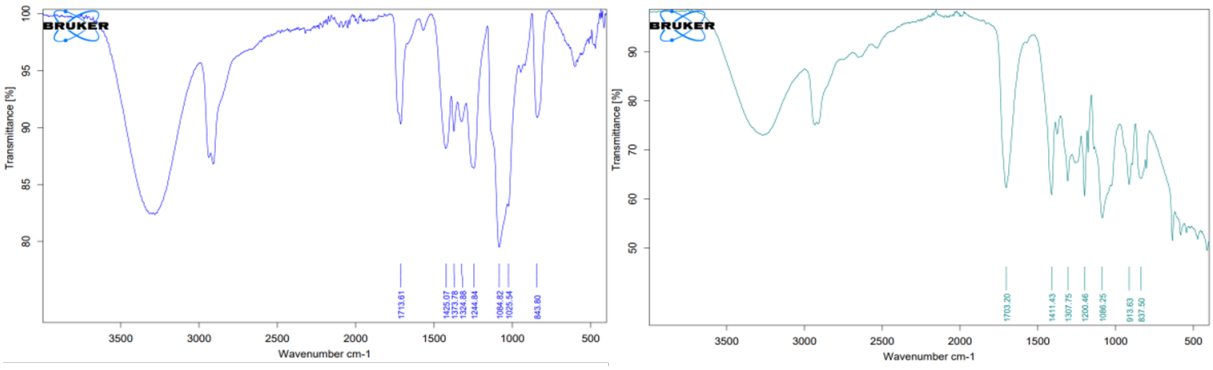

Figure S1. Representative infrared spectra of PVOH-418 (left) and succinylated PVA (right). The spectra indicate a distinct change in the carbonyl stretching region (i.e., 1600-1800 cm^{-1}) which is in agreement with the introduction of succinate moieties; i.e., 1714 cm^{-1} for PVOH-418 vs 1703 cm^{-1} for succinylated PVA.

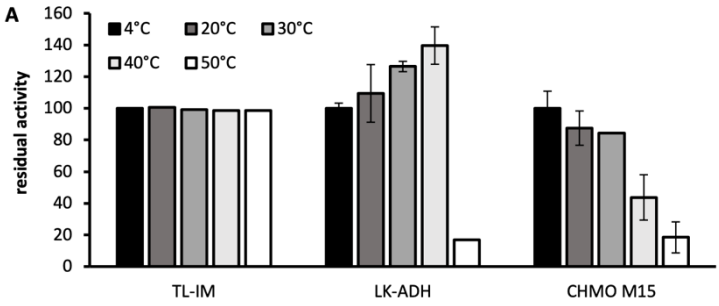

Figure S2. Investigating the optimal temperature of the enzymatic cascade. All three enzymes used in the cascade were investigated for their residual activity after incubation for one hour in a temperature range from 4-50 °C. While TL-IM remained 100 % residual activity over the whole temperature range, LK-ADH was only 20 % active after 1 h at 50 °C and the activity of CHMO M15 significantly decreased at temperatures over 30 °C.

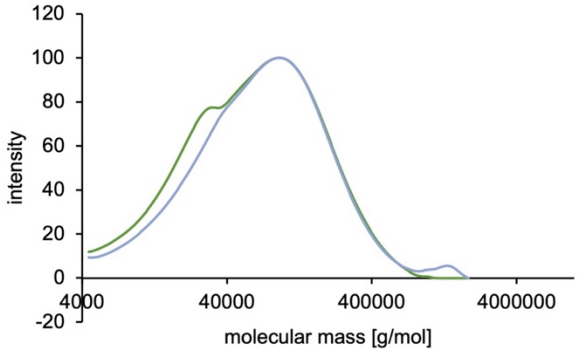

Figure S3. Representative GPC chromatogram for enzyme degraded sample (green) and negative control (blue).

Table S1. Summary of key parameters for different succinylated PVOH-418 materials. The chemical composition of the films differed in the amount of succinic anhydride: 2 g (Suc2), 4 g (Suc1) or 6 g (Suc3) were used per 30 g PVOH-418.

Criteria	Target	Suc2	Suc1	Suc3
Method of manufacturing	Pellet to film	Film via wet casting	Film via wet casting	Film via wet casting
Oxygen Transmission ($cc/m^2/day$) *23°C, 0% humidity*	<10	21.7	22.2	29.9
Water Vapour ($cc/m^2/day$) *38°C, 90% humidity*	<13.8 (1wk) <6.57 (2wk)	525.4	433.1	696.9
Avg. Gauge (µm)	25-120	42	141	95
Tensile Strength (N)	>50	196	77	60
Puncture (N)	>20	91	108	84
Dispersibility / Solubility @25°C		✓ /x	✓ /x	✓ /x
Dispersibility / Solubility @40°C (sec) (avg)		39/110	72/1151	27/102
Dispersibility / Solubility @60°C		✓ /x	✓ /x	✓ /x
Disintegration	6 months	n.a.	Small holes	8 weeks intact

References

[1] a) H. Mohamaed, A.M.Shah, Y. Nazir, T. Naz, S. Nosheen, Y. Song, *World J. Microbiol. Biotechnol.* **2021**, *38*, 10; b) J. H. Finley, *Anal. Chem.* **1961**, *33*, 1925–1927.

[2] A. Becker, D. Böttcher, W. Katzer, K. Siems, L. Müller-Kuhrt, U. T. Bornscheuer, *Appl. Microbiol. Biotechnol.* **2021**, *105*, 4189–4197

Author Contributions

Conceptualization, U.T.B., M.B.; Substrate generation and characterization, K.D., M.D.F., and M.B.; Enzyme expression, characterization and enzymatic reactions, G.H.; Gel permeation chromatography measurements, D.B.; Writing – Original Draft, G.H., and M.B.; Writing, review and editing, all authors; Supervision and funding acquisition, R.W., M.B. and U.T.B.

Eigenständigkeitserklärung

Hiermit erkläre ich, dass diese Arbeit bisher von mir weder an der Mathematisch-Naturwissenschaftlichen Fakultät der Universität Greifswald noch einer anderen wissenschaftlichen Einrichtung zum Zwecke der Promotion eingereicht wurde.

Ferner erkläre ich, dass ich diese Arbeit selbstständig verfasst und keine anderen als die darin angegebenen Hilfsmittel und Hilfen benutzt und keine Textabschnitte eines Dritten ohne Kennzeichnung übernommen habe.

Gerlis Maria von Haugwitz

List of Publications

R. Wei, G. von Haugwitz, L. Pfaff, J. Mican, C. P. S. Badenhorst, W. Liu, G. Weber, H. P. Austin, D. Bednar, J. Damborsky, U. T. Bornscheuer, Mechanism-Based Design of Efficient PET Hydrolases, *ACS Catal*., **2022**, 12, 3382−3396.

G. von Haugwitz, X. Han, L. Pfaff, Q. Li, H. Wei, J. Gao, K. Methling, Y. Ao, Y. Brack, J. Mican, C. G. Feiler, M. S. Weiss, D. Bednar, G. J. Palm, M. Lalk, M. Lammers, J. Damborsky, G. Weber, W. Liu, U. T. Bornscheuer, R. Wei, Structural Insights into (Tere)phthalate-ester Hydrolysis by a Carboxylesterase and its Role in Promoting PET Depolymerization, *ACS Catal*., **2022**, accepted.

G. von Haugwitz, K. Donnelly, M. Di Filippo, D. Breite, M. Phippard, A. Schulze, R. Wei, M. Baumann, U. T. Bornscheuer, Synthesis of Modified Polyvinyl Alcohols and their Degradation Using an Enzymatic Cascade, *Angew. Chem. Int. Ed.*, under review.

Acknowledgements

First and foremost, I would like to thank Prof. Dr. Uwe T. Bornscheuer. Uwe, thank you very much for giving me the opportunity to do my Ph.D. in your group. I very much appreciated your supervision, your unbelievably fast reply to e-mails, and the detailed knowledge that you have in each of the vast numbers of topics being researched in your group. I could always count on your support and contact you with questions regarding students, project partners, or simply research issues. The dedication and trust that you put into your students is astonishing and I am highly grateful to have had the chance to be part of your team. You always go the extra mile for us and even though you told me once that that is a given, I could not have asked for a better professor to do my Ph.D. with. Thank you!

Next, I would like to thank Dr. Ren Wei who also supervised and supported me throughout the past three years. Ren, thank you very much for always being reachable and taking the time to answer my questions in detail. You sent me many, many papers, suggestions, and creative ideas regarding my research. Thank you for always believing in my research and making publishing in journals like *ACS Catalysis* possible for me.

Furthermore, I would like to express my gratitude to the MixUp project for the financial support of my Ph.D.

A big thanks also goes to the ‘plastic people’ from the Bornscheuer group, Lara Pfaff, Carolin Buchmann, Yannick Branson, and Thomas Oïffer. Working with you as a team, discussing research, and finding solutions for what seemed like unsolvable problems was a great pleasure. You made the working environment fun and productive at the same time. I appreciate all the challenges that you went through with me, the research kind but of course also the sport/mental kinds that especially Yannick kept agreeing to.

I would also like to thank all the members of the Bornscheuer group for the productive and friendly environment not only at work but also at various meetings outside of the lab. A special thanks to Ina Menyes for helping with all the HPLC and GC measurements.

Thanks for all the support that I received from my friends and family. My deepest appreciation goes to my parents who helped me financially and mentally throughout my education. Without you, I would not be where I am today. Last but not least, I want to thank my boyfriend. Vova, thank you so much, not only for your direct support of my research but also for your patience, care, and emotional support. Thank you for listening to me day in and day out, and for going through this emotional roller coaster with me. I am so grateful to have you by my side.